ABSTRACT

GUPTA, ATUL. Surface reactions during plasma enhanced chemical vapor deposition of silicon and silicon based dielectrics. (Under the direction of Gregory N. Parsons)

Theoretical ab-initio calculations (including both the Configuration Interaction and Density Functional approaches) are used to describe some of the critical surface reactions during plasma enhanced chemical vapor deposition of amorphous and micro-crystalline silicon films. The energetics as well as the reaction mechanism are calculated for the abstraction of surface hydrogen by incident silyl and hydrogen radicals. Another important reaction involving the insertion of these radicals (silyl and hydrogen) into strained Si-Si bonds on the surface is also evaluated. Experiments involve surface topology evolution studies of plasma deposited a-Si:H films using atomic force microscopy (AFM) as well as structural and electrical characterization of silicon dioxide films using several techniques including infrared spectroscopy, ellipsometry, and current-voltage measurements. A predictive kinetic model to describe the growth of silicon films from a predominantly silyl radical flux is developed to explain experimental observations regarding the properties of plasma deposited amorphous silicon films. The model explains diffusion length enhancements under certain processing conditions as well as lays a foundation for understanding the Si-Si network formation during the deposition of a-Si films.

SURFACE REACTIONS DURING PLASMA ENHANCED CHEMICAL VAPOR DEPOSITION OF SILICON AND SILICON BASED DIELECTRICS.

by

ATUL GUPTA

A dissertation submitted to the Graduate Faculty of
North Carolina State University
in partial fulfillment of the
requirements for the Degree of
Doctor of Philosophy

CHEMICAL ENGINEERING

Raleigh, North Carolina

2001

APPROVED BY:

Dr. H. Henry Lamb	Dr. Phillip E. Russell
Dr. Gregory N. Parsons Chair of Advisory Committee	Dr. David F. Ollis Co-Chair of Advisory Committee

This thesis is dedicated to my parents, Mr. Tilak Raj and Mrs. Chandra Kanta Gupta for their loving support throughout my education, and my uncle Mr. N.L. Mahajan, for being a great mentor.

BIOGRAPHY

ATUL GUPTA was born on December 27, 1974 in the capital city of New Delhi, India. He was brought up in New Delhi, where he attended Manava Bharti School through high school (twelfth grade). He then opted for a career in Engineering and attended the Indian Institute of Technology, New Delhi, from August 1992 to May 1996, when he graduated with a Bachelor of Technology degree in Chemical Engineering. In August 1996, he moved to the United States for his graduate studies at North Carolina State University in Raleigh, NC. On the way to his Ph.D. (which he completed in October 2001), he was conferred two Master's degrees, one in Chemical Engineering (May 1999) and another in Electrical and Computer Engineering (May 2000). Upon completion of his graduate education, he plans to join Advance Micro Devices as a Module Transfer Engineer.

ACKNOWLEDGEMENTS

I would like to thank Dr. Gregory N. Parsons for his support, encouragement and direction throughout the course of this work. I am deeply indebted to Dr. Parsons for being a true mentor and good friend and especially thank him for giving me this wonderful opportunity to explore the exciting field of electronic materials. Special thanks to my fellow research group members: Easwar Srinivasan for helping me decide on this project, Ashfaqul Chowdhury and Tom Yang for their ever needed help with system, Jim Chambers, Tonya Klein and Kevin Bray for some very thoughtful discussions and collaborations, and David Terry, Kiejin Park and Leonard Nelson for taking the reins over on this work. .

I am grateful to Dr. Lee Bartolotti for his tutorials on the use of quantum chemistry packages and the North Carolina Supercomputing Center for providing the hardware and software resources without which this work would not have been possible. Special mention of the cleanroom staff personnel including Joan O'Sullivan, Henry Taylor, and Harold Morton as well as Dr. Ginger Yu for her training course on the use of some analysis tools in the facility. Also, thanks to the Analytical Instrumentation Facility for the use of the XPS instrument and Dr. Laura Smith for training me on the AFM.

I acknowledge my graduate committee members, Dr. Henry Lamb, Dr. Dave Ollis and Dr. Phil Russell for their support through my graduate years and their insight into the details of the my research at an early stage. Special thanks to Kit Yeung, our instrument

maker for his in genuine solutions in the repair/maintenance of the plasma deposition system.

I also acknowledge the financial support from National Science foundation and DARPA high definition systems program.

TABLE OF CONTENTS

LIST OF TABLES

LIST OF FIGURES

CHAPTER 1

1 INTRODUCTION

1.1 OVERVIEW OF THE DISSERTATION

The last few decades of the twentieth century have been an era of unprecedented technological advancement in the semiconductor industry. Developments in the manufacturing and characterization of high performance device materials have revolutionized the quality and diversity of the semiconductor products available to today's consumers. While further developments in device manufacturing and materials are being pursued in order to maintain this momentum, a fundamental understanding of the deposition processes controlling the material and device properties is critical towards attaining the challenging goals. This dissertation focuses on enhancing our understanding of growth mechanisms that control the electronic and morphological properties of hydrogenated amorphous silicon (a-Si:H) and silicon dioxide dielectric films deposited at low temperatures (<400°C) using plasma enhanced chemical vapor deposition (PECVD) techniques.

This dissertation aims at developing an understanding of the reaction mechanisms involving hydrogen (H) and silyl (SiH_3) radicals with the growth surfaces during plasma deposition of a-Si:H films. This is accomplished by evaluating the reaction energetics using theoretical ab-initio quantum chemical calculations that include both the

Configuration Interaction (CI) and the Density Functional Theory (DFT) approaches. Specifically, the reaction energetics for: i) the abstraction of a surface hydrogen atom by H and SiH_3 radicals; and ii) the insertion of H and SiH_3 radicals into strained Si-Si bonds are quantified. A quantitative kinetic growth model for a-Si:H deposition is developed as a predictive tool for estimating the optimum growth conditions for a given set of desired film properties. The model utilizes a novel "valence balance" approach (developed to describe "bond-specific" reactions, for example, insertion of radicals into strained bonds) in conjunction with the conventional site balances.

The search for a device quality transparent dielectric, deposited at temperatures compatible with plastic substrates for the next generation flat panel display applications, is continued through deposition and characterization of plasma deposited silicon dioxide films. The challenges include water incorporation in these films during the deposition process that degrades the electric properties of the films. The possible application of H_2 plasma anneals during the deposition of silicon dioxide films to abstract the OH groups from the growth surface of the oxide film deposited from silane (SiH_4) /nitrous oxide (N_2O) gas mixtures is explored and the possible challenges in utilizing this approach are elucidated. These studies broaden our understanding of the fundamental reactions during a-Si:H and SiO_2 film depositions as well as demonstrate the universal applications for some basic surface reactions across different deposition processes.

1.2 THIN FILM MATERIALS

Rapid developments in the telecommunication and wireless technology in the past decade have increased the demand for portable electronics manifolds. The display technology, in particular, has benefited a great deal from this boom. Large area Active matrix displays, such as those used in flat panel displays, high definition televisions and laptop computer screens typically use thin film transistors (TFT) to switch individual pixels on the screen. Various thin film materials are required in the fabrication of these TFTs. These include a semi-conducting material (either amorphous or poly–Si), a dielectric material (typically silicon nitride, or silicon dioxide) and a conducting material for contacts (Aluminum metal). The amorphous silicon and dielectric layers are typically deposited using plasma deposition techniques while the metal is deposited by sputtering or evaporation techniques.

1.2.1 Hydrogenated Amorphous Silicon

Amorphous silicon films have attracted considerable interest for applications in photovoltaic devices (Solar cells) and more recently in TFTs for active matrix displays as well as some photo-sensor applications [1]. The films are typically deposited using plasma enhanced CVD of silane/hydrogen mixtures at a temperature of ~250°C. Hydrogenated amorphous silicon lacks the long-range structural order present in crystalline silicon and this results in interesting material properties for the material. The disorder in the structure of a-Si:H films results in localized band tails, which has a strong influence on the optical and electronic transport properties [1]. For example, a-Si:H is a direct band-gap semiconductor while c-Si has an indirect band gap. The carrier

mobilities in amorphous silicon are substantially lower than those in c-Si a device quality a-Si film only has a carrier mobility of 1 cm^2/V.sec. Under typical growth conditions, the plasma deposited a-Si films contain about 10-15% hydrogen primarily as mono-hydride species in the bulk [2]. H plays an important role in determining the film properties by defect saturation, and some metastable phenomena such as the Staebler-Wronski effect [1]. References [1,3-6] are recommended for further information on a-Si films.

1.2.2 Silicon Dioxide

Silicon dioxide has been the choice material for the dielectric layer in conventional metal-oxide-semiconductor (MOS) based transistors. This has been largely due to the fact that thermally grown SiO_2 films form the best interface with silicon that is critical for superior complementary MOS based logic circuits. However, low temperature deposition processes for good quality SiO_2 films have had little success on account of the poor electronic and structural properties of these films. Nevertheless there are several other application for low temperature oxides including inter-layer dielectric materials in back-end processing of semiconductor devices and barrier applications in the packaging industry. Silicon dioxide is attractive barrier material to prevent permeation of gases through polymeric films since these films are durable, dense, and transparent. The good barrier performance results from a highly networked covalent bond structure. Silicon based insulators are unique in that all atoms in the material bond in a continuous random covalent network. Interest in low temperature SiO_2 has also been rekindled, for potential application as hermetic coatings to protect organic light emitting devices from degradation. Transparent thin film gas permeation barriers are also desired for other

situations to isolate materials from ambient exposure [7], including food packaging, and protective coatings (such as paints and varnishes). These films can also be used as selective barriers for gas separation of gaseous mixtures [8]. Additionally, the transparent silicon dioxide films are potentially more environment friendly than other clear barrier materials such as polyvinyl chloride and poly-vinylidene chloride that cause ozone depletion in the atmosphere [9].

1.3 PLASMA PROCESSING

At very low temperatures (<300°C), semiconductors or insulators cannot be grown thermally (as the available thermal energy available is too low) and other means of film growth have to be used. Growth generally involves consumption of the substrate by a thermally activated process (i.e. silicon oxidation, $Si + O_2 \rightarrow SiO_2$). A deposition process typically does not include significant substrate consumption, and the film source material is supplied in the gas phase. In order to achieve deposition at low temperature the reaction precursors are typically generated in the gas phase. Gas phase generation of precursors is commonly accomplished using a plasma, where ionization, dissociation and excitation of gaseous precursors results from an applied RF (radio frequency) or DC electric field. The field developed in the plasma accelerates electrons that collide with molecules resulting in the generation of radicals, ions, and more electrons, which in turn are further accelerated. The reactive radicals/ions present in the plasma have enough energy to overcome reaction barriers, leading to deposition on the substrate surface. The

process has some characteristics of a physical vapor deposition (PVD), but in PECVD, precursors can reflect, desorb, and/or diffuse on the surface more easily than in PVD.

The obvious advantage of plasma deposition is that semiconducting and dielectric thin films can be deposited on almost any substrate at any desired temperature. However, plasma processes typically have a narrow processing window (optimal range of process variables) and may not work well under all conditions. The key lies in the difficult task of identifying the processing parameters most likely to affect the deposition. Plasma is a complex mixture of radicals, neutrals, ions and electrons with thousands of possible reactions in the plasma and on the surface. It is almost impossible to obtain an unambiguous quantitative characterization of a plasma deposition process.

There are many different approaches to low temperature plasma enhanced chemical vapor deposition (PECVD) of gate dielectrics. The most common apparatus involves a capacitively coupled radio-frequency (RF) power source where the substrates are loaded on the cathode (grounded) while the RF power is applied to the anode. The plasma is generated between the two electrodes and the radicals generated in the plasma lead to deposition on the substrates as well as the walls. These "direct" PECVD reactors are commercially available, and are well suited for deposition over very large areas (greater than $1m^2$). Another approach to PECVD gaining popularity is the remote PECVD wherein the plasma is generated away from the substrate to minimize damage due to ion bombardment and radiation exposure during deposition. Remote PECVD allows a better control over the reaction pathways by selectively exposing specific gases to the plasma, and introducing a select set of precursors near the substrate, downstream from the plasma. This technique is not as well suited to large area deposition, but

advances in reactor and process modeling are making this technique more feasible for large area industrial applications. Many other variations to low temperature deposition techniques are reported, including electron cyclotron resonance (ECR) PECVD, and photo CVD. Various materials have been deposited using PECVD processes at low temperatures, including silicon dioxide, aluminum oxide, silicon nitride, and amorphous silicon. The focus of this dissertation is to understand the key reactions in low temperature plasma deposition of amorphous silicon (a-Si:H) and silicon dioxide films.

1.4 OVERVIEW OF THE FOLLOWING CHAPTERS.

Ab-initio calculations have been used to understand the relative importance of different surface reactions during a-Si:H deposition. A comparison of the reaction mechanisms involved in the surface reactions involving incident silyl radicals with those of H radicals has been accomplished to understand the role of hydrogen radicals during amorphous silicon deposition.

Chapter 2 focuses on abstraction of H from a hydrogen terminated a-Si:H growth surface through direct Eley-Rideal reaction mechanisms involving incident silyl and H radicals. The activation barriers and reaction mechanisms for the two different types of radicals are calculates using several ab-inito methods. Results indicate that the H radicals have a low abstraction barrier as compared with abstraction by silyl radicals. The calculated reaction barriers are consistent with experiments. We further conclude that a stable “three-center” bond proposed as a physisorption state for the silyl radical on H-

terminated surfaces does not exist and that the previously proposed growth mechanisms for a-Si deposition need to be re-evaluated.

The negligible barrier calculated for H abstraction by incident H radicals indicates a possible pathway for removal/reduction of hydroxyl (OH) groups from the surface of plasma deposited silicon dioxide films. This possibility is explored in Chapter 3 where we have characterized the silicon dioxide films in terms of the bonding environment in very low temperature (<350°C) silicon dioxide films. Hydrogen dilution of the feed gases does indeed reduce the OH content in the SiO_2 films and results in improved electrical properties (low leakage current through the films), however post deposition absorption or stability of "associated" OH groups on the surface limit the applications of these material in TFT devices.

Chapter 4 presents a new kinetic model that aims at understanding the growth of amorphous silicon films in light of recent experimental observations. The model presents a novel "valence" balance approach that is used in conjunction with the site balances and enables a quantitative description of the Si-Si network formation during the deposition process. Such network formation processes control the formation of crystalline phase within the a-Si network (resulting in μc-Si) and are therefore critical in determining the electrical and morphological properties of these films. The model is used to predict surface concentrations for several species as well as macroscopic parameters (like growth rates, sticking probability and the diffusion length of the precursors on the growth surface). The results predicted by the model compare favorably with several experimental findings. The model further offers explanations for the diffusion length enhancements

measured experimentally using surface roughness evolution studies. These topology evolution studies are reported in Chapter 5.

In Chapter 6, the mechanisms involved in an alternate growth pathway (involving the direct insertion of silyl radicals into strained Si-Si bonds) for a-Si films are evaluated using Density functional calculations. Results indicate that the insertion may be an important growth mechanism. Comparison of the insertion reactions between silyl and H radicals indicates different reaction paths for the two reactions and preclude the stability of a penta-coordinated stable intermediate state for the silyl radical where it is equidistant from the surface Si atoms as had been proposed in some recent reports.

Finally in Chapter 7, the work presented in this dissertation is summarized and some ideas for further studies are discussed.

1.5 REFERENCES

[1] R. A. Street, *Hydrogenated amorphous silicon* (Cambridge University Press, New York, 1991).

[2] J. C. Knights and R. A. Lujan, *Applied Physics Letters* **35,** 244-246 (1979).

[3] R. Galloni, *Renewable Energy* **8,** 400-404 (1996).

[4] K. H. Jung, S. Shih, and D. L. Kwong, *Journal of the Electrochemical Society* **140,** 3046-3064 (1993).

[5] C. R. Wronski, L. Jiao, R. Koval, and R. W. Collins, *Opto-Electronics Review* **8,** 275-279 (2000).

[6] N. Yamauchi and R. Reif, *Journal of Applied Physics* **75,** 3235-3257 (1994).

[7] J. T. Felts and A. D. Grubb, *Journal of Vacuum Science and Technology A* **10,** 1675 (1992).

[8] G. Rossi and M. Nulman, *Journal of Applied Physics* **74,** 5471 (1993).

[9] E. Finson and J. Felts, *Tappi Journal* **78,** 161 (1995).

Chapter 2 is a reprint of a manuscript accepted for publication in Surface Science (2001)

CHAPTER 2

2 AB INITIO ANALYSIS OF SILYL PRECURSOR PHYSISORPTION AND HYDROGEN ABSTRACTION DURING LOW TEMPERATURE SILICON DEPOSITION

By: Atul Gupta, Hong Yang* and Gregory N. Parsons[1]

Department of Chemical Engineering, North Carolina State University, Raleigh, NC 27695-7905

**Department of Chemistry, North Carolina State University, Raleigh, NC 27695*

Present location: China Center, University of Minnesota, Minneapolis, MN 55455

The energetics of silyl (SiH_3) precursor surface adsorption and hydrogen abstraction on a mono-hydride terminated silicon surface are described. The abstraction of surface hydrogen by H radicals is more exothermic, and proceeds with a smaller kinetic barrier than H abstraction by silyl. Surface adsorption and abstraction were analyzed using both multiparent-configuration interaction (CI) and several density functional approaches using the Si_4H_{10} cluster representing a mono-hydride terminated

silicon (111) surfaces, and results from the two techniques are critically compared and evaluated. Hydrogen abstraction by H is found to proceed through a kinetic barrier that is between 0.0 kcal/mol predicted by DFT and 7.2 kcal/mol determined from CI, consistent with experimental values of ~2 kcal/mol. The barrier height for H abstraction by silyl (without zero point and H tunneling corrections) is determined to be between 4.1 kcal/mol calculated using DFT, and 14.2 kcal/mol determined from the multi-parent CI. These calculations indicate that during typical low temperature silicon deposition processes, H abstraction by impinging hydrogen atoms dominates H abstraction by SiH_3 and plays an important role in creation of surface dangling bonds. None of the Si─H/silyl potential energy surfaces obtained from CI and DFT methods show evidence for stable physisorbed three-center ≡Si─H─$(SiH_3)_p$ bond, which is commonly presumed in several models of silicon thin film deposition. We discuss these results in relation to experimental analysis of surface diffusion kinetics in film deposition, and suggest alternate growth models, including H-mediated Si-Si bond breaking and/or direct silyl insertion, to describe activated low temperature silicon-based film deposition.

Keywords: Ab-initio quantum chemical methods and calculations, Density functional calculations, Models of surface chemical reactions

[1]*email:* gregory_parsons@ncsu.edu

2.1 INTRODUCTION

A fundamental description of surface reaction processes in low temperature deposition of silicon and silicon-based electronic thin films continues to be an important challenge. Hydrogenated amorphous silicon (a-Si:H) films deposited using plasma enhanced chemical vapor deposition (PECVD) or hot-wire catalyzed CVD are widely used in photo-voltaic devices and thin film transistors[1,2], but detailed mechanisms associated with defect generation, crystallization, and topology evolution during low temperature (<350ºC) deposition are not conclusively understood. Quantum chemistry is a useful tool to evaluate different reaction pathways in terms of their reaction energetics, and is thereby an important tool to understand possible surface reaction mechanisms.

Bonding environments for hydrogen are directly linked with the defect structure and stability in low temperature silicon based materials. For example, photoconductivity and stability of solar cells, and charge mobility in thin film transistors, are affected by hydrogen concentration and hydrogen-mediated defects in amorphous silicon films. Therefore, understanding reactions at the growth surface that modify or affect hydrogen concentration, binding structure, or defect incorporation, are particularly important. Hydrogen removal from the growth surface takes place by several mechanisms, including direct desorption, surface recombination and desorption, and hydrogen abstraction by impinging radicals (including H or SiH_3). These hydrogen removal processes are also important because they form dangling bonds that can get incorporated as bulk electronic defects, and/or act as chemisorption sites for impinging and diffusing growth radicals.

Plasma activated deposition is a complex process involving thousands of reactions in the gas phase and on the surface. The SiH_4/H_2 plasma is comprised of mainly H and SiH_n radicals and ions, and is an important model system to understand a broad range of reaction processes in plasma materials processing. Mass spectroscopic studies of reactions between D radicals and H-terminated amorphous silicon (and exposure of D-terminated Si to H atoms) provide strong evidence for H (or D) abstraction from the surface by D (or H) [3-8]. The kinetics for this reaction indicate a small activation barrier [3,6,8] that has been corroborated by *ab-initio* calculations [9,10].

Experimental studies of silane plasmas have identified silyl as the dominant stable radical in the gas phase [11-15]. Experimental and theoretical work has also focused on the kinetics of H abstraction reaction by silyl radicals. Molecular dynamics simulations of silyl (SiH_3) radicals impinging on a H terminated Si(100)-2x1 surface indicate that the SiH_3 radical can either abstract a surface H (activation barrier of ~0.1 eV) or be reflected back into the gas phase [16,17]. Von Keudell *et al.* have reported experiments where they monitored the loss of surface SiD groups (and the appearance of SiH groups) from a deuterated a-Si:D film when the surface is exposed to SiH_3 radicals [18]. They observed a delay in the appearance of Si-H groups that indicates a non-zero barrier for H abstraction by the SiH_3, consistent with the crystalline silicon surface studies.

The interaction between the silyl radical and the H-terminated silicon surface is critically important to understand details of the silicon growth process. A common model [15,17,19-21] for silicon deposition involves physisorption of the SiH_3 radicals on H-terminated Si sites to form a three-centered ≡Si─H─Si≡ linkage that is sufficiently stable to achieve high surface coverage at temperatures near 300°C, but is also sufficiently weak

to allow the silyl radical to diffuse with a relatively small activation barrier (~0.2 eV) on the surface at low temperature.

In this article, we describe results of various *ab-initio* calculations, including multi-parent Configuration Interaction (CI) and Density Functional Theory (DFT) approaches, for interactions between surface Si-H and impinging H and silyl radicals, including:

monohydride abstraction by H

$$(SiH_3)_3{\equiv}Si{-}H + H \rightarrow (SiH_3)_3{\equiv}Si{-} + H_2 \qquad (1)$$

monohydride abstraction by SiH_3

$$(SiH_3)_3{\equiv}Si{-}H + SiH_3 \rightarrow (SiH_3)_3{\equiv}Si{-} + SiH_4 \qquad (2)$$

physisorption of SiH_3 on H-terminated silicon in a three-center bond:

$$(SiH_3)_3{\equiv}Si{-}H + SiH_3 \rightarrow (SiH_3)_3{\equiv}Si{-}H{-}(SiH_3)_p \qquad (3)$$

The geometries used to model these reactions are shown schematically in Figs 2.1 and 2.2. We have used collinear interaction geometry to obtain the energy profiles for the radical-cluster interactions. The monohydride surface was modeled as a four-Si atom cluster with the remaining three valences of the secondary Si atoms satisfied by hydrogen atoms. Larger clusters were also used for some calculations for comparison. The Si-H bond distance was fixed at 1.48Å.

The results presented here provide a direct comparison of the expected reaction energetics for H abstraction by H and silyl, and the geometry of the Si-H-(SiH_3) interaction also allows us to evaluate the energetics of silyl physisorption on H-terminated silicon. The results allow us to advance the understanding of low temperature silicon thin film formation, and to comment on the viability of various growth models in

terms of expected radical adsorption and diffusion processes. Both DFT and CI calculation methods, described in Section II, are used here to demonstrate self-consistency in our analysis of these reactions. Results of the calculations, including discussion of particular strengths and limitations of each method, are included in Section III below.

2.2 THEORY AND CALCULATIONS

Our approach to evaluate the reaction energetics involves a) Hartree-Fock self-consistent field (HF-SCF) followed by configuration interaction (CI); b) Density functional theory (DFT) under the generalized gradient approximation (GGA); and c) a hybrid HF-DFT approach using polar and non-polar basis sets.

For the CI calculations, we followed the approach detailed by Jing and Whitten [9,22]. These calculations are performed by first obtaining the self-consistent field (SCF) for the silicon cluster and the approaching H (or SiH_3) radical. The occupied and valence orbitals are then transformed separately to obtain spatially localized orbitals about all the atoms (both the silicon cluster as well as the approaching radical). CI treatment of the system requires orbitals that are outside the space spanned by localized orbitals obtained from the transformation of the lattice wave function. Therefore in addition to the localized orbitals obtained previously, we include additional basis functions on designated surface atoms for flexibility in the valence shell basis, hence allowing for the polarization and radial changes in the atomic orbitals. The two Si atoms (the topmost surface Si atom and the Si atom in the approaching SiH_3 radical) are described at an all electron level Dunning's [6*s*4*p*] basis sets contracted from [11*s*7*p*] primitive sets of

Huzinaga, augmented by a set of *d* functions with an exponent of 0.4. Other Si atoms are described at the 3*s*, 3*p* valence electron level by a set of double-zeta five term 3*s* and a four term 3*p* basis functions and a [1*s*-2*p*] effective core potential. The H atom that undergoes the abstraction is described by a double-zeta *s* basis with an additional set of 2*p* orbitals with an exponent of 0.6. All other H atoms are described by only the double-zeta *s* basis. These are the same basis orbitals as used by Srinivasan et al. [9] to describe the reaction energetics of surface H abstraction by an impinging H radical.

CI calculations for abstraction by H radicals involve single and double excitations from multiple parent configurations within a nine-electron subspace to 61 possible localized virtual orbitals. For abstraction by SiH_3 radicals using CI, the excitations were carried out in a 15-electron subspace to 75 possible localized virtual orbitals. The configurations arising from excitations having second order interaction energies with the parent SCF configurations greater than $1x10^{-5}$ Hartrees are retained explicitly in the expansion. Configurations with coefficients greater than 0.05 are included as parent configurations.

Density functional calculations were performed using the DGauss software on a CrayT90 using the Unichem (release 4.1) interface software. The generalized gradient approximation (GGA) was used in the DFT calculations. A combination of Becke's exchange functional [23] and Lee, Yang and Parr's (LYP) correlation functional [24] was used to describe the ground state energies in these computations (BLYP method). Triple Zeta Valence Potential (TZVP) basis sets augmented with A1 auxiliary basis sets were used to describe the electron wavefunctions for all the atoms in the cluster. We also calculated the minimum energy pathway for these reactions using a hybrid HF-DFT

approach, using Becke's three-parameter hybrid exchange functional with the non-local correlation provided by LYP functional (B3LYP method) using the 6-311G basis set to describe the atomic orbitals. The calculations were carried out using Gaussian98 software [25]. As a further refinement, we have also carried out the HF-DFT (B3LYP) calculations with polarized basis functions on the interacting atoms and full geometry optimization done for the cluster at each step along the minimum energy path. The 6-31G++(3d,2p) basis set was used on the interacting atoms, the topmost surface Si atom and the Si atom in the approaching SiH_3 radical along with the H atom that undergoes the abstraction and a 6-31G basis was used on the remaining atoms in the cluster.

Fig 2.1 shows the silicon cluster used as a model for the monohydride terminated surface. The surface silicon atom (top-most) is tetrahedrally bonded to three other silicon atoms (secondary) and the surface hydrogen atom. The secondary Si atoms are saturated with three tetrahedrally bonded hydrogen atoms. The Si-H bond lengths are fixed at 1.48Å while the Si-Si bond lengths are kept at 2.35Å. The cluster is bilaterally symmetric with respect to the y-z plane passing through the top-most silicon atom. The tetrahedral bond angle is fixed at 109.28° irrespective of whether the silicon atom is bonded to silicon or a hydrogen atom. Single point energy calculations were performed for several combinations of the $Si^{(1)}$-H and $Si^{(2)}$-H bond lengths and a potential energy surface was generated as a function of these two parameters.

The H abstraction reactions by both the H and SiH_3 radicals are schematically shown in Fig 2.2. The radicals are shown approaching the surface along the axial direction with respect to the surface Si-H bond. The cluster goes through a saddle point characterized by partially formed bond between the surface H and the approaching

radical, resulting in a slightly stretched bond between the surface H and Si atoms. The bond lengths for the saddle points shown in the figure are derived from the multiparent configuration interaction calculations for the respective cluster geometries.

For reactions involving H atoms, barrier tunneling can reduce the effective barrier height. We can estimate this effect through the Wigner tunneling approximation[26] which states the probability, *P(E)* of a particle with energy *E*, tunneling through a parabolic barrier profile (peak height $=V_0$) is related to the imaginary frequency at the TS, ω as:

$$P(E) = \left(1 + \exp\frac{2\pi(V_0 - E)}{\hbar\omega}\right)^{-1} \qquad (4)$$

To determine the imaginary frequency ω, the cluster near the transition state may be viewed as a system of two masses: m_1 (corresponding to the surface H) attached to the surface through a spring with force constant k_1, and m_2 (corresponding to the SiH_3 radical) attached to m_1 through a spring with force constant k_2(shown in Fig 2.1). The frequency is then given by equation (5)

$$\omega = \sqrt{\frac{k_1}{m_1} + k_2\left(\frac{1}{m_1} + \frac{1}{m_2}\right)} \qquad (5)$$

The constants k_1 and k_2 are calculated from the curvature of the total potential energy along the minimum energy path (MEP) near the transition state. For a harmonic oscillator, a quadratic equation (eq (6)) for the minimum energy is fit as a function of the two bond distances near the transition state using the coordinates (r_1, r_2, E) that lie on the MEP.

$$E = \sum_i a_i . r_i^2 + b_i . r_i + c_i \,, \qquad i=1,2 \tag{6}$$

$$k_i = \left| \frac{\partial^2 E}{\partial r_i^2} \right| = 2 \cdot |a_i| \tag{7}$$

The force constants and the tunneling probabilities may then be directly evaluated.

In addition to tunneling, zero point corrections for the reactant clusters are also expected to reduce effective barrier heights. The zero point energy correction corresponding to the reactants will depend on the vibrational modes in the reactant cluster. A zero point energy correction of 1.7 kcal/mol was determined in previous work for H abstraction by hydrogen, using the same model cluster with MP-CI calculation methods [9]. A similar, or slightly larger, zero-point correction (~2 kcal/mol) for H abstraction by silyl may be expected because of the vibrational modes associated with the impinging silyl radical.

2.3 RESULTS AND DISCUSSION

2.3.1 Abstraction by Silyl Radicals

The potential energy surface for the abstraction of surface H by SiH_3 radicals generated using ab-initio CI (multi-parent) and DFT-GGA (DGauss) calculations are shown in Figs 2.3 and 2.4 respectively. The plots show the potential energy contours as a function of the length of the surface silicon-hydrogen bond ($Si^{(1)}$-H), and the distance between the surface hydrogen and impinging silyl radical (H-$Si^{(2)}$). The minimum energy path for the interaction is indicated by the dotted line. As the silyl radical approaches the

a-Si:H surface, the dangling bond on the radical attracts electrons, stretching the surface Si-H bond and increasing the potential energy of the cluster. The energy increases to a saddle point, which approximately defines the reaction transition state. The PES calculated here encompasses the effects of the most important geometry parameters, but the definition of the true transition state requires a more detailed vibrational analysis. Fig 2.3 shows the potential surface obtained from multiparent-CI. The energy contours near the saddle point are shown in the inset. The activation barrier is 14.2 kcal/mol and corresponds to a $Si^{(1)}$-H bond distance of 1.69Å and a Si(2)-H distance of 1.80Å. DFT calculations using the BLYP functionals show a smaller activation barrier of 4.93 kcal/mol (Fig 2.4). Using B3LYP, the barrier was 2.82 kcal/mol. The details of the saddle point geometries also varied with the calculation method. With DFT, the silyl radical approached the saddle point somewhat earlier (H-$Si^{(2)}$ distance of 1.95Å from BLYP and 1.97Å from B3LYP calculations) compared with CI (H-$Si^{(2)}$ distance of 1.80Å). Details of the calculation results are shown in Table 2.1. Both DFT calculations (BLYP and B3LYP) generally show a more negative heat of formation for the silane abstraction product compared to the CI values, as well as smaller activation barriers as compared to CI. The values obtained are reasonably close to each other and, as shown below, at each level of calculation, comparisons between H abstraction by H and abstraction by SiH_3 show a consistent trend, with abstraction by H being kinetically favored over abstraction by silyl radicals.

2.3.2 H Abstraction by H Radicals, and Comparison to Abstraction by Silyl

Calculated energetics data for H abstraction by H radicals is presented in Table 2.2. Similar to the results shown above for abstraction by silyl, the DFT results generally show a larger $-\Delta H_f$ and a smaller E_a than for CI. The calculated activation barriers are small (0 to 7.2kcal/mol) consistent with experimental values near zero[6].

A detailed comparison of minimum system energy as a function of $Si^{(1)}$-H distance for H abstraction by H and by SiH_3 is shown in Fig 2.5 and 2.6. Fig 2.5 compares the energy vs. distance for incident H and SiH_3 determined from multi-parent CI, and Fig 2.6 shows the same comparison from DFT (B3LYP) calculations. For the CI result in Fig 2.5, the SiH_3 energies were taken from the minimum energy path of the potential energy surface in Fig 2.3, and the H-related energies were taken from Reference [9]. For the HF-DFT(B3LYP) results in Fig.5(b), each value (for abstraction by H and by SiH_3) was obtained by performing a partial geometry optimization to determine minimum energy for each value of $Si^{(1)}$-H bond distance. As expected, surface H abstraction by H is more exothermic than abstraction by silyl. In all the calculations, the activation barrier for abstraction by H is smaller and narrower than the abstraction by SiH_3 radicals, indicating a larger probability for H abstraction by H vs. SiH_3 due to the larger tunneling probability for the surface H atom through the activation barriers. The tunneling probabilities for a surface H atom at a typical deposition temperature (T=523K) were calculated for MP-CI barriers for H abstraction by silyl and by hydrogen. Tunneling probability for H abstracted by SiH_3, given in Table 2.1, is found to be 10^3X smaller than that for H abstraction by hydrogen (Table 2.2). Therefore, when H and SiH_3 radicals impinge on a

H-terminated silicon surface, the H radicals are much more likely to abstract surface H (and hence create dangling bond sites) as compared to the SiH_3 radicals.

We anticipate that the energies calculated by these methods will be affected by the size of the cluster used for the calculations. In previous work, the effect of cluster size on H abstraction barrier energies was examined [9]. When the cluster size describing the Si surface was changed from Si_4H_{10} to $Si_{23}H_{31}$, the H abstraction barrier from the CI calculation decreased from 7.2 kcal/mol to 6.1 kcal/mol. We expect similar changes in for values presented here. Even with larger clusters, we expect that the barrier for H abstraction by SiH_3 will remain significantly larger than abstraction by H radicals.

The barriers calculated here may also be affected by the constraint imposed by fixing the positions of the secondary Si and H atoms in the cluster, and by the fact that basis sets did not include polarization functions. An additional set of HF-DFT (B3LYP) calculations was performed for H abstraction by silyl using the following: 1) full geometry optimization applied for each point on the reaction path; 2) a polarized and diffused basis set 6-31G++ (3d,2p) for the interacting Si and H atoms; and 3) a 6-31G basis set for the secondary (non-interacting) Si and H atoms. Results are included in Table 2.1. Fig 2.7 directly compares the constrained geometry and non-polar basis set results with those obtained using the unconstrained/polar basis set. The unconstrained/polar basis set results in an activation barrier of ~4.1Kcal/mol with $Si^{(1)}$-H ~1.7Å and $Si^{(2)}$-H ~2Å at the saddle point. This barrier is somewhat larger that the value of 2.82Kcal/mol obtained from the calculation using constrained/non-polar basis sets.

To demonstrate self-consistency in our analysis both DFT and CI calculation methods are used for each reaction. These methods each have particular strengths and

limitations. For example, CI is limited by the number of configurations that may be included within available computational time, whereas DFT is limited by the quality of the functionals. The functionals are determined from equilibrium geometries and may not be optimized to describe stretched bonds. This is expected to lead to an underestimation in transition state energies and barrier heights determined by DFT for the abstraction reactions considered in this study. Comparing calculation results with experiments further supports this expectation. The DFT calculations reported here for the surface H abstraction by H radicals (before the reactant zero-point correction) predict a zero activation barrier which is close to, but smaller than the ~2 kcal/mol reported experimentally [3,6,8]. As shown in Table 2.1, including additional configurations in CI improves the correlation energy estimation and reduces the calculated barrier energy. Therefore, the barrier height for H abstraction by silyl (before zero point and H tunneling corrections) is expected to be between 4.1 kcal/mol, calculated using the B3LYP unconstrained/polar basis sets, and 14.2 kcal/mol, determined from the multi-parent CI. We note that all DFT results reported here show reactions to be more exothermic and the kinetic barriers to abstraction to be smaller than those calculated using either single- or multi-parent CI, and all methods described here show the same trend when comparing abstraction of H by H and by SiH_3. Specifically, the barrier for H abstraction by H radicals is smaller than abstraction by silyl, and none of the methods show evidence for a stable three-center bond state for a physisorbed silyl radical.

2.3.3 Adsorption of Silyl on H-terminated Silicon, and Models for Silicon Deposition

Experiments have identified several reactions between silyl radicals and the hydrogen terminated silicon growth surface, including H abstraction and insertion into Si-Si bonds. However, there are limited experiments that clearly identify elementary surface reaction steps that lead to film growth. It is generally agreed that at typical deposition temperatures (150-350°C), precursors adsorb on the surface and diffuse in order to minimize surface energy. Recent experiments indicate that surface diffusion is an important step in film growth, and that diffusion is thermally activated with a barrier of ~5 kcal/mol (~0.2 eV)[27]. However, the details of the precursor absorption geometry and elementary steps in surface diffusion have not been directly identified by experiments. Common growth models[11,21,28] propose that silyl radicals physisorb on the surface through a 3-center ≡Si─H─Si≡ bond where the top ─H─Si≡ bond is between surface chemisorbed H and the a physisorbed silyl $(SiH_3)_p$. In order for this physisorption state to be reasonably stable, the binding energy must exceed kT (where k is the Boltzmann constant and T is the temperature) at the deposition temperature (i.e. ~1.2 kcal/mol at 325°C). Moreover, in common models, elementary diffusion steps include breaking and reforming the weak H-$(SiH_3)_p$ bonds until the physisorbed radical reaches a dangling bond where it chemisorbs. This scheme presumes that radical desorption proceeds at a slower rate than surface diffusion, so that the radical can interact with multiple surface sites before it chemisorbs. It is reasonable to expect, therefore, that if a collinear three-center ≡Si─H─$(SiH_3)_p$ bonding site is the active adsorption center, the potential energy surface would show a bonding state with binding energy close to or exceeding the value of 5 kcal/mol corresponding to the barrier for surface diffusion[27].

Any stable collinear three-centered Si-H-$(SiH_3)_p$ bond would correspond to a decrease in the system energy along the minimum energy path, close to the point where the $Si^{(1)}$-H and $Si^{(2)}$-H bonds lengths are similar. The calculated interaction energetics between silyl and the hydrogen terminated surface are shown in the potential energy surfaces in Fig 2.3 and 4. Neither of the potential energy surfaces in Fig 2.3 or 2.4 show evidence for a silyl radical adsorption state. This means that within the limits of the cluster geometry considered here, the collinear 3-center Si-H-Si surface structure is an energetic saddle point, but is not expected to be a stable bonding state on the silicon growth surface. This result indicates that common growth models that assume adsorption and diffusion by way of a collinear three-centered ≡Si─H─$(SiH_3)_p$ bond may need to be revisited in order to completely describe and understand low temperature silicon growth. Three-centered ≡Si─H─Si≡i bonds have been proposed and discussed in bulk silicon as possible defect states or as bond intermediates in photo-activated dangling-bond defect formation[29], but detailed analysis of bulk bonded H interstitial energetics has not been reported. Even so, we expect that surface bond energies to be substantially different from bulk bonds based on the additional degrees of freedom afforded to an adsorbed radical compared to lattice confined silicon atoms. Our calculations did not include a direct analysis of the effect of cluster size on physisorption state energies. Based on previous cluster size effects studied for H abstraction, we expect that larger clusters would tend to further reduce the barrier heights, but they would not modify the shape of the barriers significantly enough to indicate a stable (>5kcal/mol) physisorption state.

If three centered bonds are not stable, then what mechanisms could be active for precursor adsorption and diffusion? Another possible picture that has not previously

been discussed, for example, is that silyl radicals diffuse through Si-Si bond breaking and reforming where bond breaking is facilitated by H insertion into the (weaker) stretched Si-Si bond, and Si-Si bond formation is accompanied by molecular hydrogen formation and release. Recent experiments also support the need for a new picture for silicon growth. In models including the three-center physisorption bond, diffusion length is expected to decrease with increasing temperature because surface dangling bond density increases with temperature, and diffusion is expected to "stop" on dangling bond sites. In the Si-Si bond-breaking picture described above, we expect that adspecies diffusion length will increase with temperature, consistent with recent experimental observations[27]. Other configurations for physisorbed silyl radicals, and other processes for silyl incorporation, including direct insertion, could also be considered and must also be evaluated for a more complete understanding of the surface processes in low temperature activated silicon deposition processes.

2.4 CONCLUSIONS

Reaction energetics for H abstraction by H and by silyl (SiH_3) radicals were calculated using various *ab-initio* calculation methods. We find that calculated reaction enthalpies are more negative for DFT methods compared to CI, and the kinetic barriers to abstraction are smaller using DFT compared to CI. All methods show similar trends when comparing abstraction by H and by SiH_3; the barrier for H abstraction by H radicals (between ~0 and 7 kcal/mol) is smaller than for H abstraction by silyl (between ~4 and 14 kcal/mol), and the results are consistent with various experimental reports. These

calculations indicate that during typical low temperature silicon deposition processes, the rate of H abstraction by impinging hydrogen atoms dominates H abstraction by SiH_3. This suggests that hydrogen radicals play a critical role in creation of surface dangling bonds during low temperature silicon thin film deposition. These results also have implications for understanding other kinetic growth mechanisms. The potential energy surfaces calculated for silyl interaction with H-terminated silicon show no evidence for a stable three center ≡Si─H─Si≡ silyl physisorption state as is commonly proposed in silicon deposition models. Therefore, other growth models must be considered, including for example H-mediated Si-Si bond breaking and/or direct silyl insertion to explain observed kinetic processes in low temperature activated silicon-based film growth.

2.5 ACKNOWLEDGEMENTS

GNP acknowledges support from NSF CTS. HY acknowledges the support from US DOE. Density functional calculations were conducted on the Cray T90 available through an academic grant from the North Carolina Supercomputing Center.

2.6 REFERENCES

[1] R. Crandall and W. Luft, *Progress in Photovoltaics* **3,** 315-332 (1995).

[2] R. A. Street, *Hydrogenated amorphous silicon* (Cambridge University Press, New York, 1991).

[3] A. Dinger, C. Lutterloh, and J. Kuppers, *Chemical Physics Letters* **311,** 202-208 (1999).

[4] S. A. Buntin, *Journal of Chemical Physics* **105,** 2066-2075 (1996).

[5] W. Widdra, S. I. Yi, R. Maboudian, G. A. D. Briggs, and W. H. Weinberg, *Physical Review Letters* **74,** 2074-2077 (1995).

[6] D. D. Koleske, S. M. Gates, and B. Jackson, *Journal of Chemical Physics* **101,** 3301-3309 (1994).

[7] D. D. Koleske, S. M. Gates, and J. A. Schultz, *Journal of Chemical Physics* **99,** 5619-5622 (1993).

[8] K. Sinniah, M. G. Sherman, L. B. Lewis, W. H. Weinberg, J. T. Yates, and K. C. Janda, *Journal of Chemical Physics* **92,** 5700-5711 (1990).

[9] E. Srinivasan, H. Yang, and G. N. Parsons, *Journal of Chemical Physics* **105,** 5467 (1996).

[10] K. G. Nakamura, *Chemical Physics Letters* **285,** 21-24 (1998).

[11] J. Perrin, *Journal of Non-Crystalline Solids* **137,** 639-644 (1991).

[12] P. Kaenune, J. Perrin, J. Guillon, and J. Jolly, *Plasma Sources Science & Technology* **4,** 250-259 (1995).

[13] J. R. Abelson, *Applied Physics a-Materials Science & Processing* **56,** 493-512 (1993).

[14] G. Ganguly and A. Matsuda, *Optoelectronics-Devices and Technologies* **9,** 269-276 (1994).

[15] A. Matsuda, K. Nomoto, Y. Takeuchi, A. Suzuki, A. Yuuki, and J. Perrin, *Surface Science* **210,** 114 (1990).

[16] S. Ramalingam, D. Maroudas, E. S. Aydil, and S. P. Walch, *Surface Science* **418,** L8-L13 (1998).

[17] J. Perrin, M. Shiratani, P. Kae-Nune, H. Videlot, J. Jolly, and J. Guillon, *Journal of Vacuum Science & Technology a-Vacuum Surfaces and Films* **16,** 278-289 (1998).

[18] A. von Keudell and J. R. Abelson, *Physical Review B-Condensed Matter* **59,** 5791-5798 (1999).

[19] A. Matsuda and T. Goto, in *Materials Research Society Symposium Proceedings*, Vol. 164 (1990), pp. 3.

[20] J. L. Guizot, K. Nomoto, and A. Matsuda, *Surface Science* **244,** 22-38 (1991).

[21] J. Robertson and M. J. Powell, *Thin Solid Films* **337,** 32-36 (1999).

[22] Z. Jing and J. L. Whitten, *Journal of Chemical Physics* **98,** 7466 (1993).

[23] A. D. Becke, *Physical Review a* **38,** 3098-3100 (1988).

[24] C. T. Lee, W. T. Yang, and R. G. Parr, *Physical Review B-Condensed Matter* **37,** 785-789 (1988).

[25] G. W. T. M. J. Frisch, H. B. Schlegel, G. E. Scuseria,, J. R. C. M. A. Robb, V. G. Zakrzewski, J. A. Montgomery, Jr.,, J. C. B. R. E. Stratmann, S. Dapprich, J. M. Millam,, K. N. K. A. D. Daniels, M. C. Strain, O. Farkas, J. Tomasi,, M. C. V. Barone,

R. Cammi, B. Mennucci, C. Pomelli, C. Adamo,, J. O. S. Clifford, G. A. Petersson, P. Y. Ayala, Q. Cui,, D. K. M. K. Morokuma, A. D. Rabuck, K. Raghavachari,, J. C. J. B. Foresman, J. V. Ortiz, A. G. Baboul,, G. L. B. B. Stefanov, A. Liashenko, P. Piskorz, I. Komaromi,, R. L. M. R. Gomperts, D. J. Fox, T. Keith, M. A. Al-Laham,, A. N. C. Y. Peng, M. Challacombe, P. M. W. Gill,, W. C. B. Johnson, M. W. Wong, J. L. Andres, C. Gonzalez,, and E. S. R. M. Head-Gordon, and J. A. Pople,, (Gaussian, Inc., Pittsburgh PA, 1998).

[26] E. Wigner, *Journal of Chemical Physics* **5,** 720 (1937).

[27] K. R. Bray and G. N. Parsons, *submitted for publication* (2001).

[28] A. Matsuda, *Thin Solid Films* **337,** 1-6 (1999).

[29] H. Yokomichi and K. Morigaki, *Solid State Communications* **63,** 629-632 (1987).

Table 2.1 *Reaction*: $SiH_{3\ (g)}$+ H-Si≡ → -Si≡ $_{(d.b.)}$ + $SiH_{4\ (g)}$ H abstraction by SiH_3 radical

Calculat-ion Method	Basis Set/ Functional	Saddle point		ΔH_r kcal/ mol	E_a kcal/mol	ω x10^{13}rad/s	P(E) @250°C
		Si(1)-H (Å)	H-Si(2) (Å)				
HF-SCF	Dunning-Huzinaga.	1.69	1.85	-5.33	18.62	1.35	1.49x10^{-8}
SP-CI	Dunning-Huzinaga..	1.72	1.83	-4.42	15.08	1.19	5.16x10^{-7}
MP-CI	Dunning-Huzinaga..	1.69	1.80	-4.69	14.16	1.13	1.29x10^{-6}
DFT-GGA	TZVP/ BLYP	1.65	1.95	-8.18	4.93	1.04	0.017
HF-DFT	6-311G/ B3LYP	1.65	1.97	-6.26	2.82	0.73	0.1
HF-DFT	631G++(3d, 2p) / B3LYP	1.65	1.99	-7.22	4.09	0.58	0.029

HF-SCF : Hartree Fock self consistent field

SP-CI : single parent configuration interaction

MP-CI : multi parent configuration interaction

DFT-GGA : Density functional theory under the generalized gradient approximation(BLYP functionals)

HF-DFT : Hybrid Hartree-Fock and Density functional approach (B3LYP method)

P(E): Wigner tunneling probability for surface H atom energy corresponding to a surface temperature of 250ºC (kT=0.6 kcal/mol).

Table 2.2 *Reaction*: $H_{(g)}$+ H-Si≡ → -Si≡ $_{(d.b.)}$ + $H_{2\,(g)}$ H abstraction by H radical

Calculation Method	Basis Set/ Functionals	Saddle point		ΔH_r kcal/mol	E_a kcal/mol	ω x10^{13}rad/ s	P(E) @250° C
		Si(1)-H (Å)	H-Si(2) (Å)				
MP-CI[a]	Dunning-Huzinaga	1.69	1.06	-12.7	7.2	1.07	0.0014
UHF-SCF[b]	6-31G*	1.7	1.1	-13.6	13	-	-
DFT-GGA[b]	6-31G*/ BLYP	-	-	-26.3	0	-	-
HF-DFT	6-311G/ B3LYP	-	-	-24.4	0	-	-

[a] E. Srinivasan, H. Yang, and G. N. Parsons, *Journal of Chemical Physics* **105,** 5467 (1996).

[b] K. G. Nakamura, *Chemical Physics Letters* **285,** 21-24 (1998).

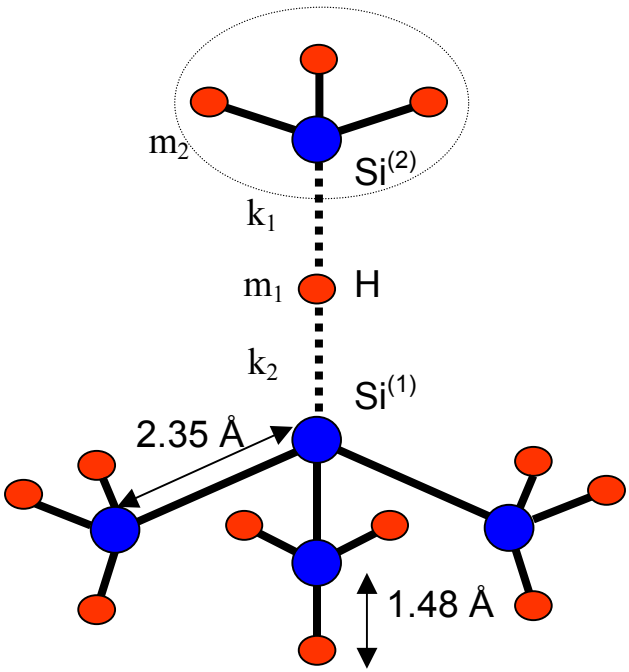

Fig 2.1 The silicon cluster used as a model for the monohydride terminated Si(111) surface. Various parameters used in the calculations are shown (see text for description)

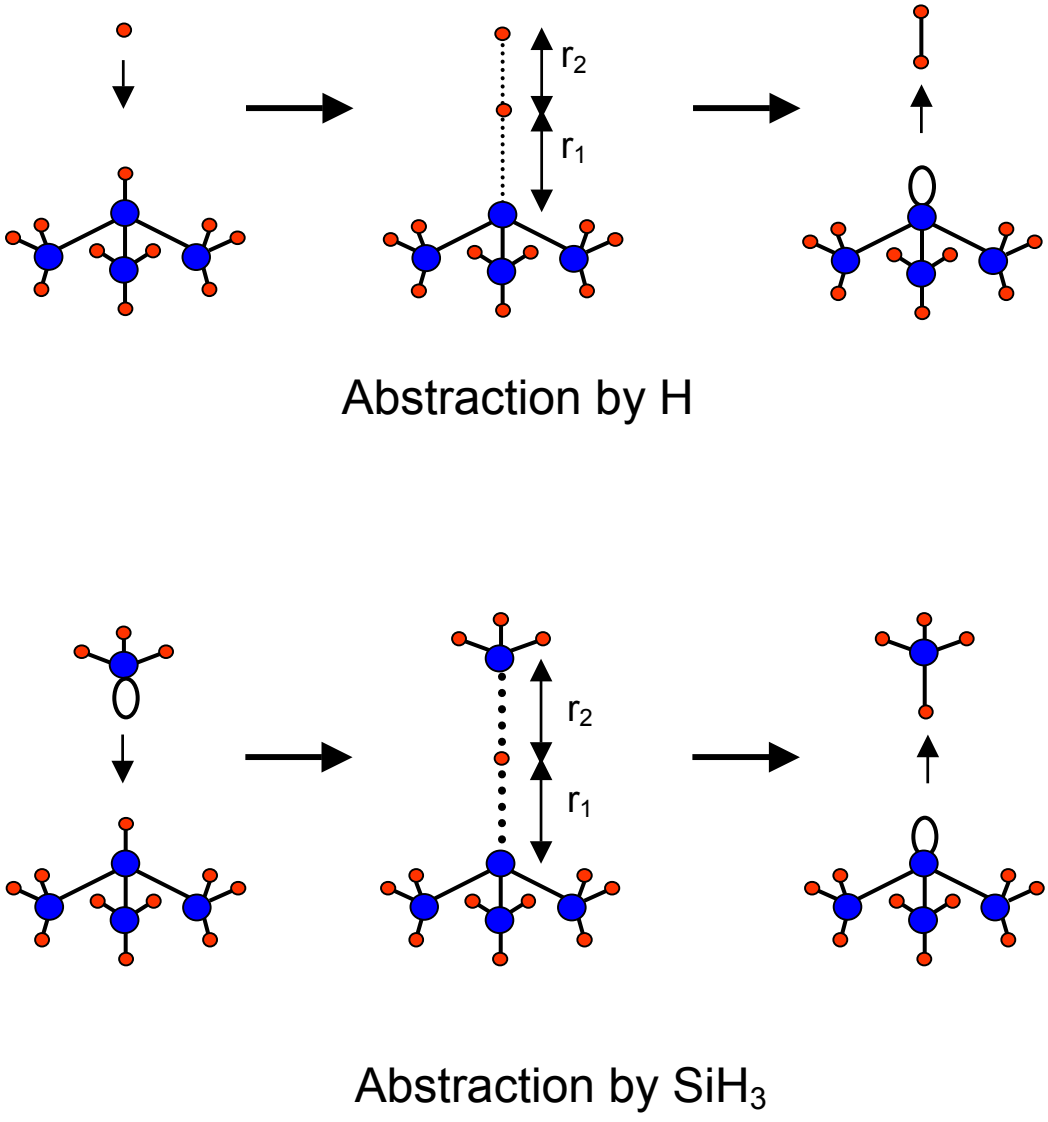

Fig 2.2 Schematic representations of the H abstraction reactions at the monohydride Si surface by both the H and SiH_3 radicals.

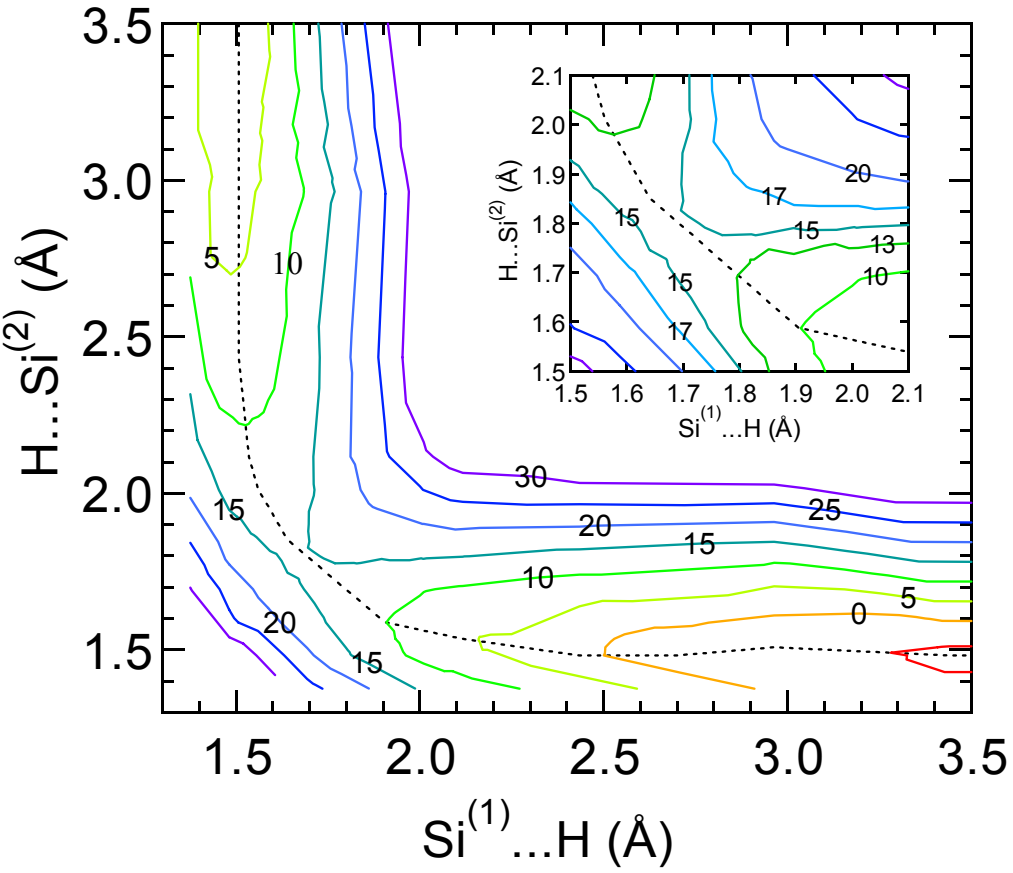

Fig 2.3 Potential energy surfaces for H abstraction by Silyl radicals plotted for the multiparent CI calculations (the parent states determined from single parent calculations) using the basis sets of Dunning and Huzinaga.

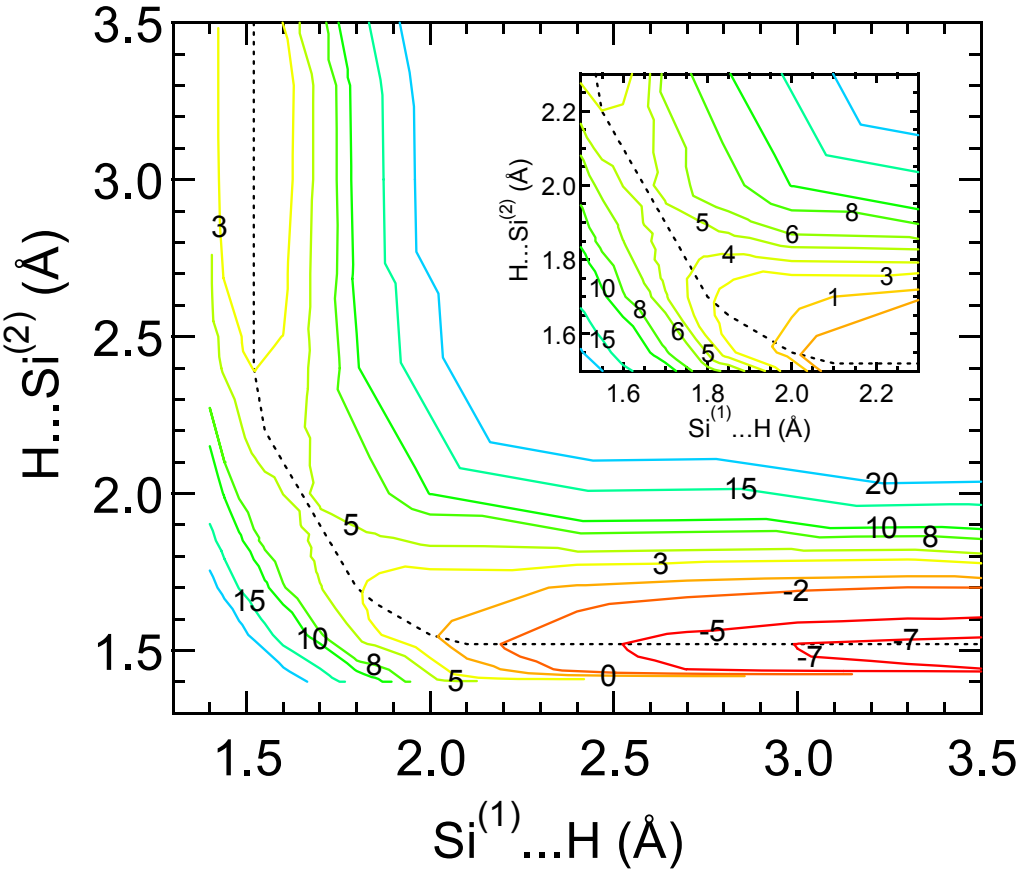

Fig 2.4 Potential energy surface for H abstraction by Silyl radicals generated using density functional calculations under the generalized gradient approximation (DFT-GGA) using the BLYP functionals and TZVP basis sets.

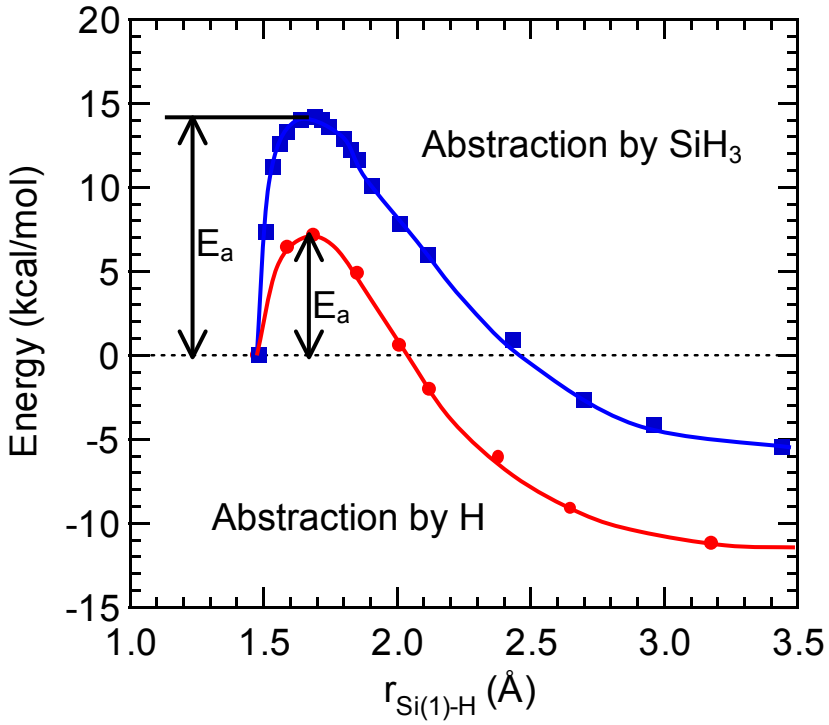

Fig 2.5 Comparison between the abstraction energetics of surface hydrogen by impinging H and SiH_3 radicals obtained from multi-parent CI calculations. The energy barrier for abstraction by H radicals is much smaller than that by silyl radicals.

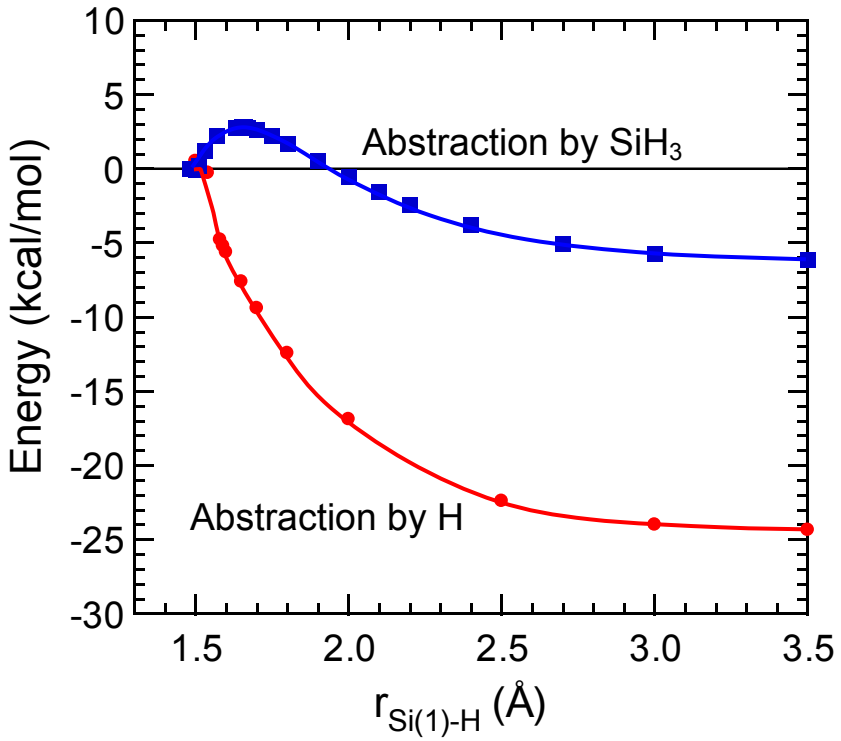

Fig 2.6 Comparison between the abstraction energetics of surface hydrogen by impinging H and SiH_3 radicals obtained from hybrid HF-DFT (B3LYP) calculations. The energy barrier for abstraction by H radicals is negligible while the silyl radicals have a higher barrier for abstraction.

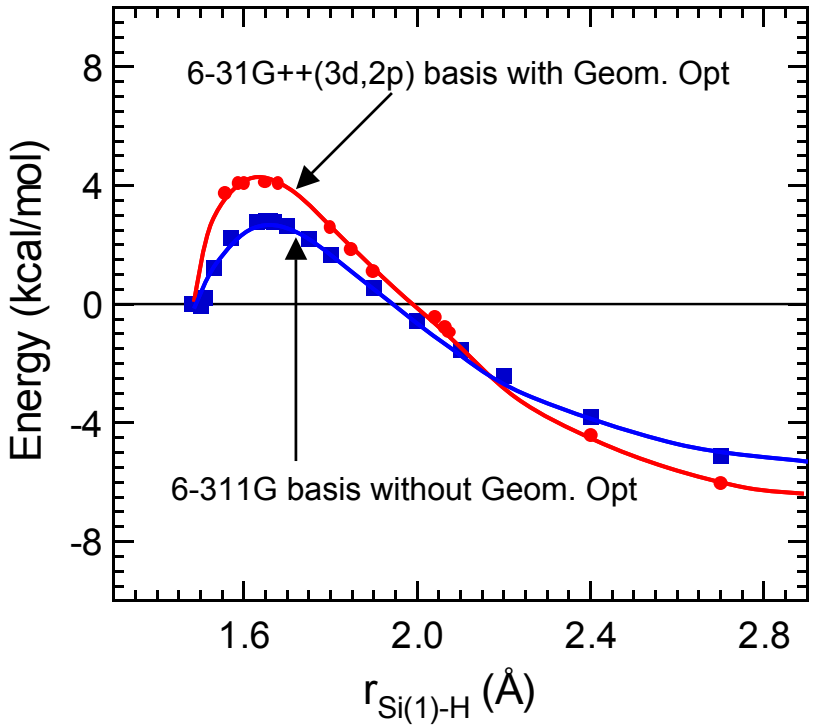

Fig 2.7 Comparison between the abstraction energetics of surface hydrogen by impinging SiH_3 radicals obtained from hybrid HF-DFT (B3LYP) calculations using unpolarized (6-311G) and polarized basis set (6-31G++(3d,2p) on the interacting atoms and 6-31G on the secondary atoms) with full geometry optimization at each point along the minimum energy path for the polarized basis set calculation. The reaction energetics are quite similar in both cases.

Chapter 3 is a reprint of a manuscript published in Journal of Vacuum Science and Technology B, vol 18 no.(3) pages 1764-1769 MAY-JUN 2000.Feb. 2000

CHAPTER 3

3 BOND STRAIN, CHEMICAL INDUCTION, AND OH INCORPORATION IN LOW TEMPERATURE (350º - 100ºC) PLASMA DEPOSITED SILICON DIOXIDE FILMS

By: Atul Gupta and Gregory N. Parsons

Department of Chemical Engineering, North Carolina State University, Raleigh, NC 27695-7905

ABSTRACT

New device concepts are being considered with very demanding requirements for low temperature processing. In this article, infrared transmission and ellipsometry is used to compare silicon oxide films formed by plasma chemical vapor deposition using SiH_4, N_2O and either He or H_2 dilution gas between 350º and 100ºC. The Si-O asymmetric stretching mode is affected by bond strain and chemical induction, and monitoring the Si-O peak position gives insight into the effect of process conditions on local bond structure. Hydrogen is expected to affect surface processes during growth, for instance, to enable

the removal of surface SiOH bonds through H-mediated abstraction, leading to improved bonding structure at low temperature. We find that exposing the surface to hydrogen atoms during growth helps eliminate isolated Si-OH bonds, leading to Si-Si bond formation. However, an increase in associated SiOH bonding groups, stabilized by hydrogen bonding, is also observed. The density of associated SiOH groups is larger at low temperature where the rate of water desorption is reduced, suggesting that the associated OH is formed by physisorbed water produced during OH removal. Films deposited with hydrogen dilution show somewhat improved electrical performance at <200ºC, but further work is required to produce high quality films at very low temperatures.

3.1 INTRODUCTION

Low temperature processing of electronic thin films has been studied for many years to reduce the "thermal budget" in integrated circuit fabrication, but there is growing interest in novel device applications where low temperature requirements are even more demanding than those for IC's. For example, flexible transparent plastics are attractive substrates for flexible active matrix displays, but most materials cannot withstand temperatures much greater than 100º - 150ºC for extended periods. Also, other new device concepts, including plastic microfluidic structures, could utilize high quality deposited inorganic thin films if they were available. Silicon dioxide is important for gate insulators and as a gas barrier layer, so a low temperature process for good quality SiO_2 would be attractive for new device concepts.

Various studies of silicon dioxide deposition processes, including experiments with organo-silane and silane source gases, show consistent results at low temperature [1-7]. Generally, films deposited at <150ºC contain significant amounts of OH bonding groups, and the Si-OH concentration increases over time due to absorption of water vapor from the ambient. Silicon-organics are known to undergo precursor-mediated adsorption, where they reversibly physisorb at low temperature, and dissociatively chemisorb at higher temperatures (typically >100ºC)[5-7]. Also, precursor oxidation results in hydroxyl (Si-OH) surface termination and physisorbed water at low temperatures. Significant understanding of silane based deposition is derived from infrared analysis of deposited materials [8,9] and mass spectroscopy and optical emission analysis of the gas-phase[1,2,4]. Production of excess oxidizing radicals, while minimizing homogeneous

reactions that form gas-phase silanol groups ($SiH_x(OH)_y$), are critical for optimum materials. In-situ IR analysis of SiH_4-based oxide deposition confirms that under conditions of excess oxidizing radicals, the surface is hydroxyl terminated due to rapid insertion of oxygen radicals into Si-H units in adsorbed silane fragments[10].

Electrical conduction in good quality SiO_2 is limited by Fowler-Nordheim injection at high field. A transition from Fowler-Nordheim to trap-mediated Poole-Frenkel conduction is observed when Si-OH density is increased, suggesting a link between OH groups and charge traps[11,12]. Average bond angle and bond strain are affected by thermal history and can also influence defect structure[8]. Silanol concentrations below the infrared detection limit have been achieved at process temperatures <150ºC by optimizing desorption kinetics (i.e. slowing the deposition rate), and by ion bombardment[10,13], but the effects of these processes on bond structure and electrical performance has not been reported.

We have re-visited low temperature plasma deposition of silicon dioxide to explore the possibility that exposing the surface to hydrogen atoms during growth may help achieve optimum bond structure and limit OH density. Hydrogen atom exposure during low temperature deposition of hydrogenated amorphous silicon can be used to control hydrogen incorporation through hydrogen-mediated abstraction reactions[14,15], and in this article, we investigate the possibility that hydrogen dilution may allow for control of SiOH density in low temperature oxide films and improve the electronic properties of films deposited at low temperatures.

3.2 EXPERIMENTAL PROCEDURE

Silicon dioxide films were deposited on 4" 1-2 ohm-cm n-type (100) c-Si wafers in a capacitively coupled parallel plate direct RF plasma enhanced chemical vapor deposition reactor. The large area of the electrodes (12"x13") allows for uniform film deposition over the substrate area. Deposition source gases were mixtures of $SiH_4/N_2O/He$ or $SiH_4/N_2O/H_2$, and the deposition pressure was fixed at 1.0 Torr. The silane and N_2O flow-rates were fixed at 3 and 375 sccm (standard cubic centimeters per minute) respectively. Generally, these conditions result in high quality materials (as determined from electrical analysis) when deposition temperature is 350°C. Variable parameters studied included substrate temperature (from 350°C and 25°C), RF power (30-150 W), and He or H_2 gas fraction. The total flow-rate was kept constant at 1900 sccm, to maintain a constant gas residence time in the reactor. Techniques for material analysis include infrared transmission spectroscopy to analyze Si-O and SiOH bond vibrations, ellipsometry (at 632.8nm) to measure refractive index, profilometry to measure film thickness, and current vs. voltage to measure dc charge leakage and trapping in capacitor structures. Fourier transform infrared transmission spectra were obtained using a Nicolet-Magna750 Spectrometer with a resolution of 4 cm^{-1} averaged over 64 scans. IR substrates were high resistivity(25-50 Ωcm) double-side polished silicon. IR transmission was measured immediately after deposition and after various exposure times to lab air to characterize the material stability with respect to ambient moisture. All spectra reported here were acquired within 30 minutes of removing the film from the deposition reactor. Before deposition, the wafers were cleaned using a standard Baker clean followed by a 10s (10:1) HF dip to strip the native oxide.

For the IV analysis, substrates were moderately-doped silicon, and aluminum dots (~2000Å thick) were evaporated onto the oxide film through a shadow-mask to form metal-oxide-semiconductor capacitors. Dynamic I-V characteristics were made with a programmable Keithley 4145 with a ramp rate of 1 V/s. Most low temperature dielectrics can have significant densities of charge trap states, and careful IV analysis is required for repeatable characterization. Therefore, the IV measurement sequence was as follows. For each wafer analyzed, a test capacitor was ramped to breakdown to determine the approximate breakdown voltage. A new capacitor was chosen, and the first IV trace was collected as the voltage was ramped from zero to close to the breakdown field. On the same capacitor, the voltage was ramped again from zero, and a second IV trace was collected up to the breakdown voltage. When a significant density of charge traps are present, the second trace will result in a significantly reduced measured current. The charges trapped during the first trace result in a built-in field that opposes the applied field, reducing the net field across the insulator, therefore leading to a lower measured current. The difference in the two traces can therefore be used characterize the density of charge traps in the material. If the leakage is sufficiently small, charge trap information can of course be directly obtained from flatband shift and hysteresis in capacitance voltage measurements.

3.3 RESULTS

Infrared transmission and ellipsometry data has been used to compare silicon oxide films deposited using SiH_4, N_2O and either He or H_2 dilution gas. These results

give some insight into the role that hydrogen plays in modifying the properties of the deposited films. Films deposited at high temperatures with He dilution show good electrical performance with bonding properties approaching that of thermally grown oxides. The Si-O asymmetric stretching peak is in the range 1055 – 1060 cm^{-1}, depending on rf power. The peak position is lower than the ~1078cm^{-1} observed in thermal oxides because of increased network bond strain in the plasma deposited films. As temperature is reduced, the Si-OH concentration increases, and the SiO(s) peak narrows and shifts to higher wavenumber. As discussed below, this trend in the SiO(s) mode results because the more highly strained Si-O-Si bonds are attacked by hydrogen or OH present in the gas phase. The same trend is observed over time when the films deposited at low temperature are exposed to ambient moisture. No evidence for H-O-H related absorption near 1650cm^{-1} was observed in any film studied.

Fig 3.1 shows the infrared transmission spectra in the Si-O stretching regime as a function of deposition temperature for films deposited using He dilution at low rf power (30 W). As the temperature is reduced from 350°C to 25°C, the position of the Si-O-Si asymmetric stretch peak shifts from 1055cm^{-1} to ~1060cm^{-1}, and the corresponding full width at half decreases from 95 to 85cm^{-1}. This is consistent with a decrease in the number of strained bonds on the lower wavenumber side of the Si-O-Si asymmetric stretch peak, which correlates with an increase in Si-OH bond units (Fig 3.2). The Si-OH stretching region in Fig 3.2 shows two distinct features: an asymmetric mode at 3650cm^{-1} and a symmetric mode near 3450cm^{-1}. The modes at higher frequency is typically assigned to more "isolated" or "partially associated" Si-OH bonds, and the peak at lower frequency is due to "strongly associated" hydroxide bonds, where the energy is reduced

by hydrogen bonding. The increased OH density also correlates with a less densely packed network, and the refractive index decreases at lower temperature, as shown in Fig 3.3. When the low temperature films are exposed to ambient moisture, the change in film structure observed by infrared is qualitatively similar to the effect of reducing temperature: an increase in SiOH is observed, with a corresponding shift in the Si-O stretch peak to higher frequency and a decrease in width.

As discussed above, exposing the deposition surface to hydrogen atoms may be helpful in controlling SiOH incorporation at low temperature. Initial electrical results of silicon oxide films deposited with H_2 and He dilution are shown in Fig 3.4. A decrease in leakage current is observed for films deposited with H_2, but the film quality is still not sufficient, for instance, for TFT gate applications. Further improvements will require understanding the effect of process modifications on material properties, and analysis of infrared absorption spectra can give quantitative insight, as shown below, into the effect of temperature and gas dilution on film structure and composition.

The IR spectra of films deposited using three different diluent compositions (pure He, He/H_2 =1 and pure H_2) at 350°C are shown in Figs 3.5 and 3.6. Fig 3.5 shows the Si-O asymmetric stretch peak shifts to lower wavenumbers (from $1055cm^{-1}$ to $1039cm^{-1}$) as the hydrogen fraction in the diluent is increased. There is a corresponding increase in the refractive index from 1.46 to 1.48 indicating an increase in silicon-silicon bonds (i.e. decrease in oxygen content). The shift of the Si-O-Si asymmetric stretch towards lower wavenumbers is consistent with the inductive effect of Si-Si bonds in the oxide network[9].

Replacing the helium dilution with hydrogen at high temperature results in an interesting change in the Si-OH modes in these films (Fig 3.6). The feature at 3650cm^{-1} (due to "isolated" Si-OH groups) diminishes, and a feature near 3380cm^{-1} (due to "associated" Si-OH groups) increases. In films deposited with pure He, the high energy feature dominates, but with H_2 dilution, the feature at 3380cm^{-1} is most pronounced. It is interesting to note that in films deposited with helium dilution, either as-deposited or after exposure to the ambient, the peak due to "associated" SiOH is observed at higher energies (typically at ~3450cm^{-1}) than observed with the hydrogen dilution process. The shift of the associated SiOH mode to lower energies in films deposited with hydrogen suggests clustering of the OH groups, promoting more hydrogen bonding effects.

The effect of hydrogen dilution on the bonding structure in films deposited at low temperature (100ºC) is shown in the IR spectra in Figs 3.7 and 3.8. There is no appreciable shift in the peak frequency of this Si-O asymmetric stretch with diluent composition (Fig 3.7) but the films do show significant changes in the Si-OH related vibration modes as shown in Fig 3.8. Similar to results at higher temperature, a distinct increase in "associated" Si-OH stretch modes is observed with increasing H_2 fraction. One may expect the higher degree of association to be linked to a higher OH concentration, but generally, for films deposited over a wide temperature range, the total integrated absorbance in the O-H bond stretching region is smaller in the hydrogen diluted films (as shown in Fig 3.9). Taking into account the difference in absorption coefficients expected for associated and isolated SiO-H [16], the change in integrated absorbance corresponds to a reduction in total SiOH concentration upon hydrogen dilution.

A series of runs were done at different temperatures (110-350°C) using pure hydrogen as the diluent to study the evolution of structural changes in the films. IR results are shown in Figs 3.10 and 3.11. Using hydrogen dilution, the effect of temperature is qualitatively similar to films deposited using helium: the Si-O peak shifts to higher frequency at lower temperature due to removal of strained Si-O-Si bonds and OH incorporation. However, the extent of the shift is more pronounced with H_2 dilution (shown schematically in Fig 3.12), so at ~100ºC, He and H_2 dilution both result in peaks near 1060cm^{-1}.

3.4 DISCUSSION

The results presented above show distinct differences in composition and structure between SiO_2 films deposited with helium and hydrogen dilution. In the helium dilution process, as temperature is reduced, the Si-O stretch mode peak position is observed to first shift to slightly lower wavenumber, then shift to higher wavenumber. The shift to higher wavenumber is accompanied by a decrease in the bandwidth. The position of the Si-O stretch peak is a good indicator of the average bridging angle in the SiO_2 network. The vibration frequency depends upon the inter-atomic distances and the change in potential energy of the atoms as a function of the respective atomic positions. A change in the bond angle will result in different potential energy due to different inter-atomic distances and hence should result in a change in the position of the vibration peak. A fully relaxed SiO_2 film shows a peak Si-O stretch frequency of ~1078cm^{-1}, and a deviation from this value in a stoichiometric SiO_2 film results from variation from the

ideal bridging Si-O-Si angle (i.e. network strain). The variation in Si-O stretch peak position results then from two competing effects: 1) increase in the network strain due to reduced thermal energy at lower temperatures, leading to a decrease in the Si-O peak position; and 2) disruption of the network due to Si-OH incorporation at temperatures below 200°C leading to the increase in the Si-O stretch peak position. As the deposition temperature is reduced from 350°C to about 200°C, the thermal energy available is not sufficient for the film structure to relax, leading to bond strain and a shift to lower Si-O stretch frequency. However the network strain cannot be increased indefinitely and beyond a threshold value, it becomes thermodynamically favorable for the atoms to relax by the insertion of OH into some of the Si-O-Si bonds. OH will break the most highly strained (low frequency) Si-O-Si bonds, resulting in the peak shift to higher frequency. This is also consistent with the observed reduction in peak width with decreasing temperature; the selective removal of highly strained Si-O-Si units by OH incorporation also decreases the width of the bond angle distribution, resulting in a narrower mode width. This picture is consistent with the decrease in refractive index values below the stoichiometric value (1.46) at deposition temperatures lower than 200°C, where OH tends to reduce film density.

Upon dilution with hydrogen at high temperature, the Si-O stretch peak is observed to shift to lower frequency. This shift results predominantly from a chemical induction effect due to silicon back-bonded to a Si-O-Si unit. For an Si-O bond with an adjacent Si-Si bond, the lower electronegativity of silicon relative to oxygen leads to an increase in the charge in the Si-O bond, increasing the bond distance and decreasing the bond frequency. For hydrogen dilution, this shift is consistent with the observed increase

in refractive index at high temperature. As temperature is reduced the Si-O peak shifts to higher wavenumbers, consistent with a decrease in Si-Si bonds and an increase in SiOH or strained Si-O-Si bond structures. Again the strained bonds are preferentially removed, resulting in further Si-OH bond formation. The distinct difference observed in the O-H bond stretching regime indicates a higher degree of bond association (i.e. hydrogen bonding) in the OH units formed in the hydrogen dilution case. Hydrogen atoms generated in a plasma can react with a hydrogenated silicon surface to remove hydrogen from the surface, creating molecular hydrogen. This process (reaction 1 below) is exothermic, and proceeds readily on silicon surfaces at moderate temperatures. The removal of SiOH and production of Si-Si bonds upon hydrogen dilution are consistent with a surface process on silicon oxide similar to that observed on hydrogenated silicon surfaces: H atoms can promote removal of OH, possibly through OH or H atom abstraction reactions, producing volatile water or hydrogen as shown in reactions 2 and 3.

$$H + \equiv Si\text{–}H \rightarrow \equiv Si\text{–} + H_2 \quad (1)$$

$$H + \equiv Si\text{–}OH \rightarrow \equiv Si\text{–} + H_2O_{(v)} \quad (2)$$

$$H + \equiv Si\text{–}OH \rightarrow \equiv Si\text{–}O\text{–} + H_2 \quad (3)$$

If reaction (2) proceeded predominantly in the forward direction, promoting direct OH removal at the surface, then it would be relatively simple to control the concentration of OH incorporated in an oxide film at low temperature by controlling the flux of hydrogen atoms onto the surface. However, these are not the only expected reactions. Mixing H_2 and N_2O in a plasma will of course result in gas phase water formation, and this will inhibit reaction (2) above. Water produced in the gas phase, or produced in the surface

OH removal reaction, will also physisorb onto the surface and react further leading to clustered OH.

$$H_2O_{(v)} \rightarrow H_2O_{(p)} \quad (4)$$

$$H_2O_{(p)} + \equiv Si\text{-}O\text{-}Si\equiv \rightarrow 2(Si\text{-}OH)_{assoc.} \quad (5)$$

The associated SiOH units are stabilized by H bonding, making them less prone to attack by H atom exposure from the plasma.

A likely growth process, therefore, involves OH removal by hydrogen exposure (step 2), followed by water back-reaction (steps 4 and 5), where water produced during deposition (either in the gas phase or on the surface) directly adsorbs onto the surface forming highly stable associated OH groups. It is consistent with the observed increase in Si-Si bonds upon hydrogen dilution at high temperature, the increase in OH bonds with reduced temperature, the decrease in total OH upon hydrogen dilution over a wide temperature range, and the significant increase in associated OH groups observed upon hydrogen dilution. This insight will be useful to design further experiments to help reduce Si-OH incorporation at low temperature. For instance, reducing the rate of gas phase reactions, utilizing lower process pressure or time-modulated gas flow, will help promote reaction (2) in the forward direction. Also, approaches that disrupt associated OH groups on the surface, including for example higher energy ion bombardment, may help impede the clustering of OH near the surface and enable oxide films with more compact covalent structure to be formed at low temperature.

3.5 CONCLUSIONS

Silicon dioxide films deposited at very low processing temperature (<200ºC) using conventional plasma processing conditions and gas composition results in poor quality films with significant OH density, not suitable for device applications. Using a surface-reducing reactant in the gas phase, such as hydrogen, can lead to some improvement in film quality. Hydrogen dilution reduces the OH incorporation, but promotes the formation of stable highly-associated Si-OH groups, likely through reactions involving physisorbed water generated in the gas phase or on the surface. The effect of hydrogen dilution on oxide film structure and composition can be understood through analysis of the infrared transmission spectra, where the Si-O asymmetric stretching peak is strongly affected by combined effects of bond strain and chemical induction.

3.6 ACKNOWLEDGEMENTS

This work was funded by the NSF through an Early Career Development Award. Special thanks are also given to Gerry Lucovsky on the occasion of his 65th birthday. As a graduate student in his group, his support and encouragement helped me (GNP) tremendously, and I am fortunate that we continue now as research colleagues.

3.7 REFERENCES

[1] G. Lucovsky, P. D. Richard, D. V. Tsu, S. Y. Lin, and R. J. Markunas, Journal of Vacuum Science & Technology a-Vacuum Surfaces and Films **4,** 681-688 (1986).

[2] D. V. Tsu, G. Lucovsky, and B. N. Davidson, Physical Review B-Condensed Matter **40,** 1795-1805 (1989).

[3] J. A. Theil, D. V. Tsu, M. W. Watkins, S. S. Kim, and G. Lucovsky, Journal of Vacuum Science and Technology A **8,** 1374 (1990).

[4] D. L. Smith, A. S. Alimonda, and T.-C. Chuang, Materials Research Symposium Procedings **204,** 475 (1991).

[5] N. Selamoglu, J. A. Mucha, D. E. Ibbotson, and D. L. Flamm, Journal of Vacuum Science & Technology B **7,** 1345-1351 (1989).

[6] S. C. Deshmukh and E. S. Aydil, Journal of Vacuum Science & Technology a-Vacuum Surfaces and Films **13,** 2355-2367 (1995).

[7] L. L. Tedder, J. E. Crowell, and M. A. Logan, Journal of Vacuum Science & Technology a-Vacuum Surfaces and Films **9,** 1002-1006 (1991).

[8] G. Lucovsky and D. V. Tsu, Journal of Vacuum Science and Technology A **5,** 2231 (1987).

[9] P. G. Pai, S. S. Chao, Y. Takagi, and G. Lucovsky, Journal of Vacuum Science & Technology a-Vacuum Surfaces and Films **4,** 689-694 (1986).

[10] S. M. Han and E. S. Aydil, Journal of Vacuum Science and Technology A **14,** 2062 (1996).

[11] D. J. Dimaria, E. Cartier, and D. Arnold, Journal of Applied Physics **73,** 3367-3384 (1993).

[12] C. Charles, G. Giroultmatlakowski, R. W. Boswell, A. Goullet, G. Turban, and C. Cardinaud, Journal of Vacuum Science & Technology a-Vacuum Surfaces and Films **11,** 2954-2963 (1993).

[13] S. C. Deshmukh and E. S. Aydil, Applied Physics Letters **65,** 3185 (1994).

[14] G. N. Parsons, Thin Solid Films **(accepted)** (2000).

[15] C. S. Yang, L. L. Smith, C. B. Arthur, and G. N. Parsons, Journal of Vacuum Science and Technology B **18** (2000).

[16] A. C. Adams, Solid State Tech. **April,** 135 (1983).

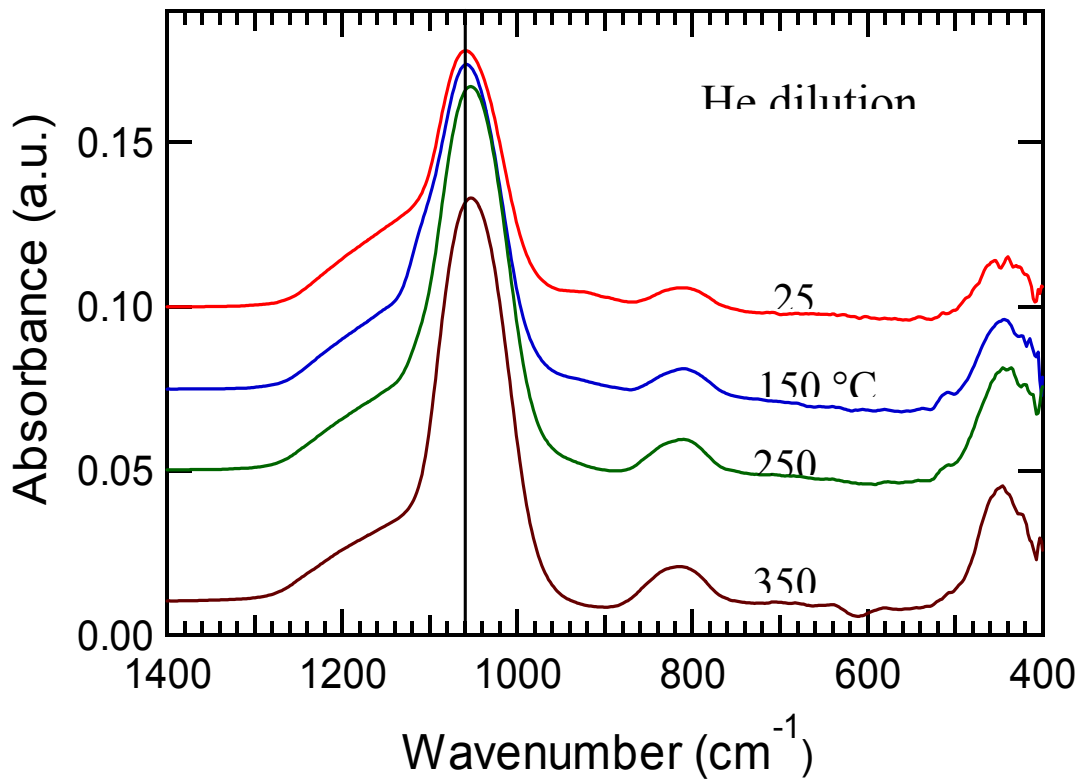

Fig 3.1 IR spectra showing the Si-O asymmetric stretch peak position as a function of the deposition temperature. Films deposited using pure He as the diluent. The Si-O peak shifts to higher wavenumbers as the deposition temperature is reduced below 250°C. Insert shows the change in the refractive index of the film as a function of the deposition temperature.

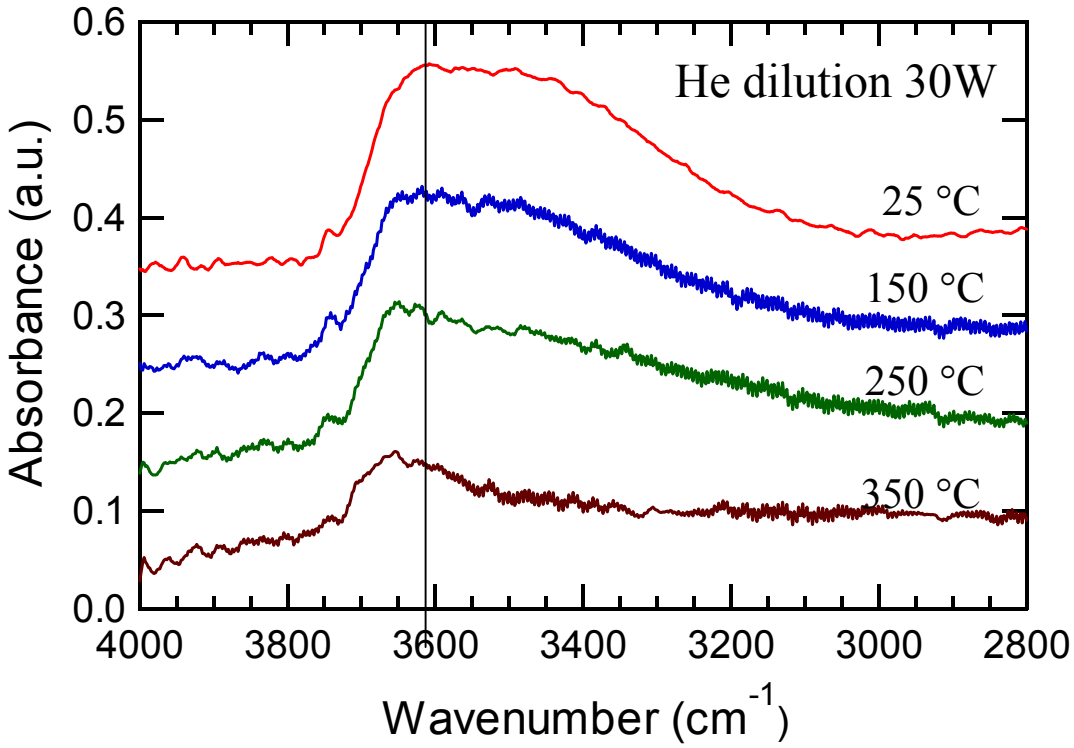

Fig 3.2 Si-OH vibration modes for He diluted films deposited at various temperatures. The Si-OH features grow as the temperature is reduced and at lower temperatures, "associated" Si-OH vibration modes (near 3380cm-1) are visible.

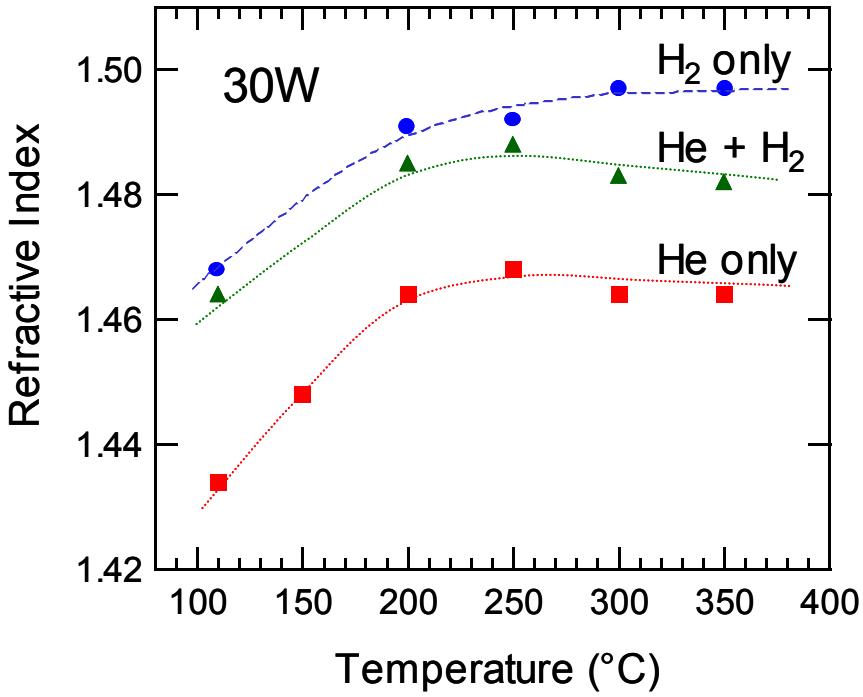

Fig 3.3 Refractive index of the films deposited using different diluent compositions as a function of the deposition temperature. Hydrogen dilution results in an increase in the refractive index at the same deposition temperature.

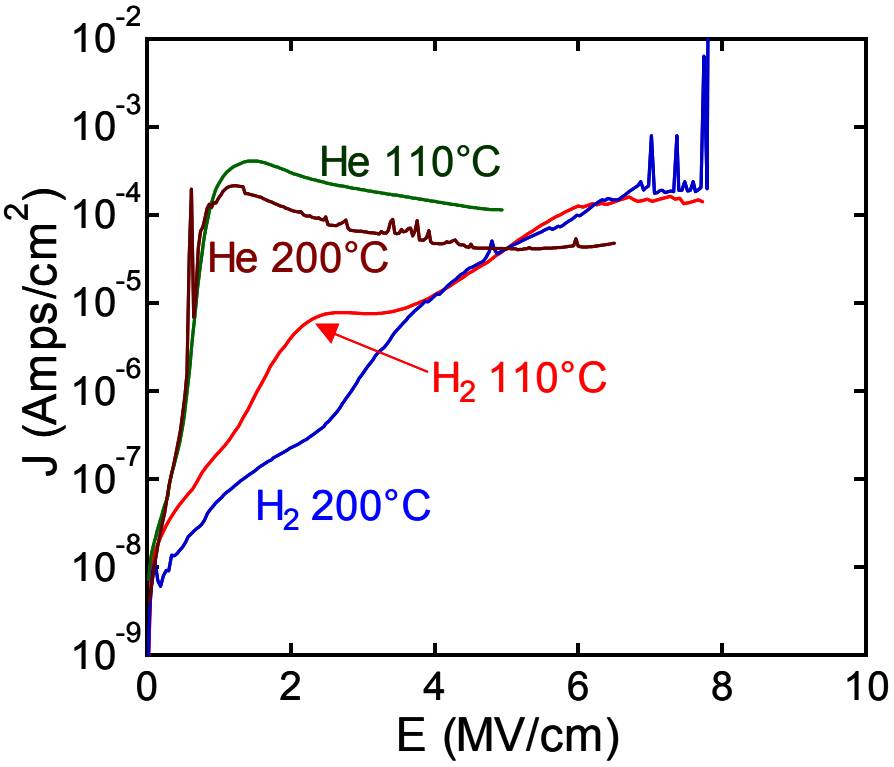

Fig 3.4 Comparison of the current voltage characteristics of the films with different diluents (He or H_2). H_2 dilution seems to reduce the leakage current at low fields but needs further improvement for device applications.

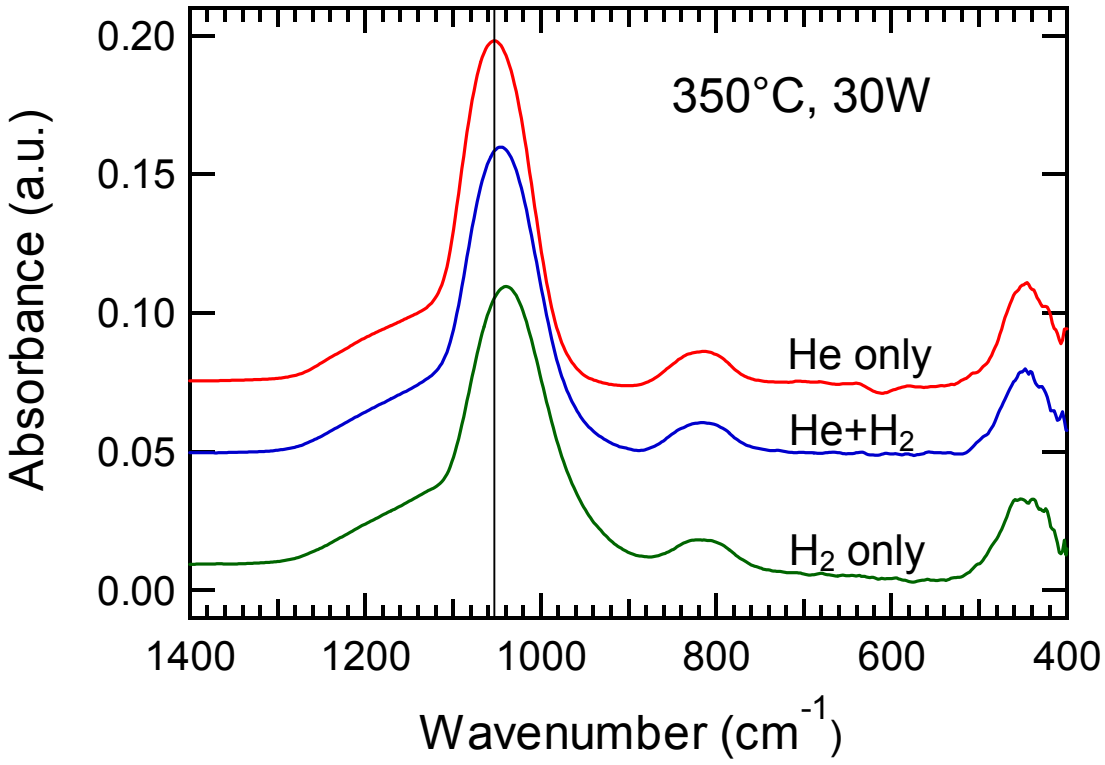

Fig 3.5 Si-O asymmetric stretch peak position as a function of the diluent composition for films deposited at 350°C. The Si-O peak shifts to lower wavenumbers as the H fraction in the diluent is increased.

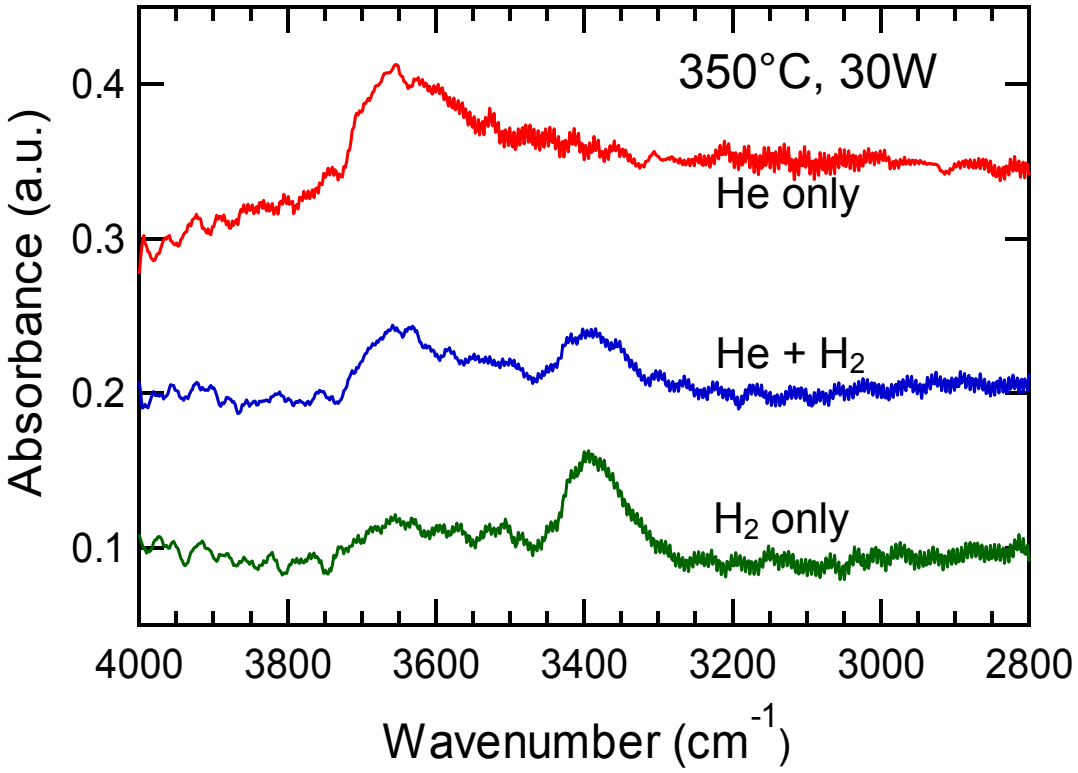

Fig 3.6 Si-OH vibration modes for films deposited at 350°C as a function of the diluent composition. H_2 dilution reduces the "isolated" Si-OH vibration band but increases the "associated" vibration modes.

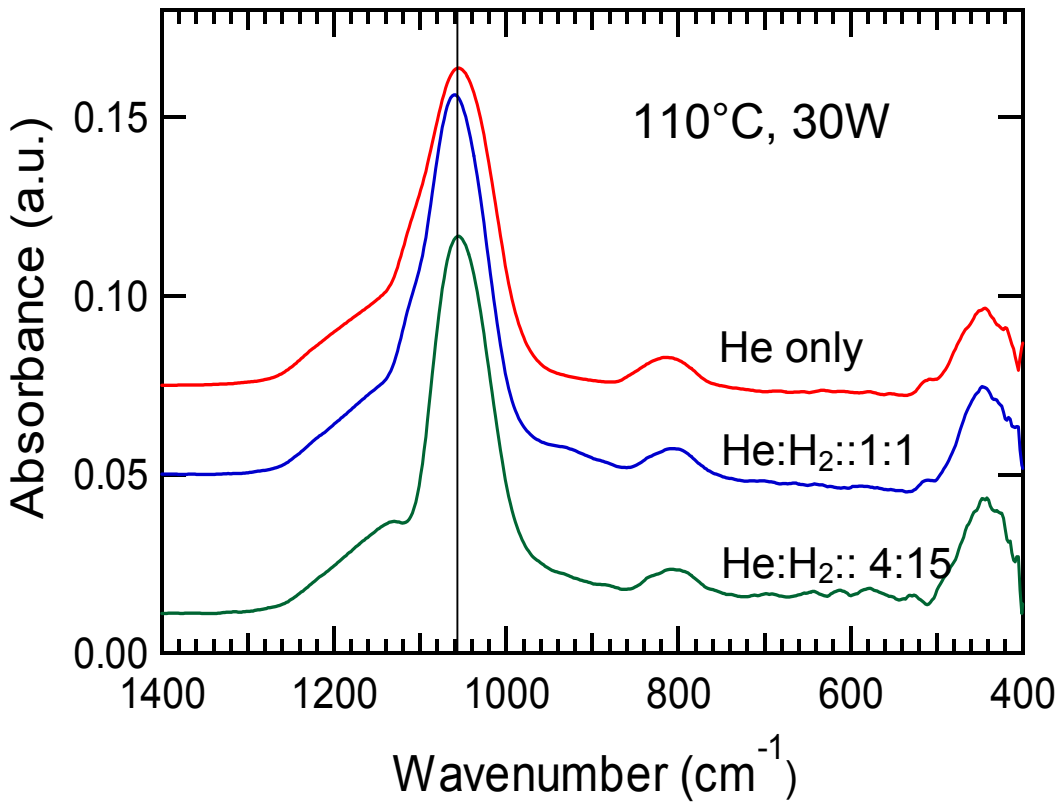

Fig 3.7 Si-O asymmetric stretch peak position as a function of the diluent composition for films deposited at 110°C. The Si-O peak does not shift appreciably with changes diluent composition

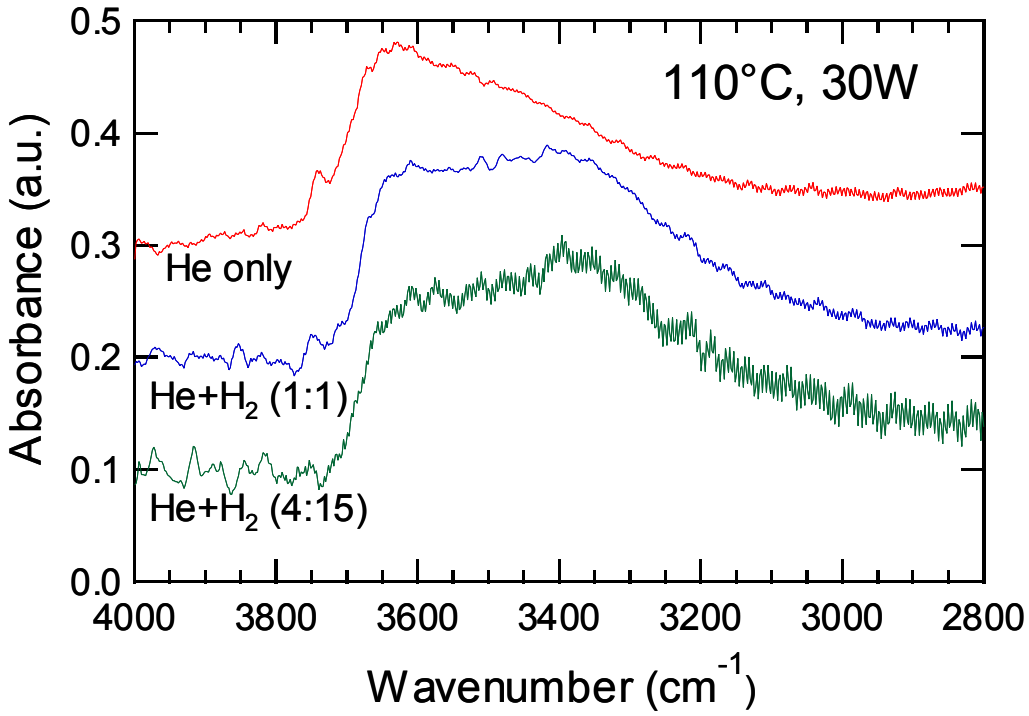

Fig 3.8 Si-OH vibration modes for films deposited at 110°C as a function of the diluent composition. H_2 dilution increases the "associated" vibration modes.

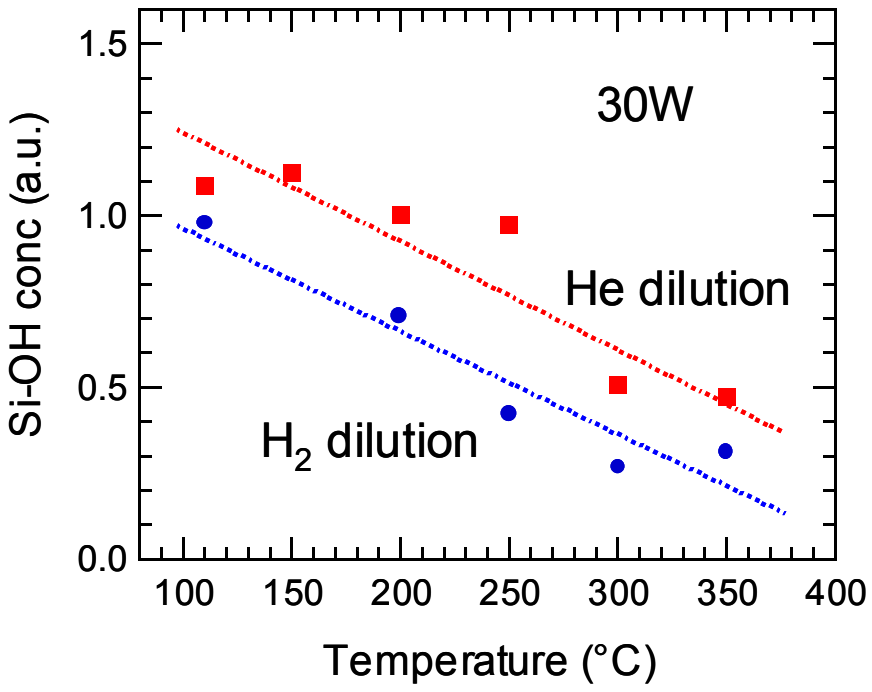

Fig 3.9 Integrated absorption for the SiOH groups (between 3200-3800cm^{-1}) as a measure of SiOH concentration in the silicon oxide films deposited using either He or H_2 dilution at 30W. H_2 dilution consistently results in a lower total concentration of OH groups under similar deposition conditions.

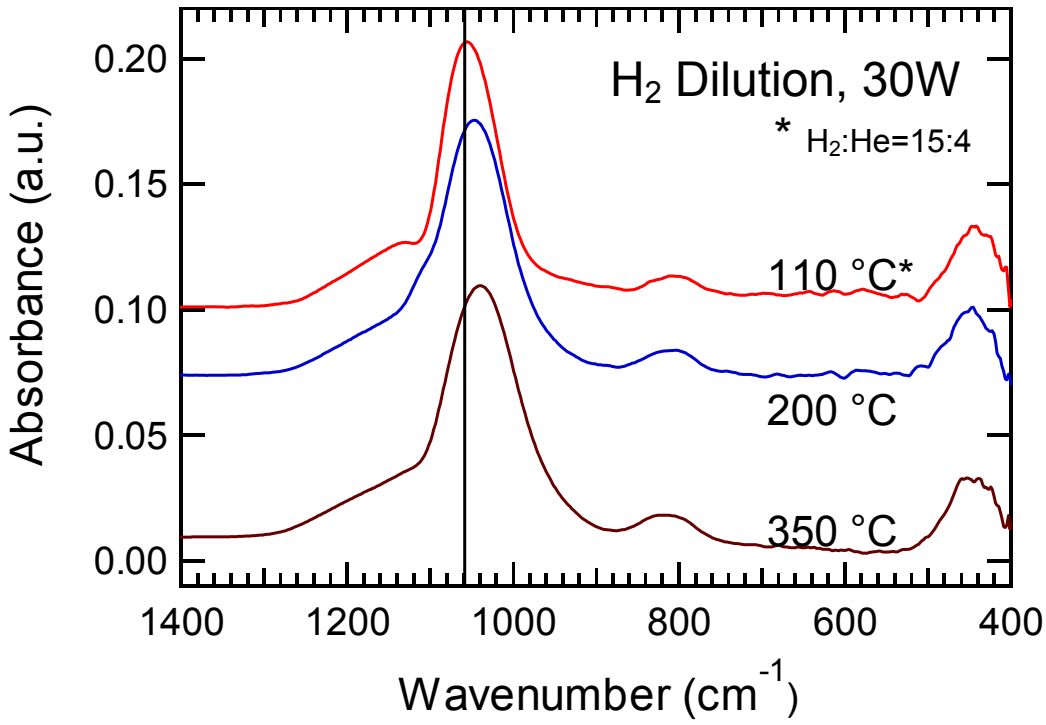

Fig 3.10 Si-O asymmetric stretch peak position as a function of the deposition temperature for films deposited using pure H_2 as the diluent. The Si-O peak shifts to lower wavenumbers as the deposition temperature is increased due to induction effect of the Si-Si bonds.

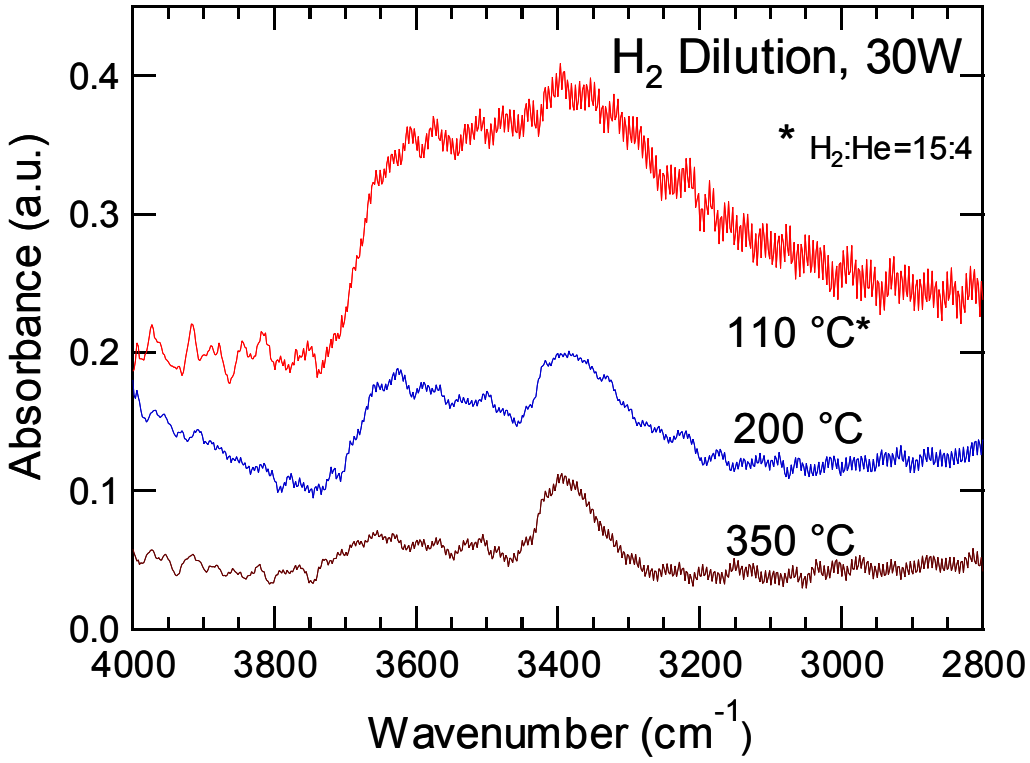

Fig 3.11 Si-OH vibration modes for H_2 diluted films deposited at various temperatures. The "isolated" Si-OH features grow as the temperature is reduced while the "associated" Si-OH vibration mode (near 3380cm-1) remains almost unchanged.

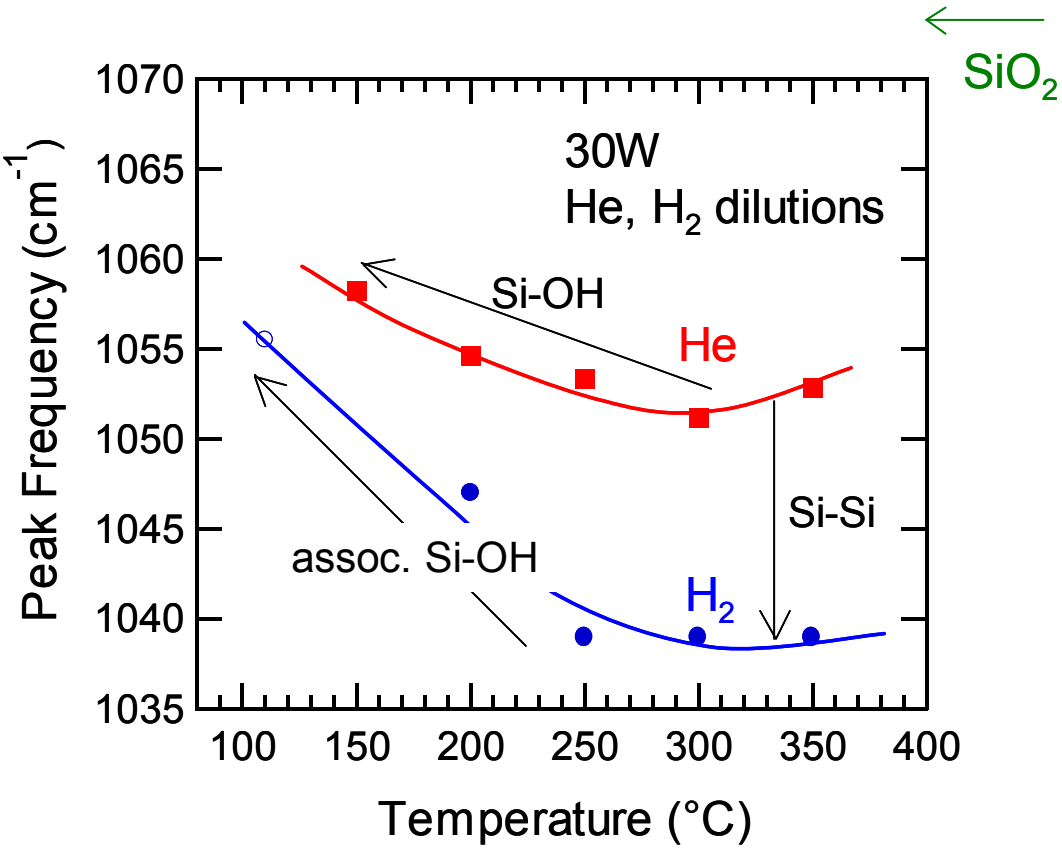

Fig 3.12 The peak position of Si-O-Si asymmetric stretch is plotted as a function of deposition temperature for films deposited (at 30W) using He and H_2 as diluents. H_2 dilution shifts the peak to lower wavenumbers. Reduction in temperature results in an increase in the peak frequency for both cases.

Chapter 4 is a preprint of a manuscript to be submitted for publication in Journal of Applied Physics

CHAPTER 4

4 A SURFACE HYDRIDE-DEPENDENT PRECURSOR DIFFUSION MODEL FOR LOW TEMPERATURE AMORPHOUS SILICON DEPOSITION

By: Atul Gupta and Gregory N. Parsons

Department of Chemical Engineering, North Carolina State University, Raleigh, NC 27695-7905

ABSTRACT

A quantitative kinetic model for low temperature hydrogenated amorphous silicon film deposition is presented. The model includes a newly developed valence balance approach used in combination with the site balance equations to describe Si-Si bond formation on the growth surface. The model describes effects of precursor physisorption and diffusion, as well as direct chemisorption and insertion into Si-Si bonds as a function of surface temperature and radical flux. Several macroscopic parameters, including precursor surface reaction probabilities, film growth rate, and surface precursor diffusion length are calculated, and values are compared with available experimental results. The model proposes that the rate of precursor surface diffusion depends on the specific surface Si-hydrogen bond distribution. The model results in an apparent activation

energy of ~0.2eV for precursor surface diffusion under typical growth rate conditions (~1Å/s), consistent with experimental results.

Keywords: Growth mechanism, Surface composition, Network formation, Morphology evolution, Diffusion length, Surface reactions

4.1 INTRODUCTION

A fundamental understanding of the growth processes that control film properties such as defect densities, topology evolution and crystallite fraction is critical for optimizing plasma activated processes such as plasma enhanced chemical vapor deposition (PECVD), reactive ion etching (RIE) and plasma surface treatment of different materials. Here we focus on the plasma deposition of hydrogenated amorphous silicon (a-Si:H) films deposited using silane/hydrogen mixtures, used for several important applications in photo-voltaic devices and thin film transistors (TFTs) [1]. The mechanisms controlling defect generation, crystallization and topology evolution during low temperature (<400°C) deposition of a-Si films and the effect of process variables as temperature and radical fluxes are discussed in terms of a new quantitative kinetic growth model that explains a broad range of experimental observations.

The primary step towards developing a growth model is to identify the important radicals/species generated in the plasma as well as the surface transport process that control film deposition. For device quality (i.e., low defect density) a-Si:H films deposited from Silane(SiH_4)/Hydrogen(H_2) gas mixtures, mass spectrometry measurements indicate that the dominant growth precursor radical is the silyl (SiH_3) radical [2,3]. Other Si containing radicals (SiH and SiH_2) are too reactive to have substantial lifetimes on the growth surface and lead to an undesirable anisotropic "columnar" growth where the radicals simply stick at contact with the surface leading to non-conformal coverage. Hence the deposition parameters described in this article are limited to the conditions where silyl radicals are the dominant growth precursors. Recent

experiments monitoring the surface topology evolution using Atomic Force Microscopy (AFM) of plasma deposited a-Si:H films indicate that surface diffusion of the physisorbed precursors dominates film growth [4,5]. Gallagher et al [6], Perrin et al [3], Ganguly and Matsuda et al [7-10] have proposed growth models based on dominant surface diffusion of physisorbed precursors. These models were later modified by Guizot et al [11] and Maeda et al [12] to further explain hydrogen dilution and network formation effects respectively. The surface diffusion growth models involve physisorption of the growth precursors, which may then diffuse around on the surface and get chemisorbed upon reaching a dangling bond site on the surface. The dangling bonds in turn are created via a two-step growth process wherein the physisorbed radicals first abstract a surface hydrogen atom the creating a dangling bond onto which other precursor radicals may chemisorb. While this picture is quite simplistic, there is much debate over dominant reaction mechanisms as well as the physisorption state of the radicals. The physisorption of the SiH_3 radical precursors on H-terminated Si sites is often proposed to proceed through a three-centered ≡Si–H–Si≡ linkage [13,14]. In this model, this three-center bond structure needs to be sufficiently stable for the physisorbed silyl radical to achieve reasonable surface coverage at temperatures near 200°C, but is also sufficiently weak to allow the silyl radical to diffuse with a relatively small activation barrier (~0.2 eV) on the surface. However, recent *ab-initio* and molecular dynamics simulations indicate that the 3-center bond may not be the most "stable" configuration for the physisorbed precursor [15,16] and suggest that the precursor radical physisorbs on the surface in some other configuration that enables bonding and transport that follow the observed surface diffusion kinetics. In addition to the debate over a "stable" physisorbed

state, other reactions have been identified as dominant growth pathways. Specifically, von Keudell et al. have reported experimental evidence for direct insertion of the SiH_3 radicals into strained Si-Si bonds [17] using *in-situ* IR measurements of the interactions between SiH_3 radicals and a deuterated (a-Si:D) film. Also, Dewarrat and Robertson [18] have recently suggested an alternate mechanism for silyl adsorption, involving a displaced surface hydride and formation of a weakly adsorbed radical.

Recent developments in experimental surface analysis techniques have enabled direct measurements of the surface species present during the growth. Yamasaki et al [19-21] have been able to measure the surface dangling bond concentrations during a-Si:H deposition using time-resolved Electron Spin Resonance techniques, and report a monotonic increase in the surface dangling bond density with deposition temperature. Based on these observations, Robertson further argued that the film properties (especially Hydrogen elimination from the films) might be determined by bulk processes rather than surface reactions [22]. However van de Sanden et al [23] have pointed out that direct abstraction reactions by silyl and H radicals may provide other pathways for H_2 elimination and still have the deposition process dominated by surface reactions. It is therefore imperative to understand how the surface composition changes under various deposition conditions. Marra et al [24] and later Kessels et al [25] have measured the distribution of the mono-, di- and tri-hydride sites on the growing amorphous silicon surface using *in-situ* Attenuated Total Reflection Fourier Transform Infrared Spectroscopy(ATR-FTIR). These changes in the surface composition and site distribution with deposition temperature may be key to understanding the hydrogen elimination processes as well as the dominant growth mechanisms. Another limitation in

these models arises from the fact that these models use only site balances where the sites are distinguished based on the number of Si-H bonds or dangling bonds on a particular surface Si atom. With this type of surface site balance it is difficult to explain the formation of a network comprising of Si-Si bonds which is critically important in understanding the transformation from amorphous silicon to microcrystalline regime. Maeda et al have tried to address this issue [12] but their model is based on the bulk SiH and SiH_2 groups rather than the surface concentrations of these hydrides.

The kinetic model described in the following section is different from previous models in the following key aspects: i) it specifically includes silyl insertion; ii) it presents a new valence balance approach (in conjunction with the site balance equations) to explain the network formation on the surface and to quantify bond-specific reactions (e.g., the insertion of SiH_3 radicals in strained Si-Si bonds); iii) it includes silyl physisorption, but it is independent of the detailed structure of the adsorption state; and iv) it maintains consistency with surface diffusion models by presenting a diffusion activation barrier that depends on surface mono-, di- and tri-hydride composition. Using this model, we are able to understand various aspects (defect densities, network formation, surface distribution of hydrides and topology evolution) of the films grown under different deposition conditions.

The valence balance approach is presented in Section II-A. Section II-B presents key surface reactions involving radicals and active surface sites, and a reaction scheme is developed. The steady state site balance equations are presented in section II-C, and the predicted results obtained from the model are compared with known experiments in section II-D. In Section III important macroscopic growth parameters are extracted from

the microscopic reaction rates developed in Section II, and these parameters are compared with available experimental results.

4.2 KINETIC MODEL

4.2.1 Valence balance for the surface atoms

Most earlier kinetic models have assumed the growth surface of a-Si:H films to be comprised of different types of surface sites. These sites include dangling bonds, surface hydrides (mono-, di- and tri-hydrides), and physisorbed precursors. The drawback in such a description of the surface is that each of the surface sites is limited to having just one type of bond and consequently some surface reactions that involve precursor reactions with specific types of bonds cannot be adequately accounted for. Such reactions are referred as "bond-specific" reactions and could include for example, the insertion of radicals into Si-Si bonds present on the surface. Bond-specific reactions may be accounted for through a "valence" or bond balance equation for the surface atoms. In the valence balance, each surface Si atom makes one bond to a bulk silicon atom (Si atom in the layer below the surface layer) and three other bonds. These other bonds may be dangling bonds, Si-H bonds, Si-Si bonds, or any combination of the three.

The valence balance for the surface atoms is developed as follows: Assume that there are N tetrahedrally coordinated Si atoms on the surface (per unit area) prior to the start of the deposition with a total of $4N$ bonds. These $4N$ bonds are comprised of dangling bonds (N_0), Si-H bonds (N_h) and Si-Si bonds (N_{Si}). The Si-Si bonds may either be to bulk Si atoms (denoted as N_b) or could be between two surface Si atoms (denoted as

N_5). Each Si atom on the surface has to form at least one Si-Si bond with the bulk Si atoms to be considered a contiguous part of the film (hence $N_b = N$). This reduces the number of "available" valences by N. Also the surface Si-Si bonds (N_5) share two valences of the surface atoms and therefore need to be counted twice in the bond-balance. It is presumed here that the presence of a dangling bond on an atom dominates the energetics and kinetics of that surface atom, rendering the other surface bonds on that atom effectively unreactive. In other words, each dangling bond effectively counts as 3 surface valences. The bond balance is therefore written as:

$$3N = 3N_0 + N_h + 2N_5 \quad (1)$$

During the deposition, there are physisorbed radicals (surface coverage = N_4) on the surface that mask some of the surface atoms from the direct impact of the incident radicals. Each physisorbed silyl radical is assumed to mask exactly one Si atom on the surface (hence a loss of 4 available bonds) but it also makes a weak bond with the surface that may undergo other reactions (an addition of 1 available bond), therefore resulting in a net reduction of $3N_4$ bonds on the surface. This modifies the bond balance as:

$$3N = 3N_0 + N_h + 2N_5 + 3N_4 \quad (2)$$

which upon normalizing with respect to the total number of valences ($4N$) gives:

$$0.75\theta_0 + \theta_h + 2\theta_5 + 0.75\theta_4 = 0.75 \quad (3)$$

Here θ_0 and θ_4 are the fractional site coverages for the dangling bonds and physisorbed radicals respectively (defined as N_0/N and N_4/N respectively) while θ_h and θ_5

are the surface Si-H and Si-Si bond fractions (defined as $N_h/4N$ and $N_5/4N$ respectively). The total number of variables needed to be solved for in this valence balance approach is limited to the 4 different types of bonds on the surface (dangling bonds, Si-H bonds, Si-Si bonds and weak bonds between the physisorbed radicals and surface atoms). If the bond-balance approach is to be used independently, all reactions need to be described in terms of interactions between different bonds and not as interactions of precursors with different surface sites. This is possible only if all like bonds were equivalent in terms of chemical reactivity and all reactions were site independent, which implies that the location of the various bonds on the surface does not influence the probability of any of the surface reactions. However, some of the surface reactions are site-specific (i.e. they depend on the particular location of bonds on the surface sites). For example the recombination of hydrides (an important hydrogen elimination step) requires two Si-H bonds to be present on neighboring surface silicon atoms. Description of such surface reactions requires a "site balance" approach that accounts for different surface sites involved in the reactions. Hence in order to describe all types of surface interactions, whether they are bond-specific like the insertion of radicals into Si-Si bonds, or site-specific like the recombination of surface hydrides, a combination of both the "site balance" and "valence balance" approaches must be used.

4.2.2 Overall site balance equation for the surface atoms

The overall site balance equation is developed to describe the site-specific surface reactions. Various types of sites may be present on the growth surface, these include mono-, di- and tri-hydrides; dangling bond sites and physisorbed radicals. In addition to

dangling bonds and the physisorbed radical sites on the surface (fractional site densities = θ_0 and θ_4 respectively), the silicon atoms may be bonded as mono-, di- or tri- hydrides with fractional site densities of θ_1, θ_2 and θ_3 respectively. These fractional coverages are constrained so that the sum of all fractional site coverages equals unity.

$$\theta_0 + \theta_1 + \theta_2 + \theta_3 + \theta_4 = 1 \qquad (4)$$

Thus there are a total of 7 variables (θ_0, θ_h, θ_1, θ_2, θ_3, θ_4 and θ_5) in the two constraint equations (the valence and the site balance equations (3) and (4)) that need to be solved for simultaneously. The total hydrogen content on the surface (θ_h) is further related to the mono, di- and tri-hydride fractions designated as θ_1, θ_2, and θ_3 (=site density/total sites, *N*) respectively as follows:

$$0.25\theta_1 + 0.5\theta_2 + 0.75\theta_3 = \theta_h \qquad (5)$$

This equation states that if, for example, the surface is completely covered by tri-hydride units, i.e. $\theta_3 = 1$, then $\theta_h = 0.75$ corresponding to each of the Si atoms on the surface having three out of four available bonds as Si-H bonds (the remaining bond being a network Si-Si bond that binds the units to the underlying layer). In order to get the remaining site balances, the individual surface reactions leading to creation and consumption of the different surface sites need to be identified and quantified. The important surface reactions influencing the surface coverage of different sites during silicon deposition and the resulting site balance equations for the dangling bonds,

physisorbed radicals, mono- and di-hydride site balances are discussed in the next two subsections.

4.2.3 Surface Reactions

This model focuses on deposition conditions that are known to result in good quality a-Si:H films from activated deposition processes where the incident radical flux is comprised primarily of silyl radicals. Surface reactions may occur either directly between the incident radicals and surface bonds/sites (through Eley-Rideal, E-R, mechanisms) or between different species on the surface (Langmuir-Hinshelwood, L-H, mechanisms). The reactions involving the incoming radicals are quantified as the product of: 1) a reaction probability; 2) the radical flux ϕ_{Si}, defined as the flux of SiH_3 radicals per unit surface site density (ϕ_{Si} = radicals per surface site, per second); and 3) the fractional surface coverage of the species involved, θ_x (where x = 0, 1, 2, 3, 4 or 5). The L-H type surface reactions are expressed as a product of: 1) the reaction rate constant, υ_n (listed on Table 4.1); and 2) the product of the fractional surface coverage of the relevant species, θ_x and θ_y (where x, y = 0, 1, 2, 3, 4 or 5). The individual surface reaction rate constants, υ_n, are expressed in terms of an Arrhenius expression with a pre-exponential frequency factor A_n and an activation energy term, E_n. The values of A_n are chosen as $k_B T/h$ (as predicted by the transition state theory) for these reactions (where k_B is the Boltzmann constant, h is Planck's constant, and T is the substrate temperature in Kelvin). The values for E_n are taken from experimental and theoretical reports in the literature wherever available and are described and tabulated below along with the individual surface reactions.

Table 4.1 enlists the reactions considered and the rate expressions for those reactions, while Table 4.2 list the corresponding values of the rate parameters used in the model. First consider the possible reactions for the incident silyl radicals as shown in Reactions A-D (Table 4.1). Molecular dynamics simulations predict that the silyl radicals impinging on the surface with the dangling bond pointed towards the surface are more likely to participate in reactions than in other configurations [16]. In this configuration, the incident SiH_3 radicals may directly chemisorb on a dangling bond (Reaction A) forming a surface tri-hydride. This elementary addition reaction is barrier free and is assigned a probability of s_0=0.25 corresponding to the approximate fraction surface area of a dangling bond on a SiH_3 radical. The silyl radical is also presumed to physisorb easily on the surface, resulting in a net addition to the number of physisorbed radicals on the surface (Reaction B), but a detailed bond configuration is not presumed, nor is it critical for the model presented here. Again the probability for this reaction is primarily determined by the orientation of the dangling bond (db) on the incoming SiH_3 radical [13] and is designated as s_1, also set equal to 0.25. The impinging SiH_3 radicals may also land upon a physisorbed radical (Reaction C). The result is formation of Si_2H_6 molecule that goes back in the gas phase making another hydride site available on the surface. We assign a probability of $s_2 \sim 0.1$ (=0.25×0.4) to this reaction since the dangling bond on the incident radical has to point towards the physisorbed radical (~0.25) and can only attack the surface bond of the physisorbed radical from the sides, i.e. fractional area ~ 0.4. We assume that this reaction has no kinetic barrier. Because they are barrier free, the kinetic rates for reactions A-C are simply taken as the product of the silyl radical flux, ϕ_{Si}, the surface site density, and the corresponding reaction probability (s_0, s_1, or s_2).

Finally the silyl radical may directly abstract a surface H thus creating a dangling bond on the surface (Reaction D) through an Eley-Rideal mechanism. The barrier for this reaction is predicted to be ~ 0.4eV [15] and the reaction probability, υ_{a1} is again taken as 0.25. It is important to note that all Si-H bonds (present on either a mono-, di-, or tri-hydride site) are considered to have equivalent chemical reactivity towards hydrogen abstraction.

Once the silyl radical gets into a stable physisorbed on the surface, there are several possible surface reactions. For example, it can simply desorb from the surface - Reaction E, or it can abstract a hydrogen atom from a neighboring hydride and leave the surface as SiH_4 (Reaction F) thus creating a db on the surface. It could also hop onto another surface site, including hopping onto a dangling bond (Reaction G) or from one hydride to another (Reaction H). The activation barriers are chosen to be 0.7eV for desorption and 0.4eV for abstraction [15,22]. Desorption is expected to have a larger barrier than for abstraction or hopping in order for the precursor to have a sufficient residence time on the surface to diffuse and find the optimal chemisorption site. The barrier for H abstraction by silyl radicals from a mono-hydride is estimated from ab-initio studies to be ~ 0.4eV [15].

When a physisorbed radical hops onto a nearby dangling bond and chemisorbs (Reaction G), two hydrides are produced on the surface (one where the silyl was physisorbed and the other replacing the db site where it chemisorbs). The radical hopping from one hydride onto another surface hydride (Reaction H) represents a critical step in the surface diffusion model since hopping on the surface is the primary pathway responsible for the conformal deposition of a-Si:H films. The apparent barrier for the

hopping reaction has been measured using surface roughness evolution to be ~0.2eV [5] (note that similar values were also assumed in previous kinetic models by Perrin and Robertson [13,14]). We believe that the hopping rate of the physisorbed radicals depends on the type of surface hydrides and hence will be different for diffusion on mono-, di- and tri-hydride sites. Different diffusion barriers are expected on different surfaces because of several factors, including: a) steric hindrance effects of extra H atoms present on the higher hydrides; and b) different binding energies for the physisorbed radicals on different hydrides, including for example, stronger dipole interactions for silyl on di- or tri-hydride surfaces. Also, the higher hydrides present a more corrugated surface at the atomic level and hence may hinder the diffusion of the physisorbed radical. This hypothesis is in agreement with the theoretical ab-initio and molecular dynamics calculations that show no Si-H-Si bound state for the silyl radical on mono-hydride terminated surface [15,16] suggesting a lower barrier for surface diffusion on these sites as compared with higher hydrides. We assign a value of 0.2 and 0.3 eV to the hopping activation barriers on mono-hydrides, and di- or tri-hydrides respectively. For hopping onto a dangling bond, the barrier is chosen to be 0.3 eV (same as the barrier for hopping on higher hydrides). These values were assigned to be compatible the measured apparent barrier, and to be consistent with surface diffusion-dominated growth. The larger barrier on higher hydride surfaces is also consistent with recent calculations that suggest a "rolling" diffusion mechanism for physisorbed silyl [18].

Two neighboring physisorbed radicals may recombine and desorb as Si_2H_6 (Reaction I). The barrier for this reaction (0.7eV) is taken to be the same as that for desorption of an isolated radical on the surface. This mechanism is expected to

contribute significantly only in the case of high physisorbed radical surface coverages on account of the 2nd order reaction rate and is not dominant in the temperature range (0 - 600 °C) considered in this study.

Recombination reactions between different surface hydrides provide an important pathway for removal of surface hydrogen and network formation through the creation of surface Si-Si bonds. Two adjacent hydrides can undergo dissociative recombination to release molecular H_2, (Reaction J) and result in the formation of surface Si-Si bonds that may or may not be strained depending on the particular configuration of the participating hydrides. These thermally activated recombination reactions are primarily responsible for the changes in the distribution of surface hydrides under different deposition conditions. Higher hydrides are more likely to undergo the recombination reactions due to the presence of fewer number of Si-Si bonds. The presence of these rigid Si-Si bonds (as compared to the Si-H bonds) restricts the rearrangement of the surface atoms and therefore the higher hydrides have lower activation barriers towards the recombination reactions. Various recombination reactions (in order of increasing activation barriers) are tri-tri(E_{33}), tri-di(E_{32}), di-di(E_{22}), tri-mono(E_{31}), di-mono(E_{21}), and mono-mono(E_{11}). Although the exact barriers for these reactions are unknown, Kessels et al have estimated an overall barrier for the inter-conversion of surface hydrides to be ~0.21eV [25]. We therefore choose the respective barriers as E_{33}~0.20eV, E_{32}~0.25eV, E_{22}~0.3eV, E_{31}~0.35eV, E_{21}~0.45eV, and E_{11}~0.6eV. The surface Si-Si bonds created as a result of these recombination reactions play a critical role in network formation and growth processes particularly under conditions where insertion reactions are significant. These surface Si-Si bonds may react directly with the impinging silyl radicals as well as the

diffusing precursors on the surface as schematically shown in Reactions K-L. During a-Si:H growth, there is a distribution of slightly different bond lengths and angles that result in a distribution of weak and strong Si-Si bonds. The radicals will likely be able to insert into only a fraction of the surface Si-Si bonds. Although the distribution of weak and strong bonds is expected to change with temperature, for simplicity we assume that only a small constant fraction (f = 0.1) of the surface Si-Si bonds have strain energy above a threshold value that facilitates the insertion reactions. The choice of this value is somewhat arbitrary but the trends predicted by our model do not change significantly by the value chosen. This effectively renders ~90% of the surface Si-Si bonds to be stable to surface reaction, similar to "network" Si-Si bonds. This model therefore provides a means for silicon network formation not present in most other models. That is, Si-Si bond formation can proceed between two neighboring silicon hydrides, and ~90% of these bonds will not be affected by further surface reaction and will remain in the film. Finally, the surface hydrides may also recombine dissociatively at elevated temperatures resulting in two adjacent dangling bonds (for example, if the Si atoms are too far apart to form a Si-Si bond) as shown as Reaction M. The energetics of this reaction have been studied extensively at high temperatures and the barriers are reported to be between 1.8-2.5eV [26] and therefore we assign a value of 1.9eV to the barrier for this reaction.

4.2.4 Site balance equations for various surface species

Having identified the key surface reactions in a-Si:H deposition, four additional independent equations required to solve for the individual coverages of the different surface species can be derived from the surface site balances for the dangling bonds (θ_0),

physisorbed radicals (θ_4), mono-hydrides (θ_1) and the di-hydride species (θ_2). Note that the surface hydrogen concentration can be determined from the hydride distribution as $\theta_h = 0.25\ \theta_1 + 0.50\ \theta_2 + 0.75\theta_3$. The surface coverage of the different species (θ_0, θ_4, θ_1 and θ_2) is expressed in terms of a set of coupled non-linear time-dependent differential equations ($d\theta_i/dt$) that account for the generation and consumption of these different sites. If we assume a steady state growth, these differential equations reduce to a set of non-linear algebraic equations (since at steady state $d\theta_i/dt = 0$). The individual steady state site balances for θ_0, θ_4, θ_1 and θ_2 are developed next.

4.2.4.1 Dangling bond balance

Dangling bonds can be created by several distinct mechanisms: i) H abstraction reactions (from mono, di and tri-hydrides) by incident SiH_3 radicals (Reaction C); ii) H abstraction by physisorbed radicals (Reaction F); iii) insertion of incident silyl radicals into strained Si-Si bonds (Reaction K,L); iv) insertion of physisorbed radicals (Reaction L); and v) desorptive recombination of hydrides (Reaction M). Dangling bonds are in turn consumed through addition (chemisorption) reactions A and G. Hence the steady state balance for the dangling bonds is given as:

$$\begin{aligned} &\nu_{a1}\phi_{Si}\theta_{HT} + \nu_{a3}\theta_4\theta_{HT} + (\nu_{i1}\phi_{Si} + \nu_{i3}\theta_4) f\theta_5 + 2\nu_{r1}\theta_{HT}\theta_{HT} \\ &- s_0\phi_{Si}\theta_0 - \nu_h\theta_0\theta_4 = 0 \end{aligned} \qquad (6)$$

where θ_{HT} is the sum of all surface hydrides $\theta_{HT} = \theta_1 + \theta_2 + \theta_3$.

4.2.4.2 Physisorbed Radical Balance

The physisorbed radical site balance involves creation through physisorption of incident SiH_3 radicals on the surface (Reaction B), and removal through; i) abstraction by incident SiH_3 (Reaction C); ii) abstraction of surface H (Reaction F); iii) thermal desorption (Reaction E); iv) recombinative desorption of radicals (Reaction I); v) insertion into strained bonds (Reaction L); and vi) hopping onto a dangling bond (Reaction G):

$$s_1\phi_{Si}\theta_{HT} - s_2\phi_{Si}\theta_4 - s_4\phi_H\theta_4 - \nu_{a3}\theta_4\theta_{HT} - \nu_{d1}\theta_4 - 2\nu_{d2}\theta_4\theta_4 - \nu_{i3}\theta_4 f\theta_5 - \nu_{heff}\theta_0\theta_4 = 0 \quad (7)$$

4.2.4.3 Surface Mono-hydride Balance

The mono-hydride sites are created through disproportionation reactions between higher hydrides, specifically two di-hydrides may recombine to form two mono-hydrides (plus a Si-Si bond and an H_2) (Reaction J_{22}), or di-hydride and tri-hydride may recombine to form a mono- and a di-hydride (Reaction J_{23}). Some of the disproportionation reactions may also consume the mono-hydrides and produce Si-Si and H_2, such as recombination of a mono- with a tri-hydride (Reaction J_{13}) or recombination of two mono-hydrides (Reaction J_{11}). Since physisorbed radicals are presumed to "mask" surface hydrides, further reactions between physisorbed radicals and the surface can lead to a net increase in available surface hydrides. For example, desorption of a physisorbed radical from a mono-hydride site (Reaction E) produces an mono-hydride available for further reaction. Likewise, whenever a radical physisorbed on a mono-hydride is

consumed through reaction with a neighbor, the monohydride under the physisorbed radical becomes available for further reaction. Examples include Eley-Rideal abstraction of another physisorbed radical (Reaction C), Langmuir-Hinshelwood abstraction of H from a neighboring hydride (Reaction F), and hopping of the physisorbed radicals (Reaction G). This results in the following site balance equations for the mono-hydrides:

$$s_2\phi_{Si}\theta_4\frac{\theta_1}{\theta_{HT}} - s_1\phi_{Si}\theta_1 - \nu_{a1}\phi_{Si}\theta_1 - \nu_{a3}\theta_4\theta_1 + \nu_{d1}\theta_4\frac{\theta_1}{\theta_{HT}} + \nu_{p23}\theta_2\theta_3 + 2\nu_{p22}\theta_2\theta_2 - \nu_{p13}\theta_1\theta_3 - 2\nu_{p11}\theta_1\theta_1 - \nu_{r1}\theta_1\theta_{HT} + \nu_h\theta_o\theta_4\frac{\theta_1}{\theta_{HT}} = 0 \quad (8)$$

4.2.4.4 Surface Di-hydride Balance

Di-hydrides are created through disproportionation of tri-hydrides and through removal of physisorbed radicals from di-hydride sites. Two di-hydrides are created upon disproportionation reactions between two tri-hydrides (Reaction J_{33}). Likewise, one di-hydride is created when a tri- and a mono hydride react (Reaction J_{13}). Several mechanisms can result in di-hydride consumption. Two di-hydrides are consumed during disproportionation of two di-hydrides (Reaction J_{22}), and one di-hydride is consumed upon reaction between a di- and mono-hydride (Reaction J_{12}). As discussed above for the mono-hydride case, abstraction, desorption or hopping of a physisorbed radical from a di-hydride site makes that site available for further reactions. This results in the following site balance equation for the di-hydrides:

$$s_2\phi_{Si}\theta_4\frac{\theta_2}{\theta_{HT}} - s_1\phi_{Si}\theta_2 - \nu_{a1}\phi_{Si}\theta_2 - \nu_{a3}\theta_4\theta_2 + \nu_{d1}\theta_4\frac{\theta_2}{\theta_{HT}} + 2\nu_{p33}\theta_3\theta_3$$
$$- 2\nu_{p22}\theta_2\theta_2 + \nu_{p13}\theta_1\theta_3 - \nu_{p12}\theta_1\theta_2 - \nu_{r1}\theta_2\theta_{HT} + \nu_h\theta_o\theta_4\frac{\theta_2}{\theta_{HT}} = 0 \quad (9)$$

Equations (3) through (9) form a complete set of 7 independent non-linear algebraic equations that may be solved simultaneously for the 7 independent variables (θ_0, θ_1, θ_2, θ_3, θ_h, θ_4, and θ_5) as a function of temperature and incoming radical flux. Note that we do not need to write the site balance for tri-hydride sites as it results in a dependent equation that may be deduced from a linear combination of the equations (6) through (9) presented above since $d\theta_3/dt = - d\theta_0/dt - d\theta_4/dt - d\theta_1/dt - d\theta_2/dt$ (as a consequence of the site balance equation (4)).

4.3 RESULTS

The steady state surface site coverages as well as the surface Si-Si and Si-H bond fractions were obtained through a numerical solution of the seven non-linear algebraic equations (equations 3-9) for deposition temperatures between 0 to 600°C for several values of incident radical flux (ϕ_{Si} = 1, 10, 100 and 400 s^{-1}). A flux of 1.0 s^{-1} corresponds to approximately 0.3Å/s. Results for the individual surface coverage fractions at steady state under different growth conditions are shown in Figs 4.1 through 4.8. We first present the effect of temperature on surface composition under a typical growth rate condition (ϕ_{Si} =10 s^{-1}, or ~3Å/sec) and then discuss the effect of flux on determined parameters.

4.3.1 Effect of temperature

Fig 4.2 shows the fractional coverage of surface mono- di- and tri- hydrides at deposition temperatures between 0-600°C for a radical flux of $10s^{-1}$. At low temperature (<100°C), the model indicates that the surface remains almost entirely covered with tri-hydrides. As expected, as temperature increases, the coverage changes to di-hydride and then mono-hydride, until ~470°C where the hydrogen begins to desorb rapidly. This is consistent with the in-situ infrared measurements of the surface hydride distribution reported by Marra et al [24] and Kessels et al [25].

The total surface hydrogen coverage vs. temperature is shown in Fig 4.5. For less than 400°C, the coverage decreases monotonically with increasing temperature, then a sharper decrease is observed, consistent with the well known decrease in bulk H content with increasing temperature [23]. The relationship between bulk and surface hydrogen is not expected to be simple because there are other processes in the near surface region and film bulk that result in H elimination. For example it has been proposed that lower thermodynamic solubility limit of H in the bulk results in a net out-diffusion of H from the bulk to the surface [22]. Therefore, bulk H content is expected to be lower than that calculated from the steady-state surface hydride coverage. It is expected, however, that under kinetically limited growth conditions, the bulk H content will follow a trend similar to the surface H content as a function of deposition temperature and film growth rate.

The steady state surface coverage of dangling bonds gives insight into the quality of the deposited film since the dangling bonds provide chemisorption sites that are essential for film growth. The effect of temperature on the surface db coverage with

substrate temperature is shown in Fig 4.6. As temperature increases from 0°C to ~400°C, the dangling bond coverage increases from ~0.1% to ~1-2%, reflecting an increase in hydrogen abstraction, then increases significantly at higher temperatures, due primarily to direct desorption. The transition occurs at a temperature that depends on the flux of incoming radicals, and will be discussed below. The trends in the surface dangling bond density with temperature have been corroborated by *in-situ* Electron Spin Resonance (ESR) measurements reported by Yamasaki et al.[19,20]. Previous models Ganguly, 1993 #11] have suggested that the dangling bond density should first decrease then increase with increasing temperature. However, both the experimental data and the model presented here show only an increase in db density with increasing temperature.

Fig 4.7 shows the physisorbed radical coverage calculated as a function of surface temperature. The radical coverage decreases monotonically with increasing growth temperatures, with a rapid decrease at higher temperatures. This indicates that physisorbed radical density decreases with increasing db density. However, for a flux of $10s^{-1}$ the physisorbed radical density decreased by a factor of 10^5 as temperature is raised from 0 and 400, whereas the db density increases by only a factor of 10. This difference is attributed to thermally activated processes involving physisorbed radicals that do not involve dangling bonds, including surface diffusion, desorption, and recombination.

The model also enables a prediction of the surface Si-Si bond fraction, and model results are shown in Fig 4.8. The Si-Si bond density will be important, for example, to understand the amorphous to polycrystalline silicon transition in growth, since conditions that favor Si-Si surface bond formation will likely promote crystallite formation. For flux = $10s^{-1}$ the model predicts that the Si-Si bond fraction reaches a maximum value of ~20%

at ~450°C. The maximum is attributed to a change in the dominant film growth process from a surface diffusion limited at low deposition temperatures, to flux limited (i.e. direct chemisorption dominated) at higher temperatures. This observed trend in Si-Si bond density with temperature correlates will with the well-known experimental trend of crystallization fraction with increasing deposition temperature, where crystalline fraction increases with temperature, then drops to zero above 400°C [27].

4.3.2 Effect of incident precursor flux on surface composition

The growth rate of the films is determined by the flux of incident silyl radicals and has a strong impact on the surface composition. The predicted effect of flux on surface hydride composition is shown in Fig 4.1-4.4. Decreasing flux from $10s^{-1}$ to $1.0s^{-1}$ results in an increase in the monohydride fraction at moderate temperatures (150°-350°C). At higher flux, the di- and tri-hydrides dominate the surface hydrogen converage. Fig 4.5 shows the related increase in surface hydrogen coverage with increasing flux at all temperatures analyzed. This increase in surface hydrogen with increasing flux is primarily due to increased flux of H in the SiH_3 radical, and a shorter time between adsorption events, leading effectively to a shorter reaction time available for hydrogen elimination reactions, such as recombination. Fig 4.5 also shows that the temperature associated with the sudden decrease in hydrogen coverage is shifted higher temperature for higher silyl flux. This reflects a decrease in the net radical desorption rate as flux increases.

Fig 4.6 shows the effect of silyl flux on dangling bond density. For low to moderate temperatures (<350°C) the dangling bond density is independent of silyl flux.

This indicates that in this temperature range, the creation of dangling bonds is dominated by L-H type reactions that involve only surface species and do not involve incident radicals. A significant effect of flux is predicted for temperatures above ~400°C. The reduction in db density with increasing radical flux at temperatures between 400° and 550°C is attributed to H desorption dominating silyl chemisorption at low flux (leading to increase in db density), whereas silyl flux dominates H desorption at high silyl flux (helping to maintain a smaller db density). As will be discussed below, this result is consistent with measurements of growth rate vs temperature during high-rate silicon deposition [23], where the deposition rate is found to be independent of temperature even to temperatures as high as 500°C.

The effect of flux on physisorbed radical density is shown in Fig 4.7. Increasing flux leads to a larger physisorbed radical density over the entire temperature range. As will be shown in the following section, an increase in surface radical density results in an increased growth rate. The effect of flux on physisorbed radical density, therefore, is consistent with the observed increase in film growth rate with increasing radical flux, independent of temperature. This is also consistent with chemisorption being the dominant contributor to film growth.

The effect of increasing precursor flux on calculated fractional concentration of Si-Si bonds is shown in Fig 4.8. At temperatures less than ~400°C, a larger radical flux leads to a decrease in the Si-Si bond fraction. This is also consistent with well known experimental results that show that lower growth rates help achieve a larger crystallite size and fraction in deposited micro- and poly-silicon.

4.4 MACROSCOPIC PARAMETERS

4.4.1 Determining the macroscopic parameters characterizing film growth

Once the steady state surface coverage of various individual species (i.e., dangling bonds, surface hydrides, physisorbed radicals and strained bonds) is determined for a particular set of process parameters, such as the substrate temperature and silyl flux, various macroscopic measurable parameters can be estimated. Macroscopic parameters of interest include: 1) the steady state film growth rate (R_G); 2) the overall surface reaction probability for incident radicals (β); and 3) the incorporation probability for incident radicals (s). Values for β and s have been measured experimentally [9,28] and are useful to check the validity of the model. The effect of process conditions on growth rate is also well known and can be determined by this model. The characteristic diffusion length (L_d) of the physisorbed radicals, and the apparent thermal activation barrier for surface diffusion (E_a) are also important parameters that can be extracted from the model. Values for both parameters have recently been obtained using silicon surface topology evolution during film growth [5].

4.4.1.1 Growth Rate

The growth rate is calculated from the rates of all the reactions that result in the formation of a Si-Si bond between a precursor and the surface Si atoms. These include direct chemisorption (on a surface dangling bond) or direct insertion (into strained Si-Si bonds) of impinging SiH_3 radicals. Si-Si bonds are also formed by chemisorption or

insertion of a physisorbed SiH_3 precursor. The addition of these Si-Si bonds extends the surface by ~ 1 Si-Si bond length ($\boldsymbol{a} \approx 2.4$Å). On the other hand, the etching of the surface by incident radicals can also occur. It is important to note that the etching reaction is only significant in the case of high hydrogen dilution, and/or when the surface coverage of the tri-hydrides is significant (i.e., at very low temperatures), and is therefore negligible for the conditions described in this study. The net growth rate (in Å/sec), $\boldsymbol{R_G}$ is therefore given as:

$$R_G = a \cdot (s_0 \phi_{Si} \theta_0 + \upsilon_{i1} \phi_{Si} f\theta_5 + \upsilon_h \theta_0 \theta_4 + \upsilon_{i3} \theta_4 f\theta_5) \qquad (11)$$

4.4.1.2 Overall Reaction Probability (β) and Incorporation Probability (s)

The overall reaction probabilities for incident silyl radicals are shown schematically in Fig 4.9. Pathway 'a' represents the incident silyl flux and all other reaction probabilities are normalized with respect to the flux of incident silyl radicals. When a radical impinges on the surface, it may simply be reflected back into the gas phase (pathway 'b'), through an elastic collision or through a H abstraction event. The probability that the radical reflects back into the gas phase is written as 1-β. If the radical does not reflect from the surface, it must adsorb, designated as pathway 'c' with a probability β. A fraction of the films that adsorb will be incorporated directly through chemisorption or insertion reactions, indicated as pathway 'd' with a probability s_a. The absorbing radicals could also go into a physisorb state and move on the surface, eventually desorb, again through direct desorption or abstraction. This pathway is designated as 'e' with probability γ. The diffusing physisorbed radical could also become

incorporated into the film, indicated as pathway 'f' with a probability s_b. The overall incorporation (or "sticking") probability, s, is the fraction of impinging atoms that end up in the film (either through pathway 'd' or 'f' and is therefore given as a sum of s_a and s_b.

The incorporation probability, s, of the radicals includes reactions that lead to a net incorporation of the impinging radical, as shown in equation (12). Reactions leading to incorporation include direct chemisorption (Reaction A) and direct insertion (Reaction K), as well as chemisorption (Reaction G) and insertion (Reaction L) of the physisorbed radicals. The first two terms in equation (12) correspond to direct incorporation pathways (and the sticking probability s_a), while the 3rd term corresponds to the product of physisorption probability of an incident silyl radical and the probability that the physisorbed radical will get incorporated in the film.

$$s = s_0\theta_0 + \upsilon_{i1} f\theta_5 + s_1\theta_{HT}\frac{\upsilon_h\theta_0 + \upsilon_{i3} f\theta_5}{\upsilon_{a3}\theta_{HT} + \upsilon_{d1} + \upsilon_h\theta_0 + \upsilon_{d2}\theta_4 + \upsilon_{i3} f\theta_5 + s_2\phi_{Si}} \tag{12}$$

The overall reaction probability, β, includes all the reaction pathways through which the SiH_3 precursor may react with the surface. This includes direct reactions between the surface and the impinging SiH_3 radicals, as well as reactions between the surface and physisorbed SiH_3:

$$\beta = s_0\theta_0 + \upsilon_{i1} f\theta_5 + s_1\theta_{HT}\frac{\upsilon_{a3}\theta_{HT} + \upsilon_h\theta_0 + \upsilon_{d2}\theta_4 + \upsilon_{i3} f\theta_5 + s_2\phi_{Si}}{\upsilon_{a3}\theta_{HT} + \upsilon_{d1} + \upsilon_h\theta_0 + \upsilon_{d2}\theta_4 + \upsilon_{i3} f\theta_5 + s_2\phi_{Si}} \tag{13}$$

Here the reaction probability of the physisorbed radicals (3rd term in equation (13)) is derived from the fraction of physisorbed radicals ($s_1.\theta_{HT}$) that react with the surface. Pertinent surface reactions include chemisorption (Reaction G), abstraction (Reaction F), insertion (Reaction L), recombination with another physisorbed radical (Reaction I), and direct abstraction through incident radicals (Reaction C). Direct desorption from the surface (Reaction G) is not included.

4.4.1.3 Characteristic Diffusion Length, and Apparent Activation Energy

The characteristic diffusion length of the physisorbed precursors is estimated from the RMS displacement of the physisorbed radicals on the mono-hydride sites. This diffusion length is related to the average number of hops, *N*, that a physisorbed radical makes on the surface before undergoing any reaction that may remove it from the physisorbed state, and the distance covered in each hop, *d*. *N* is simply calculated as the ratio of the hopping rate of the physisorbed radical from one surface site to another to the sum total of all other reactions it may participate in.

Using the "random-walk" model [29] for surface diffusion of this physisorbed radical, and assuming the average distance per hop, *d*, remains constant, the diffusion length may be estimated as $L_D = d \cdot \sqrt{N}$. The distance per hop is estimated to be ~3.7Å. This is determined from the average distance between Si atoms on the surface, $d = \sqrt{1/N_{Si}}$, where N_{Si} is the surface density of Si atoms, taken to be between 6.9x10^{14} atoms/cm^2 for the Si(100) surface and 7.8x10^{14} atoms/cm^2 for the Si(111) surface. L_d is then written as:

$$L_d = d\sqrt{\frac{\upsilon_{heff}\theta_1}{\upsilon_{a3}\theta_{HT} + \upsilon_d + \upsilon_h\theta_0 + \upsilon_{d2}\theta_4 + \upsilon_{i3}f\theta_5 + s_2\phi_{Si}}} \qquad (14)$$

where

$$\upsilon_{heff} = \upsilon_{h1}\theta_1 + \upsilon_{h2}\theta_2 + \upsilon_{h3}\theta_3$$

is the effective hopping frequency on the hydrides.

In the model presented here, it is presumed that the rate of surface hopping will depend on the nature of the hydrides covering the growth surface. We believe that it is possible that the barrier to surface diffusion will be smaller for surface diffusion of a physisorbed radical onto a mono-hydride site as compared to a di-hydride or tri-hydride site. This assumption is reflected in our choice of diffusion barriers of 0.3eV for the radical diffusion onto tri-or di-hydrides and 0.2eV onto mono- hydride terminated silicon atoms. This difference in diffusion barrier energies is possible, for example, if the physisorbed radical binds strongly to di- and tri-hydrides inhibiting further diffusion. It could also result from the nature and structure of the physisorbed state itself. Recent theoretical results [15,16] suggest that silyl does not physisorb with a bond-centered hydrogen atom as is often assumed. Therefore, other configurations for the physisorbed radical that strongly favor adsorption onto the mono-hydride surface could be envisioned. An example of such a state has recently been proposed [18], where adsorption involves movement of the surface-bound hydrogen atom into a neighboring Si-Si bond. This movement would be significantly inhibited on a di- or tri-hydride site, effectively creating a large kinetic barrier to physisorption on those surface sites.

As described below, the assumption of different diffusion barriers on different surfaces leads to a hopping distance that can increase or decrease with increasing surface temperature, depending on process conditions. Using the diffusion length data, the apparent activation energy for diffusion can be determined from a plot of $\ln(L_d^2)$ vs. 1/T, where the data is fit to a straight line over a finite temperature range.

4.4.2 Comparison with experiments

In this section, values for macroscopic parameters described above are obtained from the kinetic model and are compared with experiments. The film growth rate, R_G, determined from equation 11 is plotted under different incident radical flux and substrate temperature conditions in Fig 4.10. The deposition rate remains constant at lower to intermediate temperatures (below 350-450°C and then rapidly increases to a higher saturation value at high temperatures (>400-450°C). The temperature associated with the rise in growth increases with increasing incident flux, ϕ_{Si}. This is consistent with Matsuda et al's [9] observation of an increase in the growth rate above 400°C for films deposited at low deposition rate in a low radical flux regime, $\phi_{Si} \sim 10^{s-1}$. Under higher flux conditions, van de Sanden et al.[23] showed that the growth rate was constant with substrate temperature for temperatures as high as 500°C. Both of these observations are consistent with the model results shown in Fig 4.10.

The growth rate results also enable us to suggest which growth processes contribute most significantly as a function of temperature and radical flux. Equation 11 is the sum of four distinct mechanisms for silyl incorporation into the growing film: 1) direct chemisorption into dangling bonds; 2) direct insertion into strained Si-Si bonds; 3)

radical physisorption, diffusion, and chemisorption onto dangling bonds; and 4) radical physisorption, diffusion, and insertion into strained Si-Si bonds. The contribution of each of these individual terms is plotted vs. substrate temperature for a flux of 10 sec^{-1} in Fig 4.11. Fig 4.11 shows that in the model presented here, silyl physisorption, diffusion, and subsequent chemisorption onto a dangling bond site dominates over other growth mechanisms for temperatures up to 500°C. The physisorbed radical chemisorption flux is determined from the product of temperature dependent dangling bond surface density, θ_0, the rate of hopping onto dangling bonds, ν_h, and the physisorbed radical surface density, θ_4. The temperature independent deposition rate is observed primarily because as temperature increases, the physisorbed radical density decreases, but the rate of physisorbed radical hopping and chemisorption increases to maintain the radical incorporation rate. The importance of surface diffusion in low temperature silicon growth is consistent with studies of topology evolution in these materials [5].

Closely related to the growth rate of the films are the macroscopic reaction probabilities β and s (shown in Fig 4.12). The model results indicate that the overall reaction probability β remains constant ~0.25 in the entire range of substrate temperatures considered (-100 to 600°C) and does not vary with the changes in the surface coverages of the various surface species considered. The sticking probability s, on the other hand is observed to depend on the deposition conditions and follows the same general trends as the growth rate. The sticking probability increases from a constant value of ~ 0.12 (temperature between 0 to ~transition temperature) to ~0.24 (above the transition temperature). Typically, amorphous silicon films show smooth surface texture and

conformal coverage of steps and trenches, and measurement of profile shapes can be used to determine the overall reaction probability, **β,** as well as the sticking probability, **s,** and hence the ratio **s/β** [9]. Under low to moderate growth rates, the value of the ratio **s/β** is measured to be ~0.4 at T<350°C, and increases to ~1 above 450°C [9]. The change is generally ascribed to the substantial increase in the dangling bond density created through increased recombination reactions at higher temperatures. Under these low to moderate growth rate conditions, the values of $\beta \sim 0.26$ and $s \sim 0.11$ are observed experimentally to be independent of temperature between 25 and ~400°C, and above 400°C β continues to be constant and s increases, following the same trend with temperature in Fig 4.12.

Another important parameter is the diffusion length of the physisorbed radical on the growth surface. Fig 4.13 shows the model output for the effect of deposition conditions (temperature and incident radical flux) on the surface diffusion length of the physisorbed precursors. For a flux of 10 sec^{-1}, the diffusion length is observed to increase with temperature up to ~200°C, then decrease.

The behavior of diffusion length with temperature is governed by the ratio of effective hopping rate on hydrides to the sum of abstraction, desorption and chemisorption of the physisorbed radicals. To model surface diffusion, and achieve the experimentally observed trends in step coverage, the barrier for hopping on hydrides is typically taken to be smaller than the barriers for abstraction and desorption. This means that as temperature increases, the rate of radical removal (by abstraction and desorption) increases more rapidly that the diffusion rate, leading to a decrease in the average diffusion distance and an apparent physisorbed radical diffusion barrier (related to the

difference, $E_{h,eff} - E_a - E_d - E_h$) that is negative. Since experimental data indicates that L_d increases with temperature [5], and the barrier for hopping must be smaller than for precursor removal, a different model for surface diffusion is needed. One possible modification to previous models that is reasonable and is consistent with the observed experiments, involves assuming that the surface diffusion proceeds more easily on some parts of the surface than on others. Specifically, if the barrier for surface diffusion is smaller on mono-hydride terminated surface regions that it is on di- or tri-hydrides, then diffusion rate is expected to increase as the surface coverage changes from tri- and di-hydrides at low temperature to predominantly mono-hydride at higher temperatures. This still enables surface diffusion to dominate over desorption and abstraction under typical growth temperatures. The assumption of a surface-dependent diffusion barrier is included in the model, and results in the trends observed in Fig 4.13. It also results in reasonable values for the apparent diffusion activation barrier as discussed below.

The trends in diffusion length with temperature are therefore described as follows. The initial increase in the diffusion length at low temperatures results from an increase in the mono-hydride sites on the surface that have a lower barrier for surface diffusion. At moderate temperatures (200°C < T < 400°C for flux ~$1s^{-1}$) where there are more mono-hydrides on the surface, there is a gradual decline in L_d due to increased abstraction and desorption reaction rates, similar to previous models. As temperature continues to increase, a rapid decline in L_d results from an increase in the dangling bond density on the surface, which shortens the residence time and diffusion length of the radicals on the surface.

Increasing the radical flux at temperatures below 400°C results in a decrease in the precursor surface diffusion length. This results primarily from an increase in abstraction of physisorbed precursors by the larger flux of incident radicals. It is well documented that low deposition rates (i.e. low incident radical flux) promotes network formation and, under sufficient hydrogen radical flux, formation of crystallites. The transition from amorphous to micro- or poly-crystalline growth can then be attributed to a larger diffusion length for the physisorbed radicals (and a smaller apparent diffusion barrier), consistent with many previous models of microcrystalline growth.

The apparent barrier to physisorbed radical surface diffusion is determined from the plot shown in Fig 4.14 for several values of incident radical flux. The apparent barrier increases from ~0.15eV under very low deposition rate (~0.3Å/s) to ~0.35eV at high deposition rate (~100Å/s). This change in the apparent barrier is a direct result of the changes in the surface hydride distribution under different deposition conditions. Under very low radical fluxes, the surface is predominantly covered by mono-hydride sites on which the radicals can diffuse rapidly (hence the large diffusion length and the lower apparent barrier) while under high flux conditions the higher hydrides are present in a significant fraction that results in a smaller diffusion length and a higher barrier.

4.5 CONCLUSIONS

A newly developed valence balance approach in combination with the site balance is used in a kinetic model for low temperature silicon film deposition. The valence balance accounts for surface Si-Si bonds, which enables a quantitative analysis of

radical precursor insertion into Si-Si bonds, and the rate of Si-Si bond formation. The model enables the number density of surface silicon atoms bound to one, two, or three hydrogen atoms, as well as the surface density of dangling bonds and physisorbed radicals to be calculated as a function of temperature and precursor flux under steady state growth conditions. We find that precursor diffusion on the surface is thermally activated if the precursor surface diffusion rate depends on the nature of the surface physisorption site. If the diffusion rate for precursors physisorbed on di- and tri-hydride sites is impeded relative to those on mono-hydride sites, then at low temperatures, the diffusion length increases with increasing temperature due to an increase in the fractional surface coverage of silicon mono-hydride sites. The calculated trends in growth rate, surface reaction probability, overall sticking probability, and precursor diffusion length vs. deposition temperature and precursor flux are all consistent with available experimental results. For the surface diffusion of physisorbed precursors, the model indicates that the apparent barrier will increase from ~0.15eV under very low deposition rate (~0.3Å/s) to ~0.35eV under high deposition rate conditions (~100Å/s).

4.6 ACKNOWLEDGEMENTS

Funding from the NSF through grant numbers 9624612 and 0072784 is acknowledged.

4.7 REFERENCES

[1] R. Crandall and W. Luft, *Progress in Photovoltaics* **3,** 315-332 (1995).

[2] J. R. Abelson, *Applied Physics a-Materials Science & Processing* **56,** 493-512 (1993).

[3] J. Perrin, *Journal of Non-Crystalline Solids* **137,** 639-644 (1991).

[4] J. E. Gerbi and J. R. Abelson, *Journal of Applied Physics* **89,** 1463-1469 (2001).

[5] K. R. Bray and G. N. Parsons, *Physical Review B* **accepted for publication** (2001).

[6] A. Gallagher, *Journal of Applied Physics* **60,** 1369-1373 (1986).

[7] G. Ganguly and A. Matsuda, *Physical Review B-Condensed Matter* **47,** 3661-3670 (1993).

[8] G. Ganguly and A. Matsuda, *Journal of Non-Crystalline Solids* **166,** 31-36 (1993).

[9] A. Matsuda and T. Goto, in *Materials Research Society Symposium Proceedings*, Vol. 164 (1990), pp. 3.

[10] A. Matsuda, *Thin Solid Films* **337,** 1-6 (1999).

[11] J. L. Guizot, K. Nomoto, and A. Matsuda, *Surface Science* **244,** 22-38 (1991).

[12] K. Maeda, A. Kuroe, and I. Umezu, *Physical Review B* **51,** 10635-10645 (1995).

[13] J. Perrin, M. Shiratani, P. Kae-Nune, H. Videlot, J. Jolly, and J. Guillon, *Journal of Vacuum Science & Technology a-Vacuum Surfaces and Films* **16,** 278-289 (1998).

[14] J. Robertson and M. J. Powell, *Thin Solid Films* **337,** 32-36 (1999).

[15] A. Gupta and G. N. Parsons, *Surface Science* **accepted for publication** (2001).

[16] S. Ramalingam, D. Maroudas, and E. S. Aydil, *Journal of Applied Physics* **86,** 2872-2888 (1999).

[17] A. von Keudell and J. R. Abelson, *Physical Review B-Condensed Matter* **59,** 5791-5798 (1999).

[18] R. Dewarrat and J. Robertson, *Journal of Non-Crystalline Solids* **to be published** (2001).

[19] S. Yamasaki, U. K. Das, T. Umeda, J. Isoya, and K. Tanaka, *Journal of Non-Crystalline Solids* **266,** 529-533 (2000).

[20] S. Yamasaki, T. Umeda, J. Isoya, and K. Tanaka, *Applied Physics Letters* **70,** 1137-1139 (1997).

[21] S. Yamasaki, T. Umeda, J. Isoya, and K. Tanaka, *Journal of Non-Crystalline Solids* **230,** 83-87 (1998).

[22] J. Robertson, *Journal of Applied Physics* **87,** 2608-2617 (2000).

[23] M. C. M. van de Sanden, W. M. M. Kessels, R. J. Severens, and D. C. Schram, *Plasma Physics and Controlled Fusion* **41,** A365-A378 (1999).

[24] D. C. Marra, E. A. Edelberg, R. L. Naone, and E. S. Aydil, *Journal of Vacuum Science & Technology a-Vacuum Surfaces and Films* **16,** 3199-3210 (1998).

[25] W. M. M. Kessels, A. H. M. Smets, D. C. Marra, E. S. Aydil, D. C. Schram, and M. C. M. van de Sanden, *Thin Solid Films* **383,** 154-160 (2001).

[26] D. J. Doren, in *Advances in Chemical Physics, Vol 95 - Surface Properties*, Vol. 95 (John Wiley & Sons Inc, New York, 1996), pp. 1-60.

[27] A. Matsuda, *Journal of Non-Crystalline Solids* **59-6,** 767-774 (1983).

[28] A. Matsuda, K. Nomoto, Y. Takeuchi, A. Suzuki, A. Yuuki, and J. Perrin, *Surface Science* **210,** 114 (1990).

[29] G. A. Somorjai, *Introduction to surface chemistry and catalysis* (Wiley, New York, 1994).

Table 4.1 List of Reactions (and the corresponding rate expressions) used in the model

No.	Reaction	Description	Parameter		Rate
A	$\equiv Si- + SiH_{3\,(g)} \rightarrow \equiv Si-SiH_3$	Addition of SiH_3 to db	s_0		$s_0.\phi_{Si}.\theta_0$
B	$\equiv(SiH_x) + SiH_{3\,(g)} \rightarrow \equiv(SiH_x)SiH_3$	Physisorp. of SiH_3 on Hydride	s_1		$s_1.\phi_{Si}.\theta_x$
C	$\equiv(SiH_x)SiH_3 + SiH_{3\,(g)} \rightarrow \equiv(SiH_x) + Si_2H_{6\,(g)}$	Abstraction of Phys by SiH_3	s_2		$s_2.\phi_{Si}.\theta_4$
D	$\equiv(SiH_x) + SiH_3 \rightarrow \equiv(SiH_{x-1})- + SiH_{4\,(g)}$	Abstraction of H by SiH_3	υ_{a1}	E_{a1}	$\upsilon_{a1}.\phi_{Si}.\theta_x$
E	$\equiv(SiH_x)SiH_3 \rightarrow \equiv(SiH_x) + SiH_{3\,(g)}$	Desorption of Phys SiH_3	υ_{d1}	E_{d1}	$\upsilon_{d1}.\theta_4$
F	$\equiv(SiH_x)SiH_3 \rightarrow \equiv(SiH_{x-1})- + SiH_{4\,(g)}$	Abstractn. of H by Phys SiH_3	υ_{a3}	E_{a3}	$\upsilon_{a3}.\theta_4.\theta_x$
G	$\equiv(SiH_x)SiH_3 + \equiv Si- \rightarrow \equiv SiH_x + \equiv SiSiH_3$	Chemisorption of Phys SiH_3	υ_{hx}	E_{hx}	$\upsilon_{hx}.\theta_4.\theta_0$
H	$\equiv(SiH_x)SiH_3 + \equiv SiH_y \rightarrow \equiv SiH_x + \equiv(SiH_y)SiH_3$	Hopping of Phys on hydrides	υ_{hx}	E_{hx}	$\upsilon_{hx}.\theta_4.\theta_1$
I	$2\equiv(SiH_x)SiH_3 \rightarrow 2\equiv SiH_x + Si_2H_{6\,(g)}$	Desorption of 2 Phys SiH_3	υ_{d2}	E_{d2}	$\upsilon_{d2}.\theta_4.\theta_4$
J	$\equiv(SiH_x) + (SiH_y)\equiv \rightarrow \equiv(SiH_{x-1})-(SiH_{y-1})\equiv + H_{2(g)}$	Recombination of Hydrides	υ_{pxy}	E_{pxy}	$\upsilon_{pxy}.\theta_x.\theta_y$
K	$\equiv Si-Si\equiv + SiH_{3\,(g)} \rightarrow \equiv SiSiH_3 + \equiv Si-$	SiH_3 insertion in Si-Si	υ_{i1}	E_{i1}	$\upsilon_{i1}.\phi_{Si}.f.\theta_5$
L	$\equiv Si-Si\equiv + H_3Si(SiH_x)\equiv \rightarrow 2\equiv SiSiH_n + \equiv Si-$	Insertion of Phys SiH_3	υ_{i3}	E_{i3}	$\upsilon_{i3}.\theta_4.f.\theta_5$
M	$\equiv(SiH_x) + (SiH_y)\equiv \rightarrow 2\equiv(SiH_z)- + H_{2\,(g)}$	Recomb of Hyd. forming db	υ_{r1}	E_{r1}	$\upsilon_{r1}.\theta_x.\theta_y$

Table 4.2 List of Reaction Rate parameters used in the model. The rate constants, υ_n, are given as $A_n\exp(-E_n/k_BT)$, here k_B is the Boltzmann's constant and h is Planck's constant.

Reaction	***Parameter values***			
A	s_0		0.25	
B	s_1		0.25	
C	s_2		0.1	
D	A_{a1}	0.25	E_{a1}	0.4 eV
E	A_{d1}	k_BT/h	E_{d1}	0.7 eV
F	A_{a3}	$0.1k_BT/h$	E_{a3}	0.4 eV
G	A_h	k_BT/h	E_h	0.3eV
H_1	A_{h1}	k_BT/h	E_{h1}	0.2eV
H_2	A_{h2}	k_BT/h	E_{h2}	0.3 eV
H_3	A_{h3}	k_BT/h	E_{h3}	0.3 eV
I	A_{d2}	k_BT/h	E_{d2}	0.7 eV
J_{11}	A_{p11}	$10^{-10}k_BT/h$	E_{p11}	0.6 eV
J_{12}	A_{p12}	$10^{-10}k_BT/h$	E_{p12}	0.45 eV
J_{13}	A_{p13}	$10^{-10}k_BT/h$	E_{p13}	0.35 eV
J_{22}	A_{p22}	$10^{-10}k_BT/h$	E_{p22}	0.3 eV
J_{23}	A_{p23}	$10^{-10}k_BT/h$	E_{p23}	0.25 eV
J_{33}	A_{p33}	$10^{-10}k_BT/h$	E_{p33}	0.2 eV
K	A_{i1}/s	0.25	E_{i1}	0.5 eV
L	A_{i3}	k_BT/h	E_{i3}	0.7 eV
M	A_{r1}	k_BT/h	E_{r1}	1.9 eV

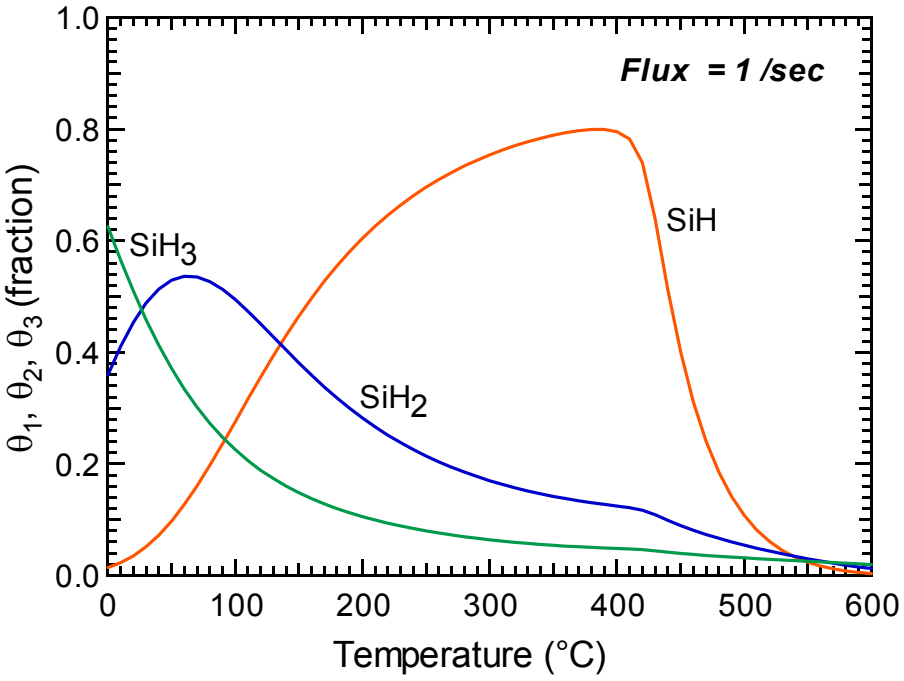

Fig 4.1 Distribution of different surface hydrides for silyl radical flux =1/sec

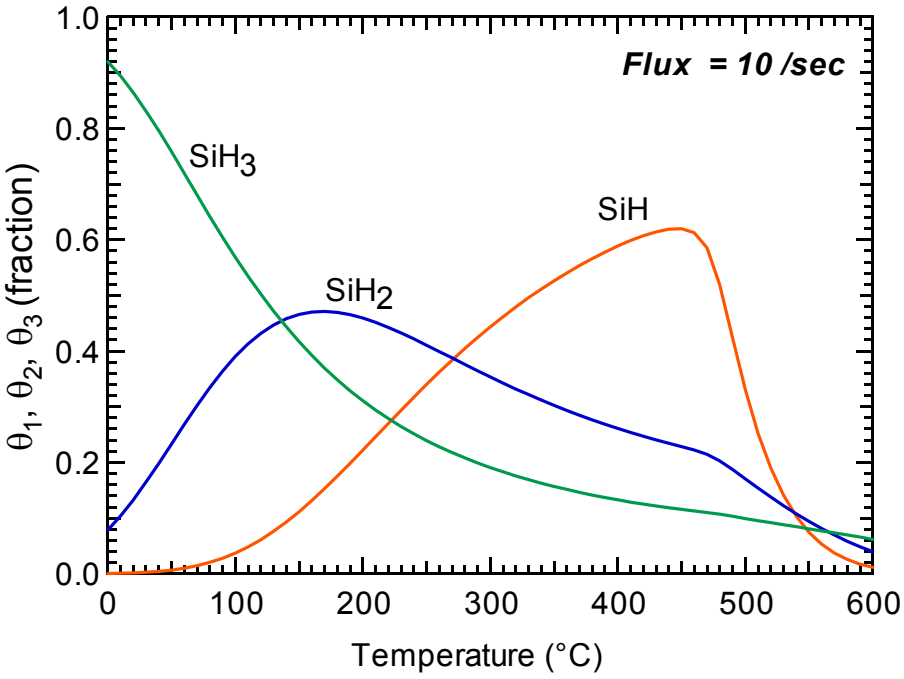

Fig 4.2 Distribution of different surface hydrides for silyl radical flux =10/sec

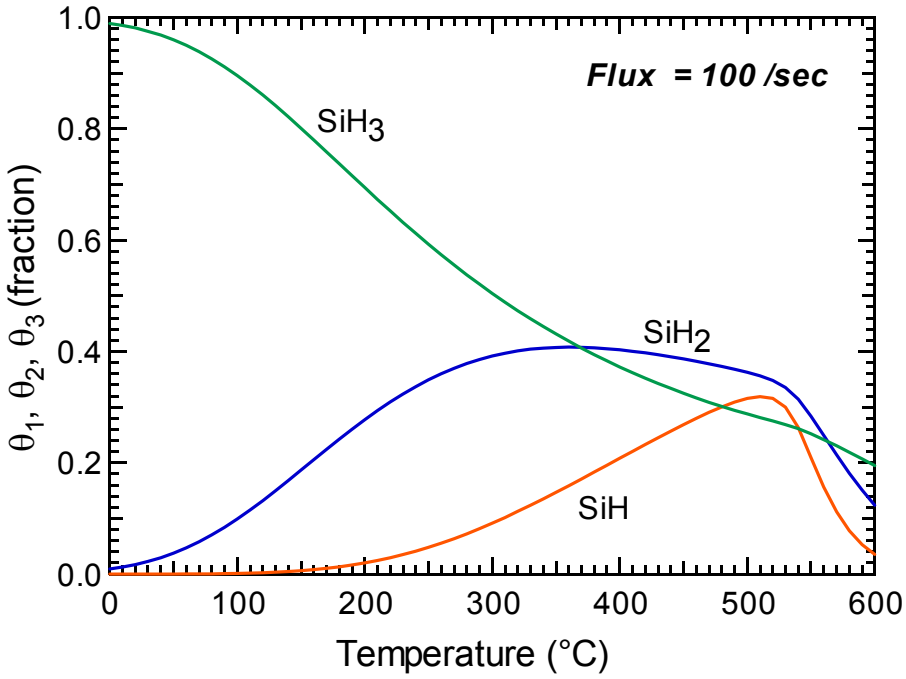

Fig 4.3 Distribution of different surface hydrides for silyl radical flux =100/sec

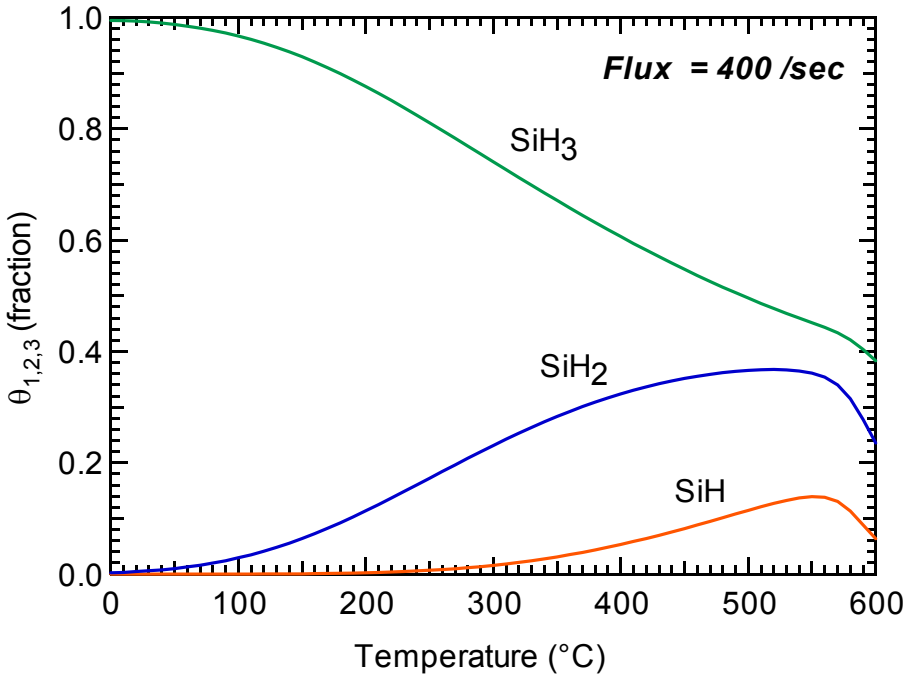

Fig 4.4 Distribution of different surface hydrides for silyl radical flux =400/sec

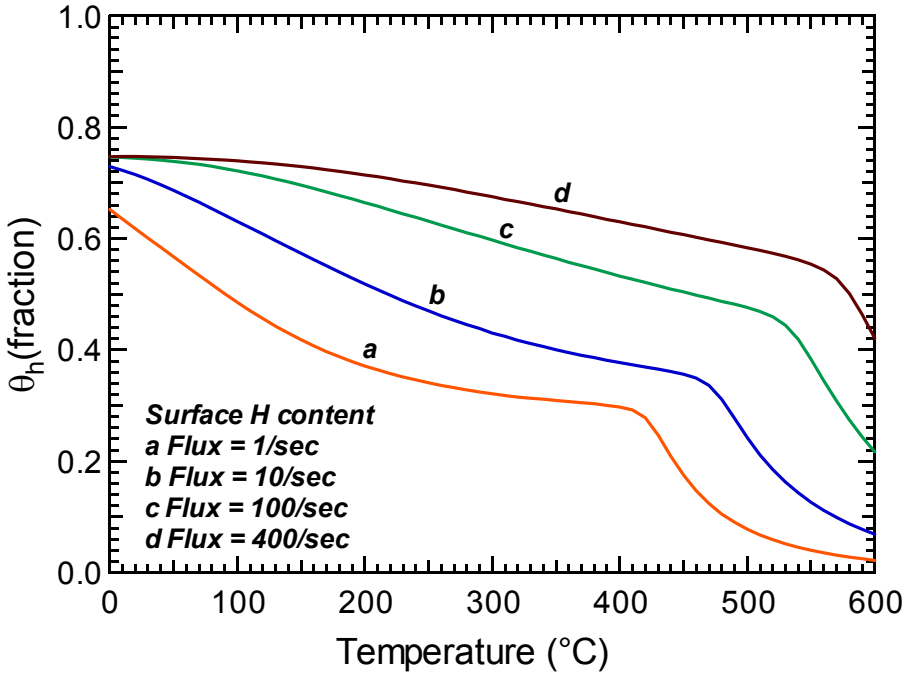

Fig 4.5 Variation of surface layer H content with deposition conditions (temperature as well as silyl radical flux)

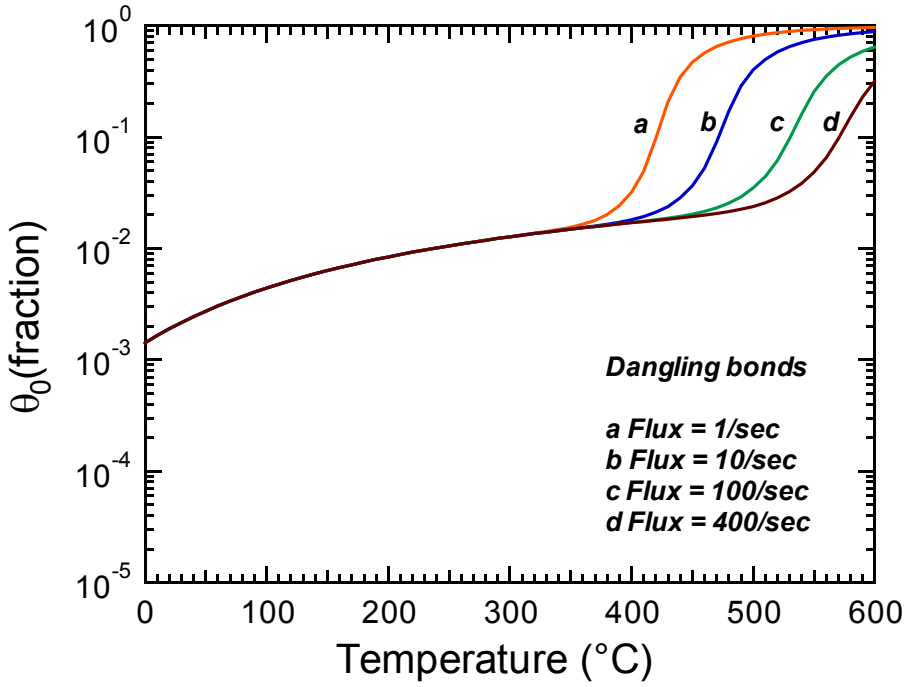

Fig 4.6 Effect of deposition conditions (temperature and silyl radical flux) on the surface dangling bond concentration.

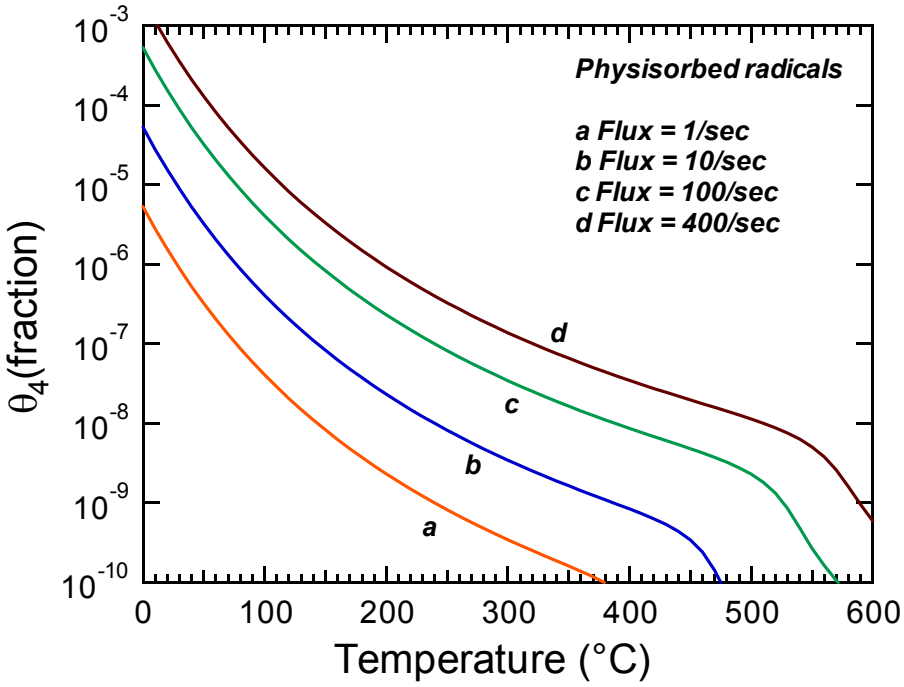

Fig 4.7 Effect of deposition conditions (temperature and silyl radical flux) on the surface coverage of physisorbed radicals.

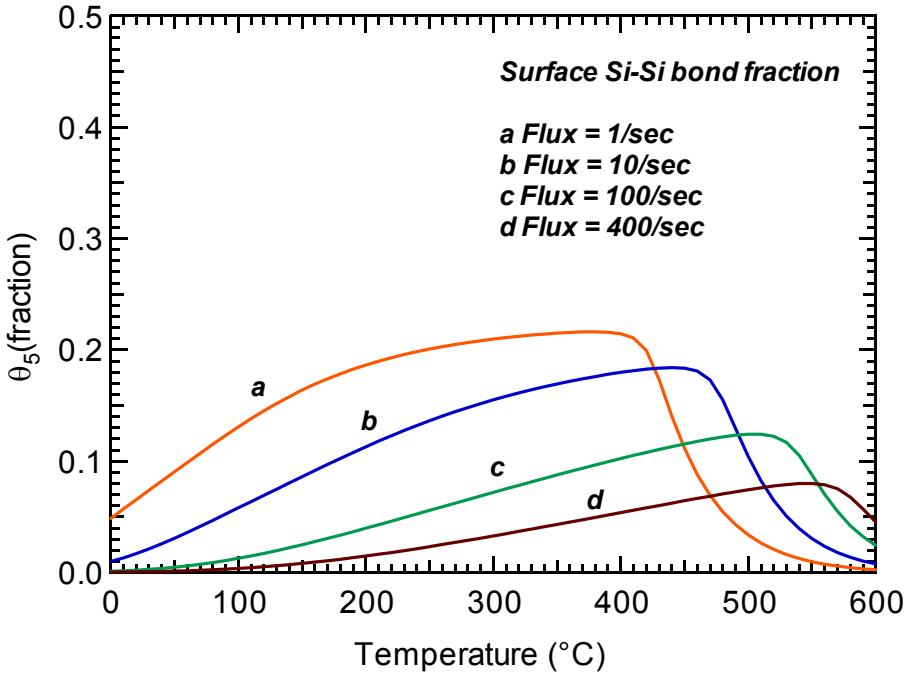

Fig 4.8 Surface Si-Si bond (θ_5) fraction under various deposition conditions

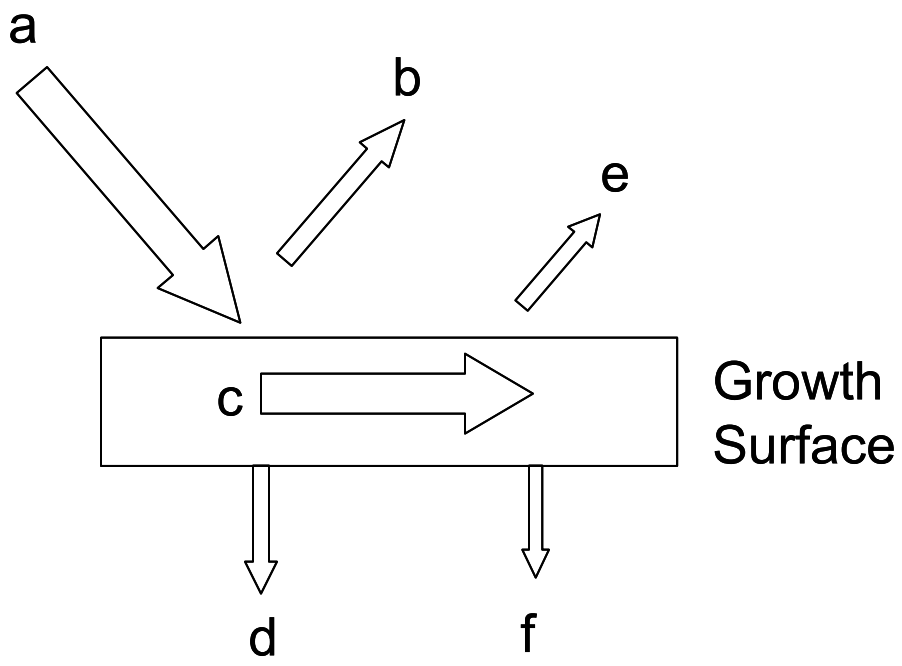

Fig 4.9 Schematic of various reaction and sticking probabilities on the surface

Probabilities associated with various growth events

a = b + c + d = 1 and c = e + f

a : Incoming Silyl Flux (=1)

b : Reflection of SiH_3/ direct H abstraction (=1-β)

c : surface reaction probability (β)

d : direct Incorporation of Silyl radicals through chemisorption or insertion (s_a)

e : Recombination, desorption of physisorbed radical (γ)

f : Incorporation of physisorbed radical (s_b)

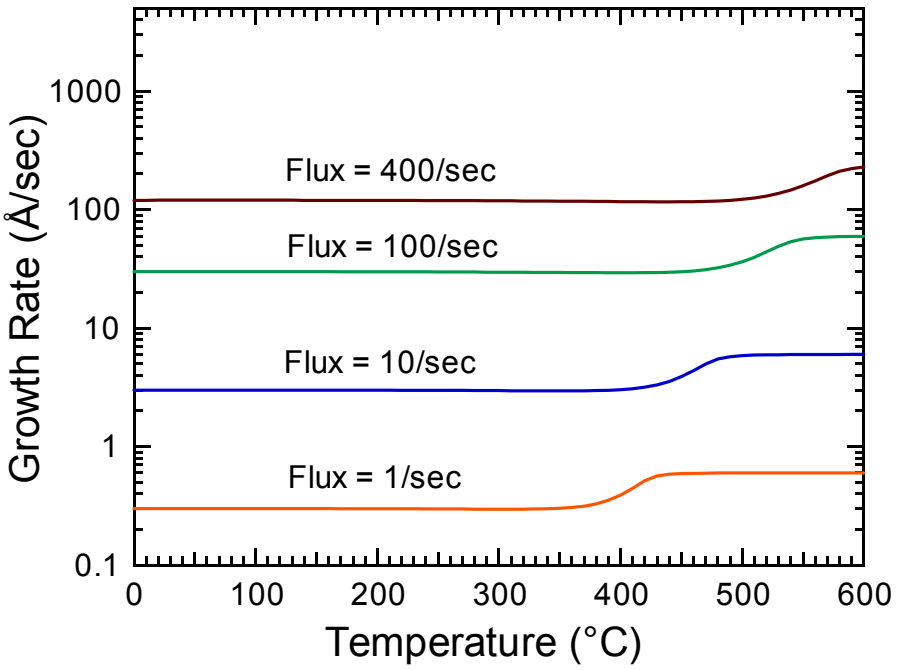

Fig 4.10 Growth rate variations with deposition conditions (temperature and silyl radical flux).

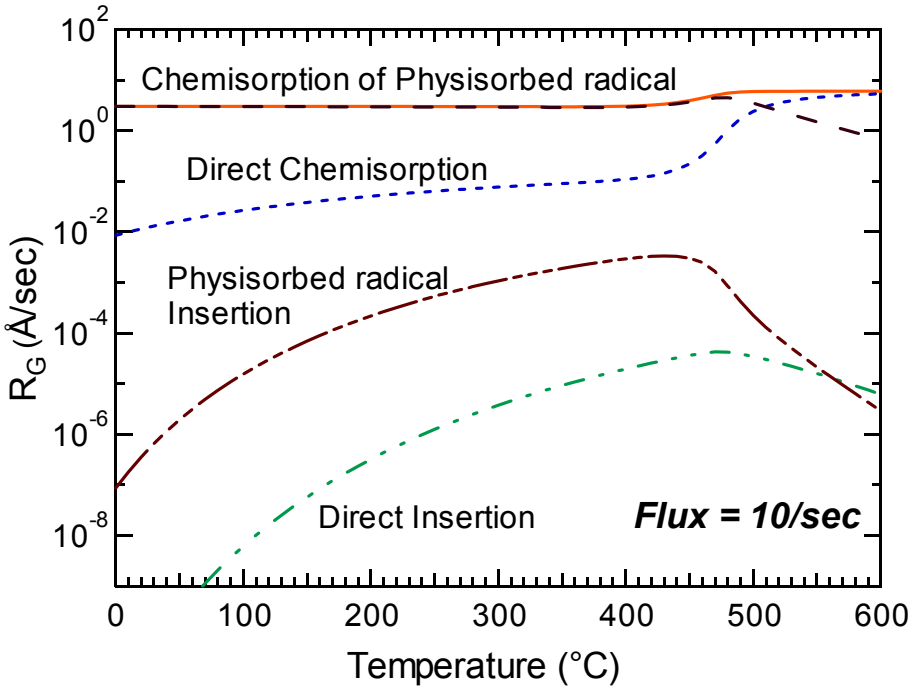

Fig 4.11 Relative contributions of different pathways towards film growth under a typical deposition rate condition. The film growth is dominated by chemisorption of physisorbed precursors at low temperatures and by direct chemisorption of incident radicals beyond the transition temperature.

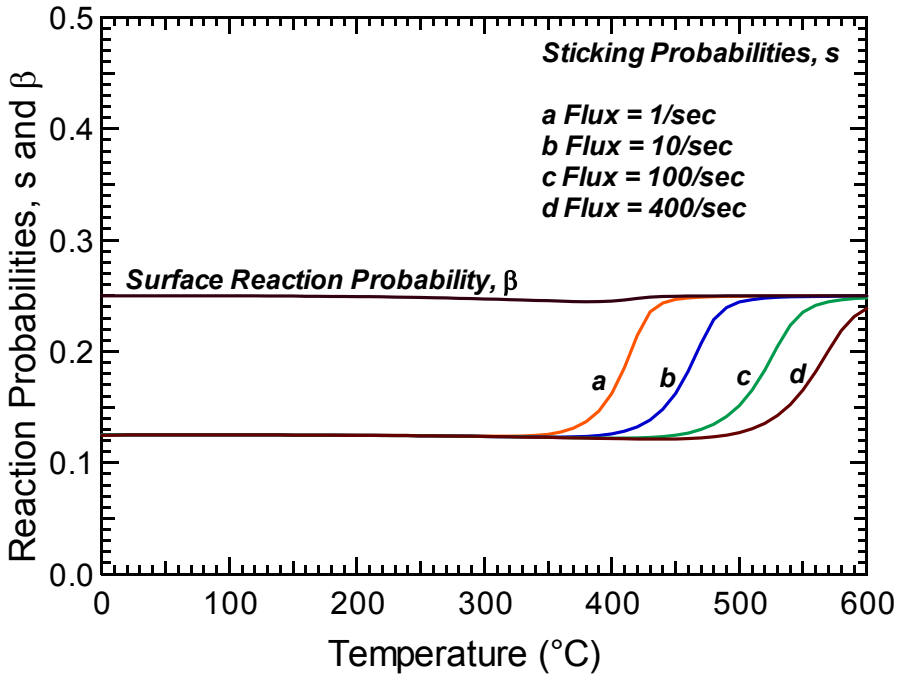

Fig 4.12 Reaction and sticking probabilities (β and s) predicted by the kinetic model.

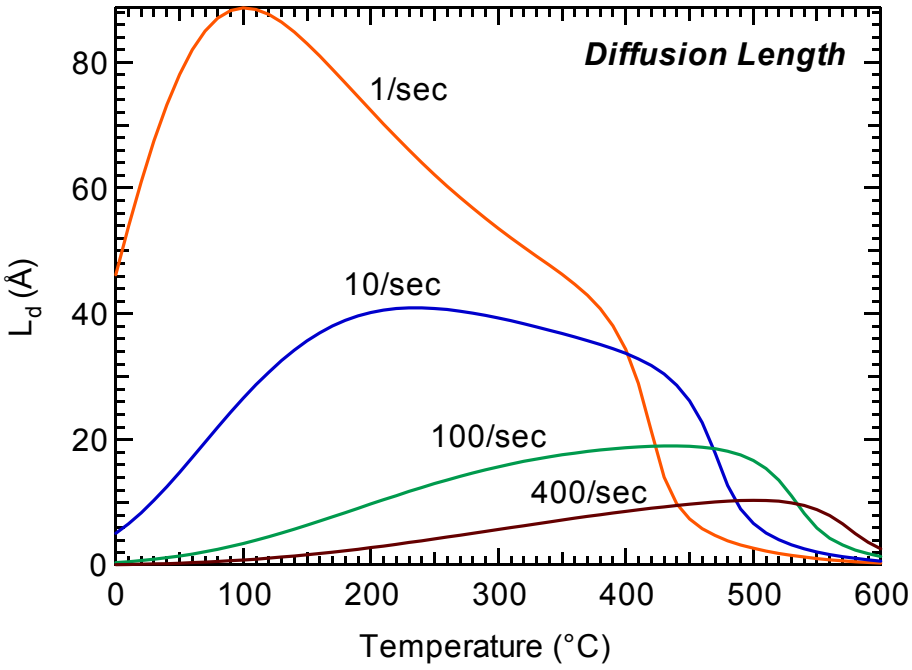

Fig 4.13 Diffusion length as a function of deposition conditions

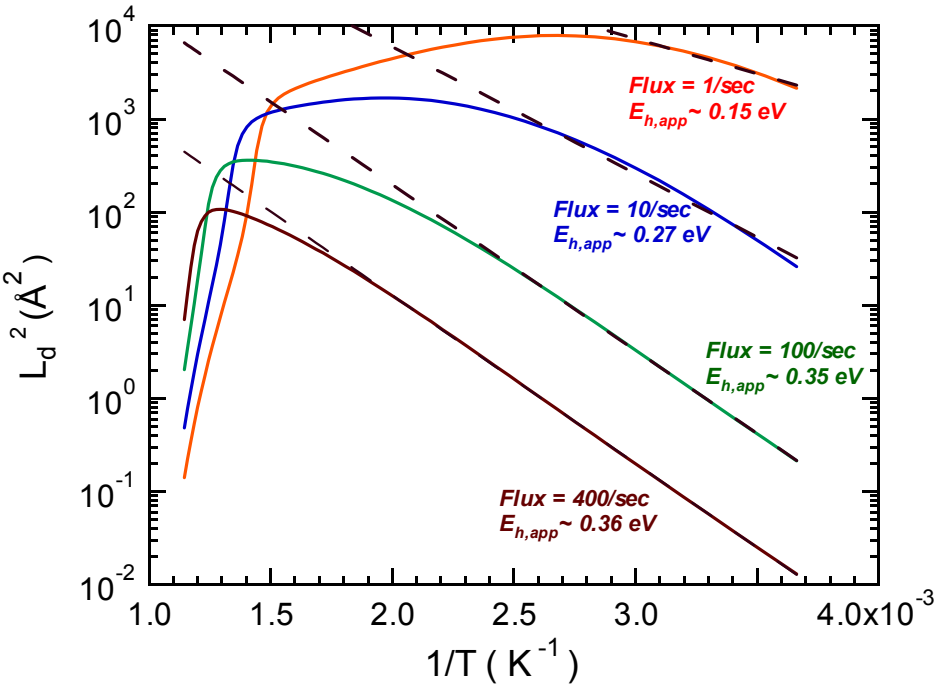

Fig 4.14 Semi-log Plot of L_d^2 vs 1/T to calculate the apparent activation barriers for the diffusion of physisorbed radicals on the surface.

Chapter 5 is a preprint of a manuscript to be submitted for publication in Applied Physics Letters

CHAPTER 5

5 DIFFUSION ENHANCEMENT EFFECTS THROUGH HYDROGEN DILUTION DURING HYDROGENATED AMORPHOUS SILICON DEPOSITION

By: Kevin R. Bray, Atul Gupta, and Gregory N. Parsons

Department of Chemical Engineering, North Carolina State University, Raleigh

Notes: My contributions towards this paper include the deposition and characterization of several a-Si:H films deposited using either pure silane gas or silane/hydrogen gas mixtures at several growth temperatures (25-350°) in a large area plasma deposition reactor. I also developed a new strategy for an accurate statistical analysis of the film surface topology and this was implemented in a Macro program written for Igor Pro software.

ABSTRACT

Fractal analysis of the surface topography is used to study the effects of hydrogen dilution and rf power density on the surface transport kinetics during the plasma deposition of hydrogenated amorphous silicon. Images obtained from atomic force

microscopy are examined using dimensional fractal analysis and surface diffusion lengths of growth precursors are extracted as the correlation length in the plots. The addition of hydrogen during deposition initially decreases the diffusion length at low H_2/SiH_4 ratios but increases the diffusion length from 45nm to 100nm at 25°C with a hydrogen dilution of 50/1. The surface diffusion activation barrier is reduced from 0.20eV for SiH_4 to 0.13eV with high hydrogen dilution. Increasing power density is shown to increase the surface diffusion length, but the activation barrier remains unchanged with power density. Results are compared for two PECVD reactors.

5.1 INTRODUCTION AND APPROACH

Plasma deposition of hydrogenated amorphous silicon results in very smooth, conformal surfaces and non-thermally activated growth rates over temperatures ranging from <25° to 400°C [1-4]. Typical models for a-Si:H growth presume that radical precursors generated in the gas phase adsorb and diffuse on the surface with low thermal barriers, giving rise to the observed smooth conformal surface coverage [2,3,5], but results are not available that directly identifying surface transport processes. Analysis of surface roughness can be used to characterize transport on a-Si:H surfaces [6-9] and determine the diffusion barrier as a function of temperature and process conditions [9-11].

In this work, the effects of hydrogen dilution and rf power density on the diffusion of surface precursors during Plasma Enhanced Chemical Vapor Deposition (PECVD) of hydrogenated amorphous silicon deposition were investigated. The a-Si:H films were deposited using two different direct PECVD reactors described elsewhere [12,13]. Hydrogenated amorphous silicon was deposited using 2% SiH_4 in He at temperatures from 25 - 150°C at 0.6 Torr and from pure SiH_4 at temperatures from 25 - 350°C at 0.4 Torr in reactors one and two respectively. The effect of hydrogen dilution was studied using H_2/SiH_4 ratios from 0 – 75 during the deposition of 1000Å a-Si:H films in reactor one. A Digital Instruments Dimension 3000 Atomic Force Microscopy (AFM) was used to image the surface topography of the deposited films. Fractal analyses were then performed on the AFM images to extract correlation lengths [9].

5.2 RESULTS

Fig 5.1 shows the dimensional fractal analysis using a plot of the root mean square (rms) roughness vs. length scale for two 1000Å thick a-Si:H films, deposited with and without H_2 dilution. For each sample, the roughness increases with measurement length, then, at the correlation length L_c, the roughness saturates at σ_{sat}. The correlation length is the maximum lateral length scale over which surface roughness correlations persist [14] and has been used as an estimate of the surface diffusion length [3,6,8].

The effect of hydrogen on the correlation length is shown in Fig. 2. As the H_2/SiH_4 ratio increases from 0 – 10, the correlation length decreases. As the ratio increases further, there is a rapid increase in the correlation length, which then saturates constant value. Helium dilution experiments were conducted to determine if the increase in the surface diffusion length with hydrogen dilution was due to surface interactions during growth or simply a gas dilution effect of reduced silyl flux to the surface. Fig 5.1 shows a small dilution effect with as the $SiH_4/(SiH_4+He)$ ratio is changed from 1/(1+49) to 1/(1+99), with the correlation length increasing 5 – 10 nm. This is much smaller than the increase observed when the same initial $SiH_4/(SiH_4+He)$ of 1/(1+49) is diluted with hydrogen to $SiH_4/(SiH_4+He+H_2)$ of 1/(1+49+50), where the correlation length doubles. Additional He dilution while maintaining a constant SiH_4/H_2 ratio of 1/50 show another slight increase in L_c as seen in Fig. 1, but again it is on the order of 10 nm. A study using attenuated total reflection Fourier transform infrared (ATR-FTIR) spectroscopy [15] has shown that the surface coverage during a-Si:H growth changes from predominantly di- and tri-hydrides to predominantly monohydride with a 20/1 H_2/SiH_4 dilution ration

during deposition. The observed increase in the diffusion length with high hydrogen dilution may be an effect of the change in the hydride surface coverage.

The increase in L_c with hydrogen dilution is consistent with the increase in the surface diffusion length with increasing hydrogen dilution indirectly observed in other studies [16-18]. Ellipsometry measurements of a-Si:H deposited using conventional PECVD showed films deposited with increased hydrogen dilution had lower surface roughness, which was attributed to increased surface diffusion lengths.[16] The effect of hydrogen dilution was also studied by depositing a-Si:H and μc-Si:H on rough substrates using dc reactive magnetron sputtering and observing the surface roughness decrease with increasing film thickness [17]. The roughness decreased more rapidly with increasing hydrogen dilution, indicating an increase in the surface diffusion. The crystalline volume fraction of microcrystalline silicon has been observed to increase with increasing hydrogen dilution [1]. This increase has been ascribed to increased diffusion lengths. The effect of hydrogen on silicon nucleation and coalescence was investigated by using Auger electron spectroscopy to observe the Si and Ga fractions during μc-Si deposition onto GaAs substrates [18]. The Ga signal goes to zero at the coalescence point. The coalescence is observed more rapidly with hydrogen dilution, indicating enhanced precursor diffusion.

The temperature dependence of the correlation length discussed above was further investigated. Using L_c as the diffusion length, the diffusion activation barrier was estimated from an Arrhenius plot of L_c^2 vs. 1/T. As shown in Fig. 3, the surface diffusion activation energy for films grown with the SiH_4/He mixture is 0.20eV. The technique for surface transport analysis presented here utilizes direct surface characterization, and does

not require identification or supposition of the particular gas-phase precursor responsible for growth, or the adsorbed surface species responsible for diffusion. The values of diffusion length and diffusion activation barrier determined from the topography analysis are close to those obtained from previous rough estimations using precursor dependent reaction models [19], estimates from direct simulation [20,21] or physical based assumptions [3,5,22]. With the addition of hydrogen dilution during a-Si:H deposition, the diffusion activation barrier decreased from 0.20eV to 0.13eV as seen in Fig. 3.

The influence of the rf power density on the correlation length was investigated by varying the power from 8 – 50 mW/cm^2 in reactor 1. No hydrogen dilution was used during the power density studies. As shown in Fig. 4, L_c increased with increasing power density. This may be due to more highly energized growth precursors arriving on the surface [23] or an increase in the hydrogen ion flux to the surface [1]. The surface diffusion barrier, as shown in Fig. 4, remained constant over the entire power density range studied.

To study if the diffusion barriers observed were universal and not an artifact linked to the reactor system used for deposition, comparisons were made between aSi:H films deposited in both reactors one and two. Fig 5.3 shows Arrhenius plots for films grown in both reactors. A surface diffusion activation barrier of 0.19eV is found from reactor two, similar to 0.20eV from reactor one. The correlation lengths are also of comparable magnitude. These results indicate that the diffusion barriers calculated are independent of the reactor used for deposition.

5.3 CONCLUSIONS

In conclusion, low hydrogen dilution (1 - 10 H_2/SiH_4) during the deposition of hydrogenated amorphous silicon decreases surface diffusion. Higher hydrogen dilutions ($H_2/SiH_4 > 10$) increase surface diffusion. Previous work [16-18] has speculated that hydrogen increases surface diffusion to explain observed results, but in our work actual diffusion lengths determined. The decrease in diffusion length with low hydrogen dilution has not previously been observed. This trend of decreasing diffusion length with increasing hydrogen dilution has been reproduced in a kinetic model of amorphous silicon growth [24]. This influence on the diffusion length is due to increased dangling bond density on the surface through atomic hydrogen abstraction of surface hydrogen. Increasing rf power density used for deposition slightly increases the diffusion length, but does not change the activation barrier. The activation barriers calculated were independent of the reactor system used for depositions.

The authors would like to acknowledge the NSF for support of this research.

5.4 REFERENCES

[1] A. Matsuda, *Journal of Non-Crystalline Solids* **59-60,** 767 (1983).

[2] J. Perrin, M. Shiratani, P. Kae-Nune, H. Videlot, J. Jolly, and J. Guillon, *Journal of Vacuum Science and Technology A* **16,** 278 (1998).

[3] J. Robertson, *Journal of Applied Physics* **87,** 2608-2617 (2000).

[4] A. Matsuda, *Plasma Physics and Controlled Fusion* **39,** 431-436 (1997).

[5] G. Ganguly and A. Matsuda, *Journal of Non-Crystalline Solids* **164-166,** 31 (1993).

[6] D. M. Tanenbaum, A. L. Laracuente, and A. Gallagher, *Physical Review B-Condensed Matter* **56,** 4243-4250 (1997).

[7] M. Kondo, T. Ohe, K. Saito, T. Nishimiya, and A. Matsuda, *Journal of Non-Crystalline Solids* **227-230,** 890 (1998).

[8] W. M. Tong, E. J. Snyder, and R. S. Williams, *Surface Science* **277,** L63 (1992).

[9] K. R. Bray and G. N. Parsons, *to be published* .

[10] L. Bardotti, C. R. Stoldt, C. J. Jenks, M. C. Bartlet, J. W. Evans, and P. A. Thiel, *Physical Review B* **57,** 12544-12549 (1998).

[11] B. Reinker, M. Moske, and K. Samwer, *Physical Review B* **56,** 9887 (1997).

[12] E. Srinivasan, D. A. Lloyd, and G. N. Parsons, *Journal of Vacuum Science and Technology A* **15,** 77 (1997).

[13] C. S. Yang, W. W. Read, C. Arthur, E. Srinivasan, and G. N. Parsons, *Ieee Electron Device Letters* **19,** 180-182 (1998).

[14] W. M. Tong and R. S. Williams, *Annual Review of Physical Chemistry* **45,** 401 (1994).

[15] D. C. Marra, E. A. Edelberg, R. L. Naone, and E. S. Aydil, *Applide Surface Science* **133,** 148-151 (1998).

[16] H. Fujiwara, Y. Toyoshima, M. Kondo, and A. Matsuda, *Journal of Non-Crystalline Solids* **266-269,** 38 (2000).

[17] J. E. Gerbi and J. R. Abelson, *Journal of Applied Physics* **89,** 1463-1469 (2001).

[18] A. Matsuda, *Thin Solid Films* **337,** 1-6 (1999).

[19] K. Maeda, A. Kuroe, and I. Umezu, *Physical Review B-Condensed Matter* **51,** 10635-10645 (1995).

[20] M. J. Kushner, *Journal of Applied Physics* **62,** 4763-4772 (1987).

[21] K. K. Gleason, K. S. Wang, M. K. Chen, and J. A. Reimer, *Journal of Applied Physics* **61,** 2866-2873 (1987).

[22] R. Robertson and A. Gallagher, *Journal of Chemical Physics* **85,** 3623-3630 (1986).

[23] S. C. Saha, A. K. Barua, and S. Ray, *Journal of Applied Physics* **74,** 5561 (1993).

[24] A. Gupta and G. N. Parsons, *to be submitted* .

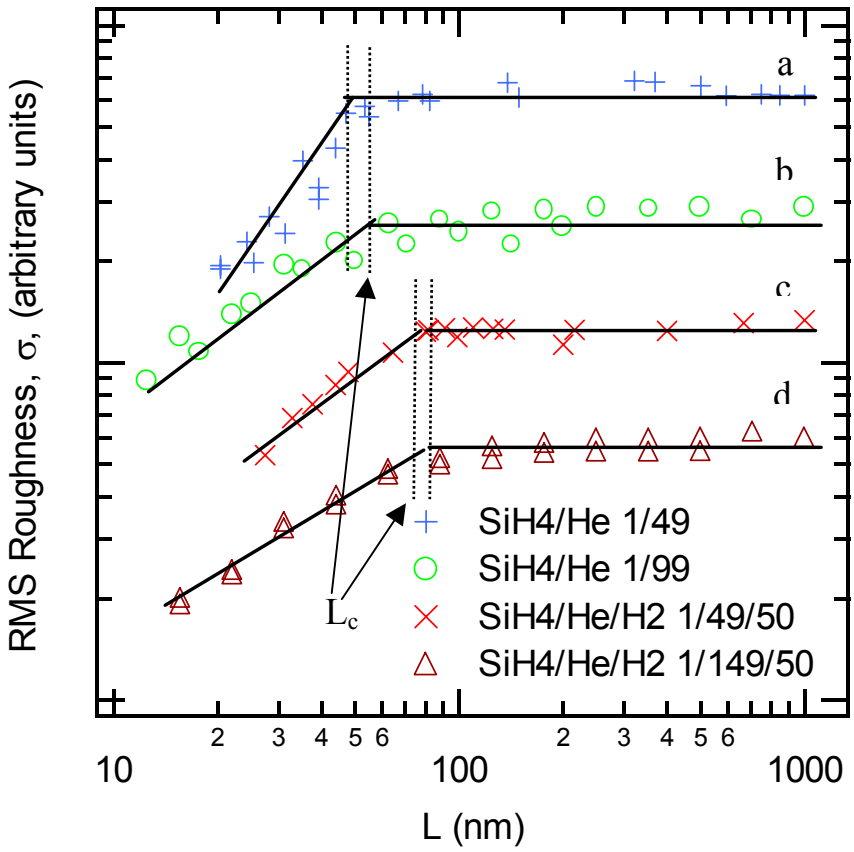

Fig 5.1 Fractal analysis of 1000Å a-Si:H films deposited with varying helium and hydrogen dilutions. a) SiH_4/He 1/49, b) SiH_4/He 1/99, c) SiH_4/He/H_2 1/49/50, d) SiH_4/He/H_2 1/149/50. The correlation length, L_c, where the RMS roughness saturates with length, increases with hydrogen dilution. The curves are offset of clarity. Lines are guides for the eye.

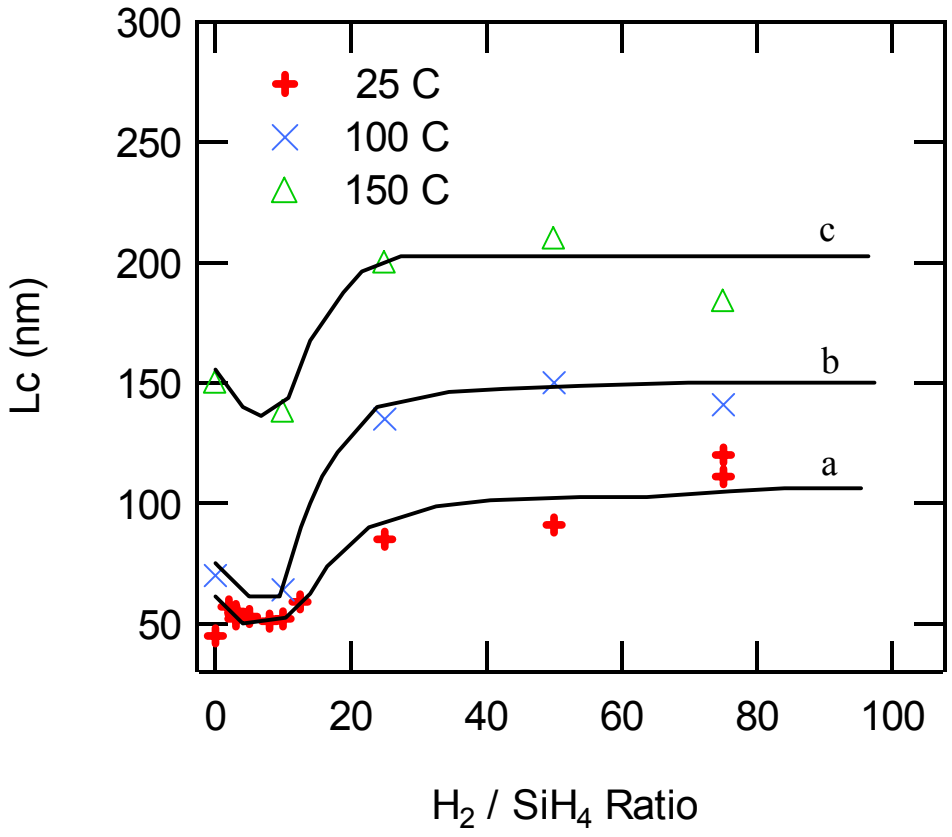

Fig 5.2 The correlation length, L_c vs. the H_2/SiH_4 ratio. Lc remains constant with low H_2 dilutions, then increases with high hydrogen dilutions for films deposited at a) 25°C, b) 100°C, and c) 150°C. The lines are guides for the eye.

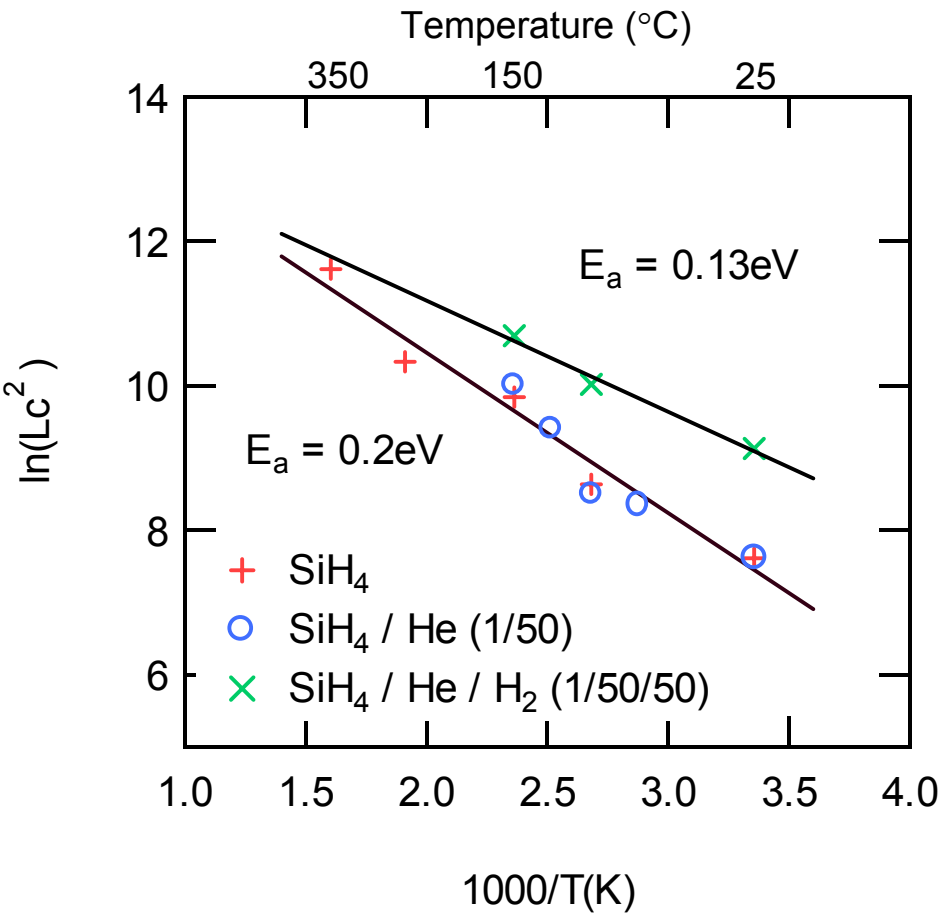

Fig 5.3 Arrhenius plots of $\ln(L_c^2)$ vs. 1/T for a-Si:H films deposited from SiH_4 (from reactor two), SiH_4/He and SiH_4/He/H_2 mixtures (from reactor one).

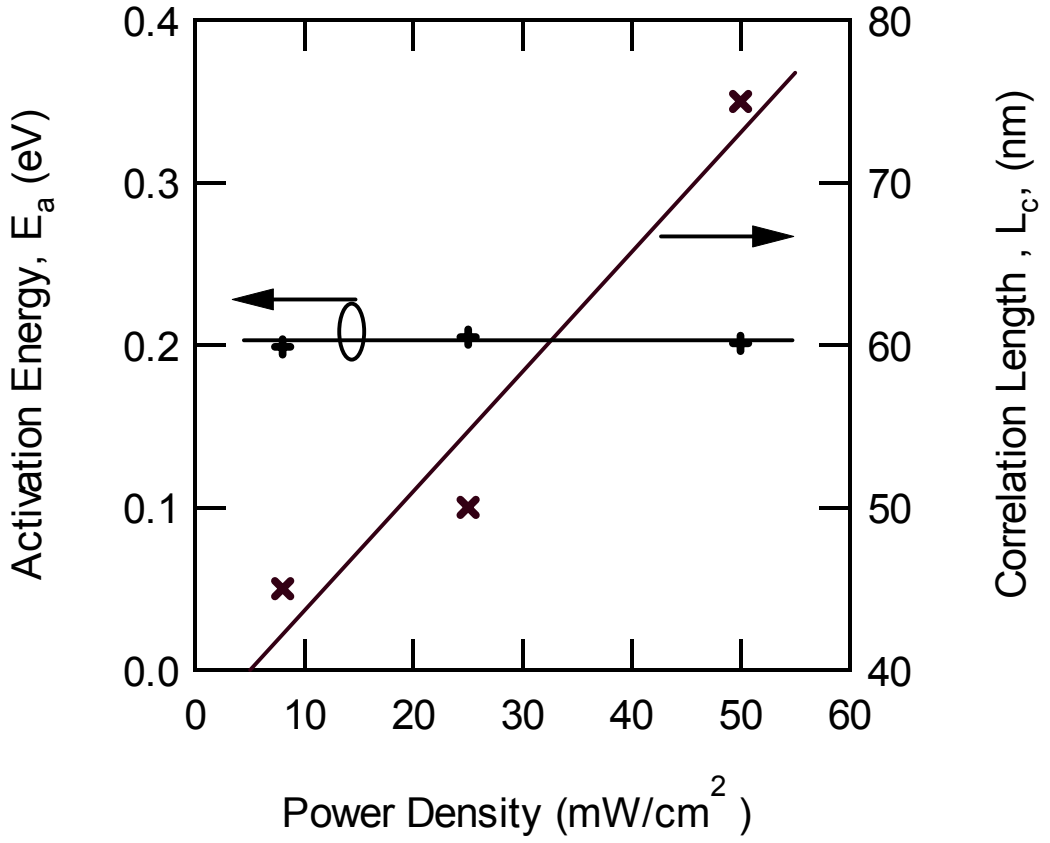

Fig 5.4 Effect of power density on the correlation length and the surface diffusion activation barrier. Lines are guides for the eye.

Chapter 6 is a preprint of a manuscript to be submitted for publication in Journal of Chemical Physics

CHAPTER 6

6 DENSITY FUNCTIONAL STUDY OF THE INSERTION REACTIONS OF H AND SIH_3 RADICALS INTO STRAINED SI-SI BONDS.

Atul Gupta and Gregory N. Parsons

Dept. of Chemical Engineering, Box 7905, North Carolina State University, Raleigh

ABSTRACT

The energetics of silyl (SiH_3) and hydrogen (H) radical insertion into strained Si-Si surface bonds during plasma deposition of a-Si:H films are described. Ab-inito calculations based on Density Functional Theory (DFT) using the hybrid Hartree- Fock methods were performed on Si_9H_{15} and $Si_{10}H_{17}$ clusters to elucidate the reaction mechanisms. The H radical inserts has a barrier of ~3.6 kcal/mol while the SiH_3 radical has a barrier of 21.6kcal/mol along a reaction path where the H and silyl (specifically the Si atom) radicals are kept equidistant form the surface silicon atoms. The minimum energy path for the silyl radical is different from the above trajectory and the actual barrier for silyl insertion may be ~13 kcal/mol. Furthermore the penta-coordinated state

for silyl radical during the insertion reaction is found to be unstable and cannot be considered as a reaction intermediate. These results indicate that the insertion reactions may present an alternate pathway to the conventional growth models for a-Si:H films and are consistent with recent experimental reports.

Keywords: Surface reactions, amorphous silicon, strained Si-Si bonds, Reaction energetics, Growth mechanisms

6.1 INTRODUCTION

Hydrogenated amorphous silicon (a-Si:H) films find several applications in photo-voltaic devices and thin film transistors [1,2]. These films are typically deposited at low substrate temperatures using plasma enhanced chemical vapor deposition (PECVD) or hot-wire catalyzed CVD to make them compatible with transparent glass or polymeric substrates and significant scientific effort has been dedicated towards the characterization of these films in terms of its bulk material properties such as defect density, microcrystalline silicon (μc-Si) fraction. Details of the deposition and growth mechanisms that control these bulk properties are still being debated in light of new experimental observations that have been made possible through technological advancements in the available experimental techniques [3-7].

Plasma deposition of amorphous silicon films is typically carried out using silane/hydrogen (SiH_4/H_2) gas mixtures. Under conditions that yield device quality films (i.e., low defect density, conformal step coverage, and smooth films), the dominant growth precursors are the silyl (SiH_3) radicals [8-11]. A significant flux of the hydrogen radicals is incident upon the surface when the silane gas is diluted with hydrogen and is responsible for improved material properties since H radicals can saturate the dangling bonds in the film thereby reducing the defect density. The silyl and H radicals may participate in several surface reactions including abstraction of surface hydrogen atoms, chemisorption onto dangling bonds, etching of tri-hydrides from the surface or insertion into strained Si-Si bonds among other possible reactions. Several experiments have focused on studying the reaction energetics of these reactions to elucidate the growth

mechanisms. For example, the abstraction and etching reactions involving incident H radicals has been studied using real time mass spectroscopy [12] and von Keudell et al have reported experimental evidence for the insertion of H and SiH_3 radicals into strained Si-Si bonds [13,14]. However the energetics of some of these reactions are difficult or impossible to evaluate experimentally. The use of ab-initio calculations and molecular dynamic simulations has gained importance in elucidating the mechanisms of these reactions [15,16]. These theoretical approaches have helped in gaining new insight into the microscopic processes that control a-Si:H film formation and have questioned the previously proposed mechanisms. One such example is the physisorption of silyl radicals on a hydrogen terminated silicon surface. The physisorption was presumed to occur through a three-center bond in which the Si atom in the silyl radical forms a partial (weak) bond on a surface hydride such that the H atom is partially bound to both, the Si atom of the radical, as well as the Si atom on the growth surface. The resulting potential energy surfaces from several ab-initio calculations indicated that such a three-center bond configuration is not stable and pointed towards alternate physisorption states for the radicals [15]. These theoretical results confirm the observations made by von keudell and Abelson about an alternate pathway for radical incorporation during film growth [14]. Their experiments involved monitoring the loss of surface SiD groups (and the appearance of SiH groups) from a deuterated a-Si:D film surface upon exposure to a purely SiH_3 radical flux using in situ real time infrared spectroscopy. The observed time delay between the appearance of Si-H groups and the loss of Si-D groups from the surface upon introduction of the SiH_3 radical flux indicates a non-zero barrier for H abstraction by the SiH_3, and points towards a direct insertion mechanism for the silyl

radicals. Such insertion reactions likely involve strained Si-Si bonds present on the surface during a-Si:H deposition. Similar insertion reactions between the incident H radicals and strained Si-Si bonds are also possible. Jackson and Tsai proposed that the H radicals insert into strained Si-Si bonds to form hydrogen platelets [17]. Von Keudell and Abelson have also reported direct experimental evidence for insertion of H radicals into Si-Si bonds [13].

The energetics of the silyl insertion were explored using molecular dynamics simulations and pseudopetential DFT calculations by Walch et al who found that the silyl radical dissociatively adsorbs on the surface in two steps [18,19]. The first step involves breaking the Si-Si dimer bond and has an activation barrier (~0.9eV) with the Si atom in the radical partially bound to both Si atoms of the dimer. The second step involves the formation of a Si-Si bond between the radical and one of the surface Si atoms accompanied by a transfer of one of the H atoms from the silyl radical to the other Si atom comprising the original dimer bond on the surface. This step is endothermic (~0.16eV) and has a barrier of ~0.37eV. However the reaction pathway is does not include the effect of an off–center approach path by the radical that may have a lower barrier for the insertion into the dimer bond. In this article, the mechanisms for insertion reactions of both H and silyl radicals into the Si(100)2x1 dimer bonds and the stability of the reaction intermediate for the silyl insertion reaction are analyzed using density functional (B3LYP) calculations in light of the new experimental evidence for these reactions.

6.2 THEORY AND CALCULATIONS

The strained Si-Si bonds are modeled as a Si(100) 2x1 reconstructed surface using a 9 Si atom, and 14 H atom Si_9H_{14} cluster. The reconstructed dimer on the 2x1 surface represents the strained Si-Si bond into which the hydrogen and silyl radicals insert. Including the incident radicals with this cluster we get two structures (shown in Fig 6.1 and Fig 6.2), one with the empirical formula Si_9H_{15} and the other as $Si_{10}H_{17}$, that are used to evaluate the energetics of the H and SiH_3 insertion reactions respectively. The reaction energetics are calculated from optimized energy of these clusters under different geometric configurations. The Si_9H_{14} cluster which is used to represent the strained Si surface has been widely used by other researchers to study several reactions on 2x1 reconstructed Si(100) surfaces [20,21]. The cluster consists of four layers of Si atoms. Two Si atoms in the first (top) layer form the dimer linkage and are in turn covalently bonded to four other Si atoms (comprising the second layer) with no direct bonds between the 4 atoms in this layer. The third layer again comprises of two Si atoms each sharing one covalent bond with two Si atoms in the second layer. Both the Si atoms in the 3rd layer are held together through a covalent bond each with the lone Si atom in the fourth (bottom) layer. The remaining two valences on each of the Si atoms in the 2nd and 4th layers, as well as the lone valency for the dimer atoms and the 3rd layer atoms are saturated with H atoms.

The hydrogen and silicon atoms in the cluster are distinguished into two categories (a) H_{int} and Si_{int} are the hydrogen and silicon atoms that interact with the approaching radicals and (b) H_{bulk} and Si_{bulk} are the hydrogen and silicon atoms that are

used to build the underlying layers. The surface H and Si atoms (comprising the top layer) are assumed to interact with the approaching radicals. The bulk atoms on the other hand do not have a significant electronic interaction with the radicals but help in restricting the atoms from drifting apart during a full geometry optimization calculation. It is for this reason that a higher level basis set, 6-31G++(3d,2p), with both the diffuse and polarization functions superimposed upon the gaussian type orbitals is used to describe the electron distributions in the surface atoms as well as the incident radicals (H and SiH_3). The bulk atoms are described using a 6-31G basis without the diffuse and polarization functions. Partial geometry optimization calculations using the hybrid Hartree-Fock and Density Functional Theory approach (HF-DFT) were performed using the commercially available GAUSSIAN98 quantum chemistry package to identify the reaction pathways for the insertion of both H and SiH_3 radicals into strained Si-Si bonds [22]. The calculations were run on a 48 processor (400MHzMIPS R12000) SGI workstation cluster available through the North Carolina Supercomputing Center. The HF-DFT calculation method uses Becke's three-parameter hybrid exchange functional [23]in combination with the non-local correlation functional of Lee, Yang and Parr [24]. The method is commonly referred as the B3LYP method indicative of the functionals used.

Fig 6.1 and 6.2 show the geometry of the model clusters used in the calculation of reaction energetics for the insertion of H and SiH_3 radicals in the Si_9H_{14} cluster. The model clusters indicate several degrees of freedom that are critical in determining the potential energy surface. Some of the important parameters include; i) distance between the surface Si atoms (the length of dimer bond, $L_{Si\text{-}Si}$); ii) distance of the radical (either

the H radical or the Si atom in SiH_3 radical, R_{Rad}) from the dimer bond; iii) the approach direction for the radical i.e. along the perpendicular bisector of the dimer bond or off-center; iv) the orientation of the H atoms within the silyl radical itself etc. A comprehensive study of the effects of all these parameters on the minimum energy path requires exhaustive computational resources. The effect of changing the approach direction of the H radicals towards the surface has been reported in another *ab-initio* study of H insertion into Si-Si bonds using Si_2H_6 molecule as the model structure [25]. It was shown that the smallest barrier (3.0 kcal/mol) was observed for H approaching normal to the Si-Si bond axis, resulting in a transition state where the hydrogen is bonded to both Si atoms and a larger barrier (5.8 kcal/mol) was obtained for H approaching along the Si-Si axis. Based on their studies, only one H approach angle, normal to the Si-Si dimer linkage, was considered in this study. Also, any stable intermediate that exists during the insertion reactions is likely to result from partial bonds between the radical and both the surface Si atoms. Therefore the minimum energy path for the radicals is likely where the approaching radical is equidistant from the surface Si atoms and the cluster is symmetric. Such symmetry constraints are easily implemented through a z-matrix definition of the cluster geometry, which uses the internal coordinate system. In this system, the position of each new atom added to the z-matrix is described in reference to 3 previously defined atoms in the cluster in terms of a bond distance, bond angle and a dihedral angle. This reduces the number of variables to be optimized and helps in implementing geometry constraints where any change in the coordinates of one atom may be directly correlated with the changes in another. Hence characteristic bond lengths and angles etc. in the structure may be defined using the same variables. The actual cluster

geometries (in internal coordinates) used in the calculations for both the insertion reactions are detailed in Appendix A.

6.3 RESULTS AND DISCUSSION

The optimized energies and cluster geometries were calculated for several radical distances (R_{Rad}) measured from the center of the Si-Si strained bond. Optimization was based on a gradient corrected method available as the default for B3LYP calculations performed in G98 software. The convergence criteria for the energy were set at 10^{-6} Hartrees for H insertion and 10^{-5} Hartrees for SiH_3 insertion reactions.

Results for the insertion of H radicals into strained Si-Si bonds on the Si(100)2x1 reconstructed surface, including the calculated total energy (UB+HF-LYP) of the cluster and the surface Si-Si bonds distance (length of the dimer bond), are shown in Fig. 6.2. Energies are plotted in reference to the cluster energy when the radical is far from the surface (R_{Rad} = 15Å). We observe that the total energy of the cluster increases as the H radical begins to interact with the surface atoms and reaches a local maximum at a distance of ~1.9Å from the surface. This maxima represents the activation barrier for the insertion of H into the dimer bond and is calculated to be ~3.6 Kcal/mol. As the radical comes closer to the surface the cluster energy begins to decrease due to the formation of a partial bond between the H radical and the two Si atoms on the surface. However, since the radical is confined to be equidistant from the Si atoms, the insertion reaction cannot be completed (as seen from the negligible change in the Si-Si dimer bond length). This results in an increase in the cluster energy as the H radical comes closer than begins to

increase again that corresponds to a local minima in the energy and may represent a physisorption state for the H radical. However for the completion of the insertion of H radicals into the dimer bond, the radical must bond to one of the surface Si atoms accompanied by a cleavage of the dimer linkage. Additional calculations without the centerline approach constrain on the H radical results in a geometry where the surface Si atoms are separated from each other with the H radical forming a covalent bond with one of the Si atoms. This step is thermodynamically favored since the SiH bond is stronger than the dimer linkage and the resulting geometry is about 33 kcal/mol lower in energy than the reference state, i.e. the insertion of H radicals into the dimer bond is exothermic by 33Kcal/mol.

Fig 6.3 shows the optimized cluster energies when a silyl radical approaches the surface Si-Si bond in a manner similar to the H radical. Here the Si atom in the silyl radical is presumed to approach along the perpendicular bisector of the dimer bond. The H atoms in the approaching radical are oriented such that one of the H atoms lies in, while the other two atoms lie symmetrically on the opposite sides of the plane containing the interacting surface atoms. The reaction energetics for the SiH_3 insertion show a distinct difference in the shape of the activation barrier as compared with the smooth barrier observed for H insertion. The barrier height along this reaction path is determined to be ~21.6kcal/mol and is observed when the Si atom in the radical is ~2.4Å from the surface dimer. However, the shape of this transition barrier (steep gradient) indicates that there are other possible states for the radical at the same distance from the surface. This interpretation is further supported by the abrupt (step) change observed in the Si-Si bond distance ($L_{Si\text{-}Si}$) at R_{Rad} ~2.5Å indicating that this transition is not a true barrier as was the

case for H insertion where $L_{Si\text{-}Si}$ remains ~constant near the barrier. Moreover the abrupt change in the For example if we move the radical slightly off the centerline, i.e. closer to either of the surface Si atoms at same distance between the radical and the surface, the cluster energy decreases as the radical moves away from the center. This is shown in Fig 6.4 where the cluster energies and the surface Si-Si bond length ($L_{Si\text{-}Si}$) are plotted as a function of the bond length d_2 (refer Fig 6.2). The plot clearly shows that the approach along the centerline is the least favored trajectory. In fact at any fixed distance (R_{Rad}) from the surface dimer, the radical prefers to orient itself close to the atom labeled Si1 corresponding to a decrease in the value of bond distance d1 between Si1 and the dummy atom. This lowering of the cluster energy is more apparent for smaller R_{Rad} values (i.e. when the radical is in close proximity to the surface) as seen from the comparison of energy changes for R_{Rad}= 2.5Å and 2.7Å. This trajectory which requires the silyl radical to be closer to one of the Si atoms, provides a lower energy path for the insertion reaction and hence the effective reaction barrier has to be much lower than the ~1eV barrier calculated in earlier reports [18].

These results have important consequences in the silicon deposition process. The silyl insertion reaction results in a net growth of the film through the formation of a new Si-Si bond and is an important growth mechanism as indicated in some experiment. Both the H and insertion reactions provide alternate pathways for relaxation of network strain as well as result in the formation of a dangling bond on the surface (on the surface Si atom in the dimer that the radical *does not* bond to). These dangling bonds may act as chemisorption sites for the incident radicals and also may play an important part in determining the defect density in a-Si films.

The insertion of H radicals into strained Si-Si bonds has been proposed as a critical mechanism in H_2 plasma annealing and etching of a-Si:H films. The H radicals are believed to sequentially insert into Si-Si bonds resulting in the formation of tri-hydrides on the surface that are etched away by incident H radicals as SiH_4 molecules.

Etching of crystalline silicon films by atomic hydrogen has been studied experimentally using mass spectroscopy, and the energy barrier for the etching on reconstructed Si(111) surfaces was estimated to be 1.8 kcal/mol [26]. This value is slightly smaller than the 3.6 kcal/mol value obtained for H insertion into the Si(100) dimer . However, Si-Si bonds on the reconstructed Si(111) surface are more highly strained than the (100) dimers, and therefore, a smaller barrier for insertion is expected on the reconstructed (111) surface. This apparent barrier height for H insertion may be further lowered due to atomic hydrogen tunneling, and on account of the translational and vibrational energies in an experimental environment.

The silyl insertion reaction provides an alternate pathway for film growth different from most kinetic models reported in the literature. Such models assume a two-step growth process wherein; the first step involves abstraction of a surface H to create a chemisorption site (dangling bond) on the surface; followed by a growth step involving the chemisorption of another radical on this newly created surface dangling bond. The direct insertion pathway may only be important is the barrier for insertion of silyl radicals is comparable to the abstraction barrier. The barrier for abstraction of H by silyl radicals has been estimated to be ~0.4eV (10 kcal/mol) from ab-inito calculations [15] whereas previously reported theoretical calculations estimate the barrier for the insertion reaction at ~0.9eV (~22kcal/mol) [18], a value that is significantly higher than the abstraction

barrier. Our results indicate that the barrier of ~22kcal/mol corresponds to a constrained reaction path for the approaching radical along the centerline and that the minimum energy path for the silyl radical does not coincide with this particular approach trajectory although the same trajectory may define the minimum energy path for the insertion of H radicals. The actual barrier may actually be less than 13 kcal/mol obtained when the radical is allowed to approach the surface without any constraints which is similar to the barrier for the abstraction reation. The reason for a difference in the minimum path trajectories for the H and SiH_3 radicals lies in the asymmetric electron distribution within the silyl radical. The Si atom in SiH_3 radical is sp^3 hybridized and the directional nature of these hybrid bonding orbitals (that results in a tetrahedral geometry for the SiH_3 radicals) results in a minimum energy path where this Si atom is not equidistant from both the surface Si atoms. This is in contrast to the case of H radical insertion, where a spherically symmetric electron distribution for the H radical (1*s* and 2*s* orbitals), results in minimum energy path that is equidistant from both the surface Si atoms. Our calculations further suggest that the penta-coordinated state for the physisorbed silyl radical is not a stable intermediate as proposed in the literature.

6.4 SUMMARY

Density functional calculations have been performed on a Si_9H_{14} cluster representative of the Si(100) 2x1 reconstructed surface, to elucidate the reaction mechanisms for the insertion of H and SiH_3 radical into strained Si-Si bonds. The radicals are constrained to follow a path such that the incident atoms (H radical and Si

atom of the silyl radical) are equidistant from the two surface Si atoms comprising the Si-Si dimer bond. The activation barrier for the H insertion along this reaction path is calculated to be 3.6Kcal/mol and corresponds to the minimum energy path for the reaction. The insertion of silyl into the surface Si-Si dimer bond has a calculated barrier of 21.6 Kcal/mol along this reaction path. However the minimum energy path for silyl insertion does not coincide with this reaction path, and the insertion of silyl radicals has a different reaction path which presents a much smaller activation barrier. The minimum energy path involves an asymmetric off-center approach of the silyl radicals wherein the radical is closer to one of the surface Si atoms. The symmetric penta-coordinated state proposed as an intermediate for this reaction is not a "stable" state for the silyl radical.

6.5 ACKNOWLEDGEMENTS

The authors acknowledge the computational resources (hardware and software) available through an academic grant from the North Carolina Supercomputing Center (NCSC) as well as financial support from NSF.

6.6 REFERENCES

[1] R. A. Street, *Hydrogenated amorphous silicon* (Cambridge University Press, New York, 1991).

[2] R. Crandall and W. Luft, *Progress in Photovoltaics* **3,** 315-332 (1995).

[3] J. Robertson, *Journal of Applied Physics* **87,** 2608-2617 (2000).

[4] G. N. Parsons, *Journal of Non-Crystalline Solids* **266,** 23-30 (2000).

[5] M. C. M. van de Sanden, W. M. M. Kessels, R. J. Severens, and D. C. Schram, *Plasma Physics and Controlled Fusion* **41,** A365-A378 (1999).

[6] A. von Keudell, *Plasma Sources Science & Technology* **9,** 455-467 (2000).

[7] J. E. Gerbi and J. R. Abelson, *Journal of Applied Physics* **89,** 1463-1469 (2001).

[8] A. Matsuda, K. Nomoto, Y. Takeuchi, A. Suzuki, A. Yuuki, and J. Perrin, *Surface Science* **210,** 114 (1990).

[9] J. Perrin, *Journal of Non-Crystalline Solids* **137,** 639-644 (1991).

[10] J. R. Abelson, *Applied Physics a-Materials Science & Processing* **56,** 493-512 (1993).

[11] G. Ganguly and A. Matsuda, *Optoelectronics-Devices and Technologies* **9,** 269-276 (1994).

[12] E. Srinivasan and G. N. Parsons, *Journal of Applied Physics* **81,** 2847-2855 (1997).

[13] A. von Keudell and J. R. Abelson, *Applied Physics Letters* **71,** 3832-3834 (1997).

[14] A. von Keudell and J. R. Abelson, *Physical Review B-Condensed Matter* **59,** 5791-5798 (1999).

[15] A. Gupta and G. N. Parsons, *Surface Science* **accepted for publication** (2001).

[16] S. Ramalingam, D. Maroudas, and E. S. Aydil, *Journal of Applied Physics* **86,** 2872-2888 (1999).

[17] W. B. Jackson and C. C. Tsai, *Physical Review B* **45,** 6564-6580 (1992).

[18] S. P. Walch, S. Ramalingam, E. S. Aydil, and D. Maroudas, *Chemical Physics Letters* **329,** 304-310 (2000).

[19] S. P. Walch, S. Ramalingam, S. Sriraman, E. S. Aydil, and D. Maroudas, *Chemical Physics Letters* **344,** 249-255 (2001).

[20] P. Nachtigall, K. D. Jordan, and K. C. Janda, *Journal of Chemical Physics* **95,** 8652-8654 (1991).

[21] C. J. Wu and E. A. Carter, *Chemical Physics Letters* **185,** 172-178 (1991).

[22] G. W. T. M. J. Frisch, H. B. Schlegel, G. E. Scuseria,, J. R. C. M. A. Robb, V. G. Zakrzewski, J. A. Montgomery, Jr.,, J. C. B. R. E. Stratmann, S. Dapprich, J. M. Millam,, K. N. K. A. D. Daniels, M. C. Strain, O. Farkas, J. Tomasi,, M. C. V. Barone, R. Cammi, B. Mennucci, C. Pomelli, C. Adamo,, J. O. S. Clifford, G. A. Petersson, P. Y. Ayala, Q. Cui,, D. K. M. K. Morokuma, A. D. Rabuck, K. Raghavachari,, J. C. J. B. Foresman, J. V. Ortiz, A. G. Baboul,, G. L. B. B. Stefanov, A. Liashenko, P. Piskorz, I. Komaromi,, R. L. M. R. Gomperts, D. J. Fox, T. Keith, M. A. Al-Laham,, A. N. C. Y. Peng, M. Challacombe, P. M. W. Gill,, W. C. B. Johnson, M. W. Wong, J. L. Andres, C. Gonzalez,, and E. S. R. M. Head-Gordon, and J. A. Pople,, (Gaussian, Inc., Pittsburgh PA, 1998).

[23] A. D. Becke, *Physical Review a* **38,** 3098-3100 (1988).

[24] C. T. Lee, W. T. Yang, and R. G. Parr, *Physical Review B-Condensed Matter* **37,** 785-789 (1988).

[25] K. D. Dobbs and D. J. Doren, *Journal of the American Chemical Society* **115,** 3731-3738 (1993).

[26] J. Abrefah and D. R. Olander, *Surface Science* **209,** 291-313 (1989).

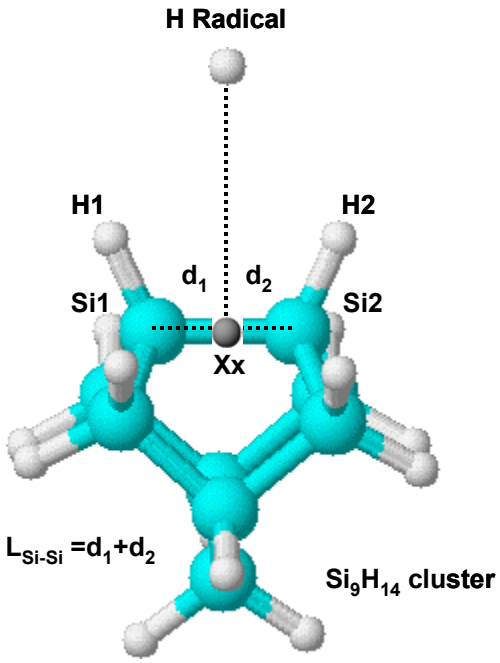

Fig 6.1 The cluster used for describing H insertion into strained Si-Si bonds.

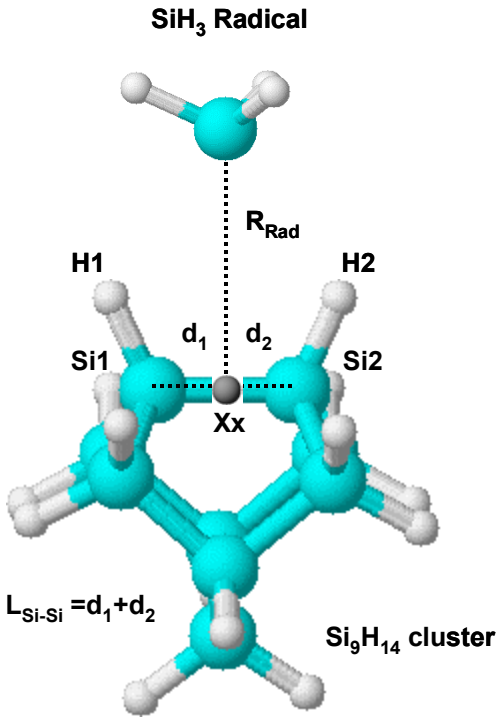

Fig 6.2 The cluster used for SiH_3 insertion into strained Si-Si bonds.

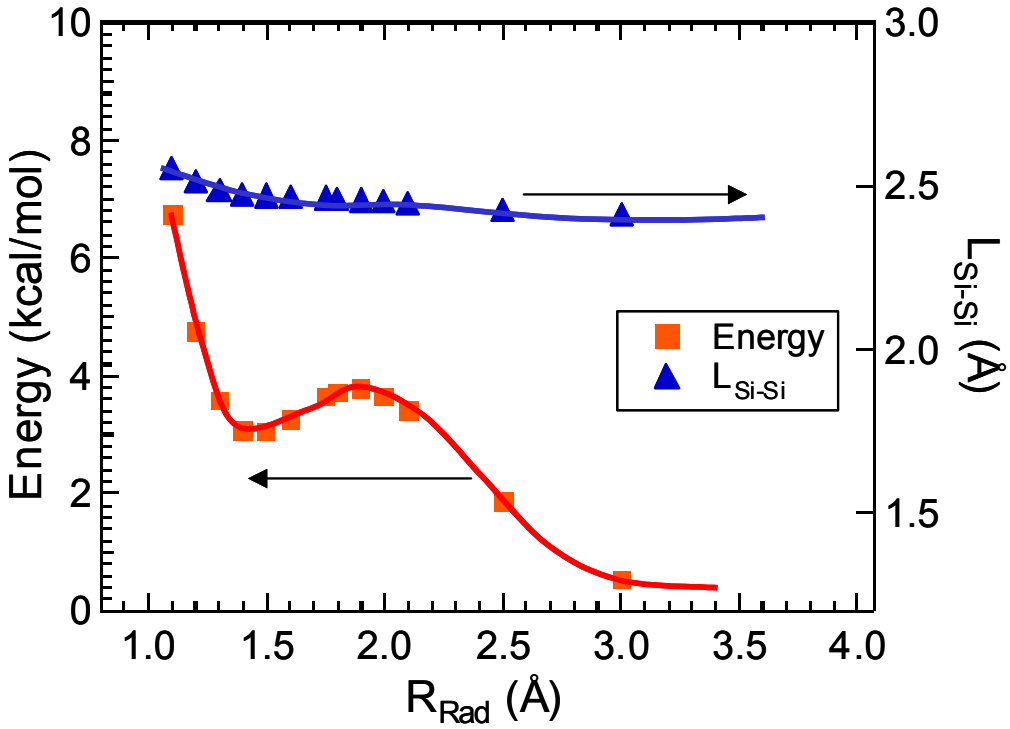

Fig 6.3 Reaction energetics for the insertion of H radicals into a Si-Si dimer bond on a reconstructed Si(100) 2x1 surface. The energies are calculated along a reaction path where the H radical remains equidistant from the two surface Si atoms.

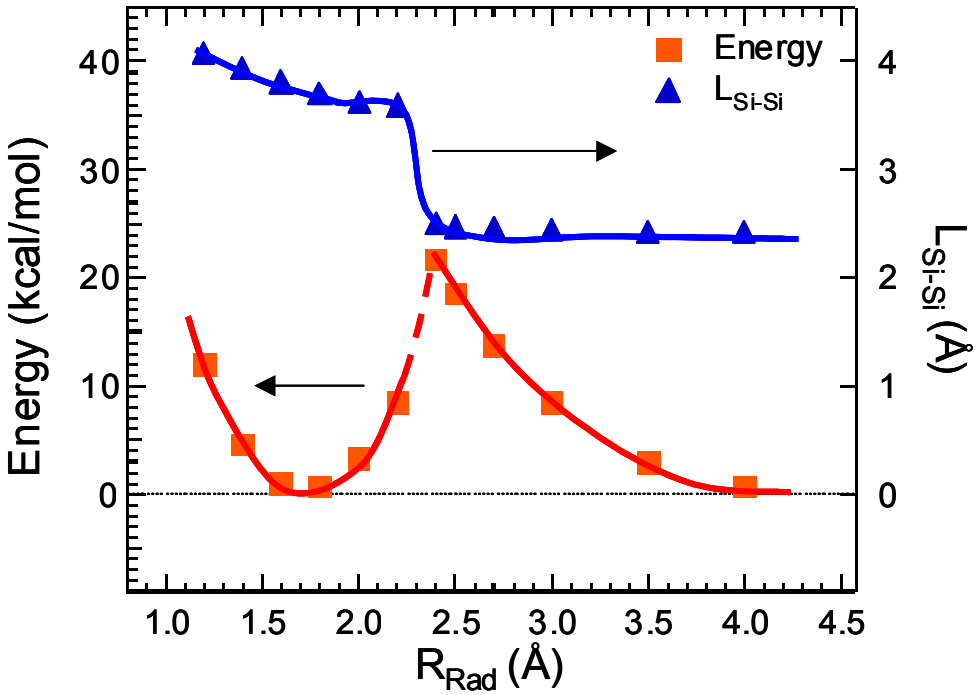

Fig 6.4 Reaction energetics for the insertion of H radicals into a Si-Si dimer bond on a reconstructed Si(100) 2x1 surface. The energies are calculated along a reaction path where the H radical remains equidistant from the two surface Si atoms.

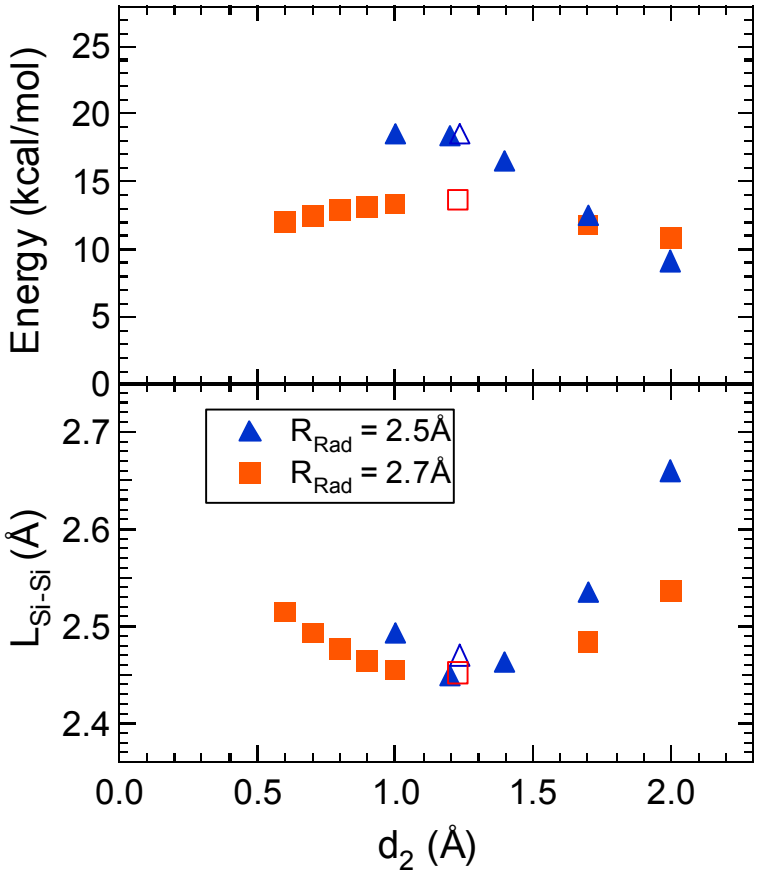

Fig 6.5 Effect of an off-center reaction path for the insertion of silyl radical into a Si-Si dimer bond. The radical does not form a stable intermediate (indicated by the maxima rather than a minima in the cluster energy) when constrained to a position equidistant from the surface Si atoms.

CHAPTER 7

7 CONCULSIONS AND FUTURE STUDIES

7.1 CONCLUSIONS

Plasma deposited hydrogenated amorphous silicon is an important material in today's world with its applications in photovoltaic devices and in thin film transistors that drive the pixels in active matrix displays. Understanding the correlation between deposition conditions and film properties is key towards optimizing the plasma deposition process. A kinetic model describing a-Si:H growth from silane plasmas has been developed to explain various experimental observations reported in the literature. The model incorporates newly reported growth pathways and a new approach to account for network formation during a-Si:H growth. Ab-initio calculations using both configuration interaction and density functional methods were used to describe the reaction energetics of several key reactions in a-Si deposition and the resulting barriers were used in the kinetic model. These calculations also provide a new perspective on the microscopic reaction mechanisms and challenge long-standing hypotheses about the geometric configurations of the physisorbed radical states. The possible applications of H abstraction reactions as a pathway for hydrogen elimination from the film have been explored for the plasma deposition of silicon dioxide at very low temperatures.

Ab-initio quantum chemical calculations of the reaction energetics for the abstraction of hydrogen from the surface of hydrogenated amorphous silicon films by incident hydrogen and silyl radicals help in identifying the mechanisms involved in H elimination from the a-Si:H surface. Results indicate that the H radicals are more likely to abstract the surface H as compared to the silyl radicals on account of a negligible activation barrier and higher tunneling probabilities. Furthermore the potential energy surface describing the H abstraction by SiH_3 radicals along a collinear reaction geometry, does indicate the presence of a stable three-center bond configuration for the approaching silyl radical. This raises new questions about the surface mechanisms involved in a-Si deposition and challenges the long held view of a stable physisorption state for the SiH_3 radicals on hydrogen terminated a-Si surface.

A comparison of the reaction pathways for direct insertion of both H and SiH_3 radicals into a Si-Si dimer bond on a Si(100) 2x1 reconstructed surface (modeled using a Si_9H_{14}) cluster indicates distinctly different mechanisms for the two reactions. Insertion of H radical into the dimer bond has a saddle point at a point equidistant from the two Si atoms comprising the dimer bond and a small barrier of ~3.8 kcal/mol. Insertion of the silyl radical into the same dimer bond, on the other hand, proceeds along a path that is asymmetric with respect to the two dimer Si atoms. The minimum energy path for this reaction does not lie along the perpendicular bisector of the Si-Si dimer linkage, i.e., it is energetically favorable for the incident radical to approach the surface atoms along a path that takes it closer to one of the two Si atoms forming the dimer. The actual barrier for the insertion of SiH_3 into Si-Si bonds is likely to be ~10-12kcal/mol which is lower than the reported values of ~20kcal/mol obtained for a reaction path where the Si atom of the

silyl radical is kept equidistant form the two surface Si atoms. Furthermore, these results indicate that the penta-coordinated transition state proposed as an intermediate for this reaction is not an energetically favored state.

These microscopic mechanisms have been considered in a newly developed kinetic growth model for a-Si:H deposition. The kinetic growth model includes bond-specific reactions such as direct insertion of silyl radicals into strained Si-Si bonds through a novel valence balance approach which is used in conjunction with the site balance equations. Precursor diffusion on the surface is found to be thermally activated if the surface physisorption site determines the precursor surface diffusion rate. If the diffusion rate for precursors physisorbed on di- and tri-hydride sites is impeded relative to those on mono-hydride sites, then at low temperatures, the diffusion length increases with increasing temperature due to an increase in the fractional surface coverage of silicon mono-hydride site. The model calculates the density of different surface sites as well as number of Si-Si bonds between surface atoms and the calculated values for several macroscopic parameters such as the film growth rate, radical reaction probabilities and precursor surface diffusion lengths are consistent with available experimental data.

The effect of using hydrogen dilution as an alternate pathway for removal of surface H in low temperature plasma deposition of silicon dioxide films has also been explored. Hydrogen dilution of silane/nitrous-oxide gas mixtures resulted in and a reduced overall OH incorporation, but promoted the formation of stable highly-associated Si-OH groups, likely through reactions involving physisorbed water generated in the gas phase or on the surface. The effect of hydrogen dilution on oxide film structure and

composition can be understood through analysis of the infrared transmission spectra, where the Si-O asymmetric stretching peak is strongly affected by combined effects of bond strain and chemical induction.

7.2 FUTURE STUDIES

7.2.1 Ab-initio Studies

There are several key reactions in both a-Si:H and SiO_2 plasma deposition processes that may play a key role in determining the film properties. Ab-initio calculations provide the means for evaluating different reaction pathways in terms of the reaction energetics and help in identifying the key processes operative under different deposition conditions. With advances in computational algorithms and hardware resources, it may be possible to use ab-initio methods on much larger clusters that provide more realistic models for understanding surface reactions, especially the effects of secondary or tertiary neighbors atoms on the reaction energetics.

For a-Si:H deposition, there is much debate over the microscopic mechanisms that result in precursor diffusion on the surface as well as the configuration of the physisorbed precursor. Specifically the binding energy of the radicals on different types of hydrides should be calculated to test the site dependent precursor diffusion mechanism. The stability of different physisorbed radical configurations may be tested following a similar approach as presented in this dissertation. Furthermore the reaction energetics for surface recombination reactions between the different types of hydrides may be quantified to

better explain the hydrogen elimination processes as well as network formation during a-Si deposition.

Theoretical studies may also be used to understand fundamentals of SiO_2 deposition. Specifically the reaction energetics for the abstraction of H or OH by H radicals from the oxide surface may provide a key to the role of hydrogen radicals in the removal of OH groups from the silicon dioxide films. The hydrogen radicals generated in the plasma may either attack the H bonded to the oxygen atom on the surface or attack the Si-O bond itself. The line of approach of these H radicals may influence the reaction energetics and help explain the preferred removal of "isolated" OH groups as compared to the "associated" OH groups as was observed in our experimental work on low temperature SiO_2 deposition.

7.2.2 Role of H radicals in a-Si growth kinetics

The incident H radicals play an important role in the deposition chemistry. Hydrogen dilution is used to reduce the defect density and improve the formation of μc-Si. As predicted by our calculations, the H radicals are much more reactive than the silyl radicals may participate in several reactions during a-Si:H deposition. Some of these reactions are listed below in equations (1) - (4).

$$\equiv Si– + H \rightarrow \equiv SiH \quad (19)$$

$$\equiv (SiH_x)SiH_3 + H \rightarrow \equiv (SiH_x) + SiH_4 \quad (20)$$

$$\equiv SiH + H \rightarrow \equiv Si– + H_2 \quad (21)$$

$$\equiv Si–Si\equiv + H \rightarrow \equiv SiH + \equiv Si– \quad (22)$$

The site balance equations need to be appropriately modified to account for such additional reactions. However there are other issues that are important to consider when including H radicals in the model. These H radicals may diffuse to sub-surface regions and participate in other reactions in the bulk. Thus a model that accounts for the bulk processes needs to be developed in order to explain all the film properties and to have a complete understanding of the film growth mechanisms.